VISION UNDER MANIPULATED ABERRATIONS: TOWARDS IMPROVED MULTIFOCAL CORRECTIONS

By Pablo de Gracia Pacheco

Thesis Advisor: Susana Marcos Celestino

A THESIS SUBMITTED TO
COMPLUTENSE UNIVERSITY OF MADRID
for the degree of
Doctor of Philosophy
Department of Optics
June 2013

PREFACE

"He who says he can and he who says he can't are both usually right"
Confucius

I believe that innovation and education are the keys for a better future and I am fully committed to strive during my life to make a difference on these matters. I started this long trip towards the completion of a PhD degree on visual sciences when I was chosen to take part on the Undergraduate Summer Fellowship Program in Vision Science of the University of Rochester. There and then I realized that I wanted to expand my background to be able to develop my professional life beyond clinical practice. Therefore I want to express my gratitude to Prof. Miguel Antón and Dr. Geunyoung Yoon who offered me the tools and the spot to participate in this program. Both of them have kept giving me their continuous support during all my doctoral studies and I cannot express in words the unbelievable support and reference they have been.

I am grateful to my supervisor Prof. Susana Marcos for giving me the opportunity to start a proper career as a researcher in a world-class laboratory in the field of Visual Science providing the environment for me to grow both personally and academically.

Also I am grateful to Prof. David Atchison for having me in his lab during a short stay. Short stay that I cherish since it was then when I started to realize that I had all that was necessary to be really good at research and that I could in truth make a living out of it.

I want to express my sympathy to all the people of the Institute of Optics with whom I have interacted during the last 5 years and say to them that I will never forget the laughs we have shared. Special thanks to the past and present members of the office 2304 (five years in a room leave plenty of time for everything). We have seen each other grow and develop. Thanks to the ones who played the best soccer and basketball games that we are likely ever to play again in our lives (Javi, Pablo… We are getting old friends!). I am also grateful to Lucie and Enrique for having an operative AO system ready when I first arrived to the Institute and for receiving me with total aperture into what later was known as the "AO team".

To my all-time friends (those whom I known since I have memory or a little bit later), thank you for listening, partying, playing sports, travelling... for being there, I hope we will stay there for each other at least till we lost our memory. Kaccie, thank you for sharing your experience with me! It is been an unbelievable asset. I am sure that without your counsel I would not have enjoyed this process nearly as much. Thanks to Bea for staying there and for showing me that sometimes there are things that you cannot count with your fingers. Thanks to Marta for helping me to awake to my freedom and authenticity with all my bright parts and my shadows (or at least what I considered my shadows).

I want to express to my parents and sister my deepest gratitude since they are one of the central pillars of my live and sustain who I am and who I want to be.

Last but not least I want to acknowledge to the American Academy of Optometry and to the International Society for Optics and Photonics for the awards they have conceded me during the length of this thesis that have undoubtedly paved the way for allowing me to continue a successful career in research. Since I received your awards I have grown in confidence what is one of the most (if not the most) important tools for a researcher.

The last part of this thesis corresponds with a summary on Spanish that is a requirement from University Complutense of Madrid in order to be able to present the rest of the work in English.

PABLO DE GRACIA PACHECO,

June 2013

To my family and all who shared with me these last five years…

FUNDING

The work performed in this thesis would have not been possible without the funding received from public and private institutions.

- Consejo Superior de Investigaciones Científicas. Predoctoral Fellowship JAE-Pre to Pablo de Gracia.
- Collaborative agreement with Essilor (PI: Susana Marcos).
- Ministerio de Ciencia e Innovación y Ministerio de Economía y Competitividad, Spanish Government grants FIS2008-02065 y FIS2011-25637 (PI: Susana Marcos).
- EURHOROCS -ESF European Young Investigator Award Essilor EURYI-05-102-ES (PI: Susana Marcos).
- ERC Advanced Grant ERC-2011-AdG-294099 (PI: Susana Marcos).

Table of contents

Chapter-1 Introduction

1.1. Motivation

The motivation is to increase the available knowledge about the current solutions for presbyopia and to try to improve their optical performance. Solutions for presbyopia are currently one of the hottest topics in vision research because presbyopia affects everyone beyond 45 years of age and all currently available solutions only partially address the condition.

1.2. Optical aberrations and optical quality

The refractive properties of the human eye are classically characterized by their defocus (myopia or hyperopia) and astigmatism. The correction of myopia is known to have started in Florence around the 15th century [1] and Johannes Kepler formally described the optics of myopia and hyperopia and their correction as early as the 17th century. The characterization of astigmatism was achieved in the beginning of the 18th century by Thomas Young[2]. A historic note of relevance for the Institute of Optics where this thesis is been performed is that it is named after Benito Daza de Valdés who in 1623 published a study called “The use of Spectacles”. The correction of astigmatism and defocus removed most of the perceivable blur in the vast majority of the population. Therefore, less effort was put into correcting vision further over the next two centuries.

It is now known that the eye's optics cannot be completely characterized by only three degrees of freedom. Defocus and astigmatism, as typically used in ophthalmic solutions, only allow modeling the optical imperfections of the eye with essentially a sphere in which the two principal meridians (separated 90º) can take on different radii of curvature (cylinder). First attempt to measure the aberrations of the eye beyond that of astigmatism and defocus date from 1962. Smirnov, evaluating the slopes of the light rays through psychophysical measurements (data obtained relied on subject observations and responses), measured for the first time such aberrations in an actual eye[3]. Today’s methods typically do not include psychophysical measurements (although

cross cylinder based techniques and inverse Shack-Hartman sensors still do) but rather take advantage of the advances in technology that have occurred since then (superluminiscent diodes, CCD cameras…) to objectively measure the aberrations of the eye.

1.2.1 Aberrometers (Shack- Hartmann)

The most widely used aberrometer in vision nowadays is the Shack-Hartman (SH) sensor. It was developed out of a need to solve a problem unrelated to vision. At the end of the 1960´s, the US Air Force wanted to improve the quality of ground images of satellites[4]. The optical media that introduced the aberrations in this case was the atmosphere. In the early 1970´s, the first Shack-Hartman sensor was delivered to the Air Force to be used in satellite tracking. But it was not up until 1994 when the first Shack-Hartman sensor was used to measure the eye[5].

Figure 2.1 is a represents a scheme of the procedure. A spot is projected onto the retina by a led source (typically near infrared). Scatter from this spot acts as a source, and on the way out of the eye, captures the optical properties of the combination of the crystalline lens and the cornea with respect to the retina (defined at the paraxial focus). The whole set of rays of light coming out of the eye are called a wavefront. Different rays passing through different areas will recollect information from different parts of the crystalline lens and the cornea (resulting in different optical pathways). A wavefront coming out of a perfect eye will be completely flat, and when arriving at the lenslet array, each microlens will generate a spot. All spots coming for the different microlenses will be distributed over a perfectly rectangular grid (Fig 1.1.A).

In a real eye, the resulting wavefront will not be flat and these differences from the ideal wavefront will produce a non-uniform pattern of spots (Fig 1.1.B).

From the departure found on the spot diagram of a given subject to that of the ideal one, the local slope of the wavefront can be reconstructed. These slopes are used to generate the coefficients weighting the Zernike polynomials a_n^m in equation 1.3 [6].

Zernike coefficients are the standard used for the representation of the ocular wave aberration. The fact that the Zernike polynomials form an orthonormal

basis is one of its major advantages. A second advantage is that second order Zernike polynomials can generate any classical refraction (sphere+cylinder). Zernike polynomials are composed by a radial component $R_n^m(\rho)$ and an angular component $\cos(\mathrm{m}\varphi)$ where the radial orders (n) are positive integers, and the angular orders (m) vary between –n and +n. The rest of m and n is always an even number. The general expression of a Zernike polynomial is:

$$Z_n^m = R_n^m(\rho)\, cos(m\varphi) \qquad (1.1)$$

Where the radial component of the Zernike is given by:

$$R_n^m(\rho) = \sum_{k=0}^{(n-m)/2} \frac{(-1)^k (n-k)!}{k!\,((n+m)/2-k)!\,((n-m)/2-k)!}\, \rho^{n-2k} \qquad (1.2)$$

And the complete reconstruction of the wavefront is in the form:

$$W(x,y) = W(\rho,\varphi) = \sum_{n,m} a_n^m Z_n^m \qquad (1.3)$$

Once all the Zernike coefficients are obtained the global ocular wave aberration can be reconstructed. Wave aberrations up to 6th order Zernike polynomials are used for all the measurements shown in this thesis. We used the OSA convention for the ordering and normalization of Zernike coefficients [7]. Figure 1.3 shows the wave aberrations of 4 subjects measured in our lab for calibration presented in chapter 2 (section 2.1.2).

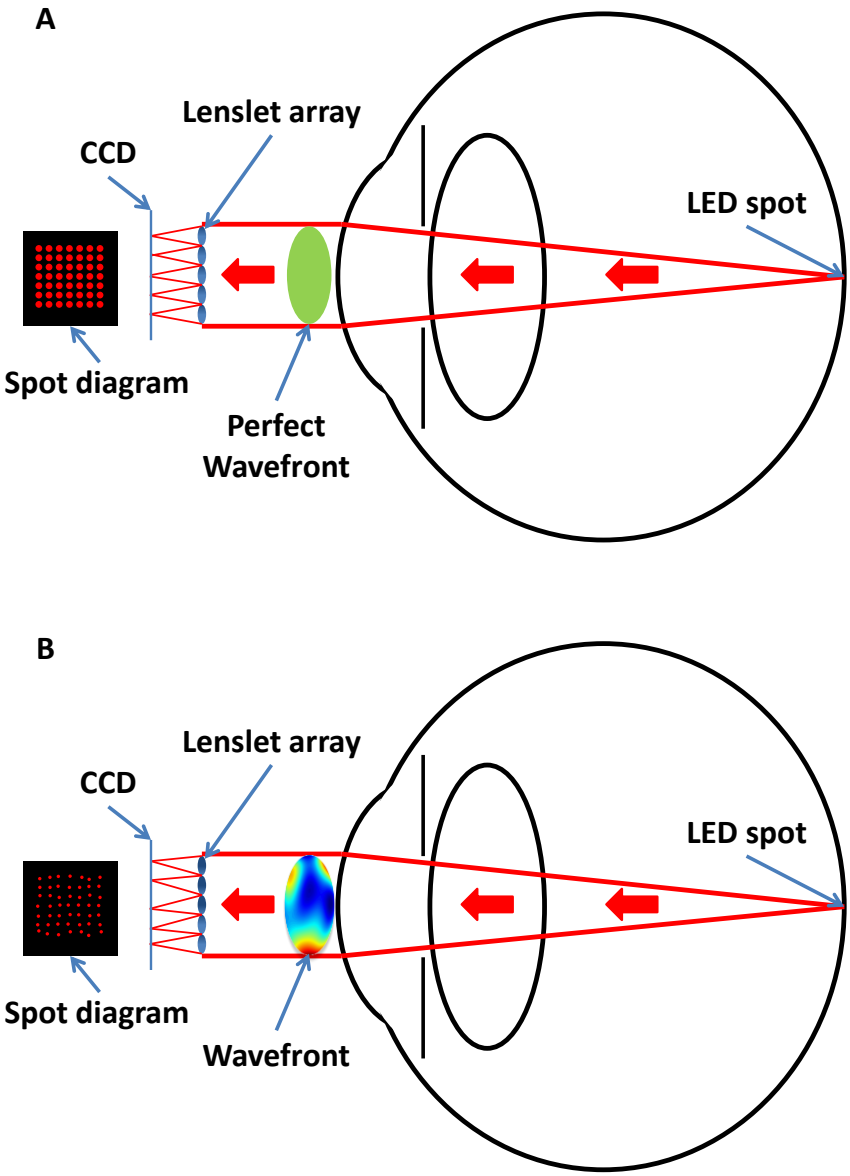

Figure 1.1. Schematic representation of how a Shack-Hartman wavefront sensor works. A) Ideal eye were the wavefront coming out of the eye is completely flat. B) Measurement typically obtained from a normal subject.

Figure 1.2 shows the expansion of the Zernike polynomials up to 7th order.

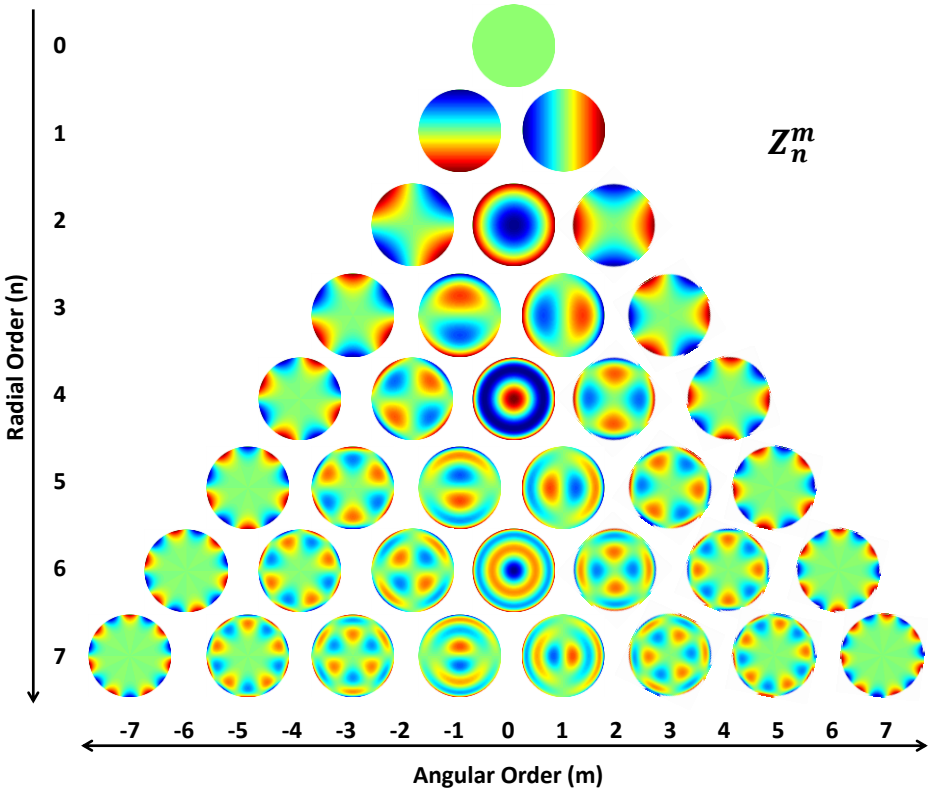

Figure 1.2. Representation of the Zernike polynomials up to 7th order (Z_n^m).

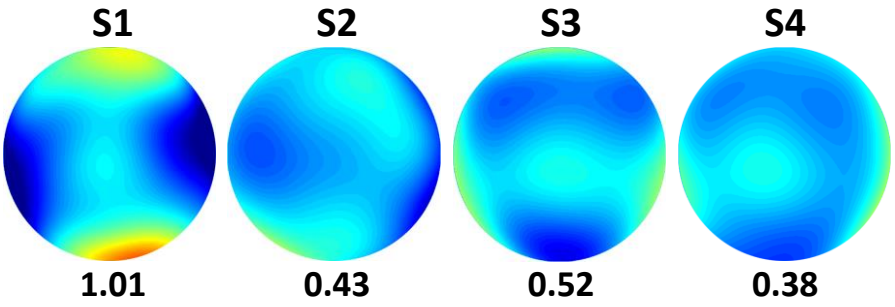

Figure 1.3. Examples of the wave aberrations of the four subjects used for the calibration of the AO system in chapter 2. Pupil diameter 6-mm

1.2.2 Optical Quality Metrics

During the last decade, much effort has been put into obtaining a subject´s refraction of someone directly from the set of Zernike coefficients. As a result of these efforts many different metrics have been developed [8]. A good evaluation of the performance of different metrics can be found in Marsack et al. [9].

The next section briefly explains some of the most common metrics that typically form the basis for most of the optical quality metrics that are currently used in vision science.

The first and simplest is the Root Mean Square of the wavefront error (RMS) (a_n^m in equation 1.3). The RMS up to 6th order of a list of Zernike coefficients is given by:

$$RMS = \sqrt{\sum_{n=0,m=-6}^{n=6,m=6} {a_n^m}^2} \qquad (1.4)$$

The point spread function (PSF) is the image of a point source. If the system is close to the limit imposed by diffraction (and the aperture is sufficiently large for the effects of diffraction to be small) the image of a point will be close to a point. Conversely if the aberrations of an optical system are high, the image of a point will no longer be a point (see chapter 2 for seeing the mathematical expression). The Strehl Ratio (SR) is the ratio between the peak of a PSF limited by optical aberrations and the one limited by diffraction alone. The resultant retinal image is the convolution of the system PSF with that of the Stimulus. The Modulation Transfer Function (MTF) characterizes the contrast of the image after it passes through the optical system as a function of spatial frequencies. The MTF can be restricted to a certain range of frequencies originating other MTFs (e.g. $MTF_{3\text{-}12}$ or $MTF_{5\text{-}15}$). The Visual Optical Transfer Function (VSOTF) is computed by weighting the MTF by a neural contrast sensitivity function (CSF)[10]. The VSOTF is the most successful metric to date in predicting visual performance [9]. Figure 1.4 shows: Wavefronts, PSFs, convolutions, and MTFs. They are presented both for a normal eye (upper representations) and under adaptive optics (AO) correction.

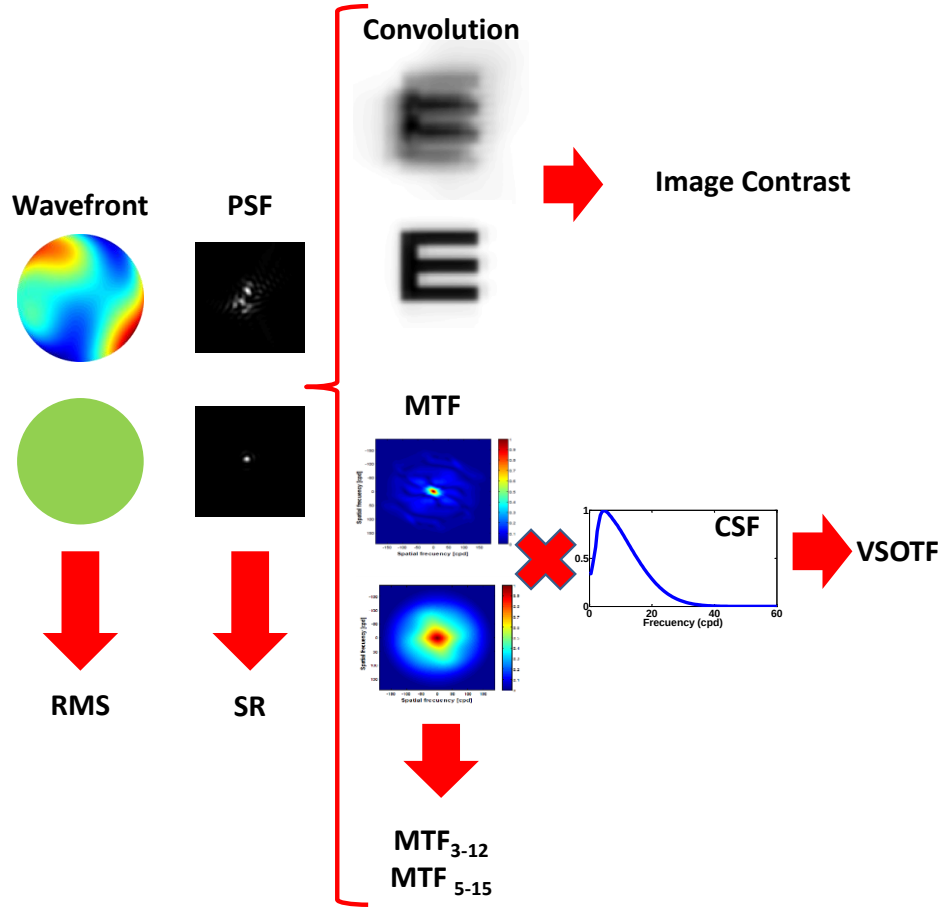

Figure 1.4. Schematic chart representing some of the most common metrics. From left to right: Wavefronts computed from equation 3. The Root Mean Square (RMS) of the list of coefficients that generate the wavefront (as calculated in equation 4). The PSF is the image that an optical system forms of a point source (see chapter 2 for seeing the mathematical expression). The Strehl Ratio (SR) is the ratio between the peak of a PSF limited by optical aberrations and the one limited by diffraction. The convolution is the result of convolving the PSF of the system with a target. The Modulation Transfer Function (MTF) specifies the loss of contrast of frequencies (contrast of the image/contrast of the object) generated by the optical system. If it is limited to a certain band of frequencies you obtain other MTFs known as the $MTF_{3\text{-}12}$ or the $MTF_{5\text{-}15}$. By weighting the MTF with a CSF you obtain the VSOTF. Wavefronts, PSFs, Convolutions, and MTFs, are presented both for a normal eye (upper representations) and under AO correction of the aberrations of the eye (lower representations).

1.3. Adaptive Optics

Once the aberrations are measured, the wave aberrations can be corrected. During the last 25 years the application of adaptive optics technology, first developed for correcting atmospheric turbulence in astronomy, to measuring and correcting the eye's optics has opened the door for the measurement and correction of the optical properties of the eye in a fast and noninvasive procedure [11-14]. The first trial to create and AO system dates from 1989 when Bille's group made an early attempt but the wavefront sensor and the wavefront corrector were not fully developed [15]. David Williams' group in 1997 provided the first results of an adaptive optics system applied for vision correction. Although these first works aimed at imaging the retina, the first results of visual performance tested under adaptive optics correction were also presented [14,16].

Currently, there are four primary technologies aimed at wavefront correction. Figure 1.5 shows 4 schemes representing each one of the technologies. In a), a reflective surface on top of an array of actuators is capable of reproducing local deformations in the surface. In b), a set of pistons regulate the height of the segmented mirrors that can also be tilted. Liquid crystal spatial light modulators work in a similar fashion but induce change in the index of refraction of the material rather than displacing the mirrors. In c) membrane mirrors that are composed of a grounded, reflective, flexible membrane positioned between a top transparent electrode and an underlying set of patterned electrodes. In d), a bimorph mirror consisting of a layer of piezo electric material is positioned between a continuous top surface electrode and a patterned electrode array on the bottom. The top layer over the continuous electrode is mirrored. An applied voltage drop will create a deformation in the top mirrored surface. The two adaptive optics mirrors (shown in figure 1.6) that have been used in this thesis are based in the technology presented in figure 1.5c.

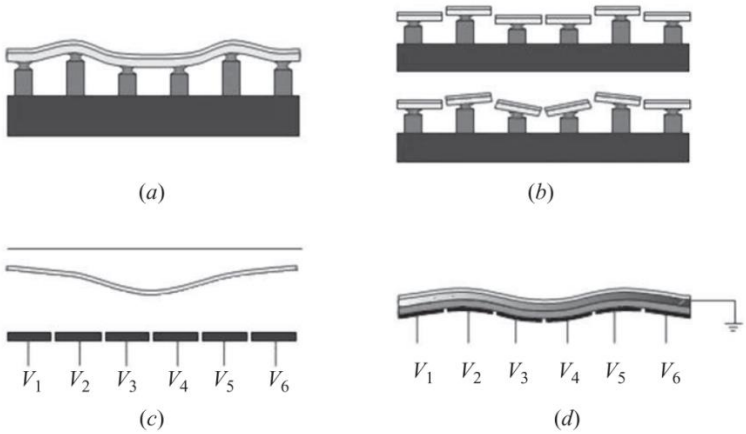

Figure 1.5. Different adaptive optics technologies. a) A reflective surface and an array of actuators are capable of reproducing local deformations in the surface. b) A set of pistons regulate the piston, tip and tilt of the individual mirror segments. Liquid crystal spatial light modulators work in a similar fashion but induced changes in the index of refraction of the material rather than displacing the mirrors. c) Membrane mirrors, are composed of a grounded, reflective, flexible membrane positioned between a top transparent electrode and an underlying set of patterned electrodes. d) Represents a bimorph mirror consisting of a layer of piezo electric material positioned between a continuous top electrode and a bottom, patterned electrode array. There is a mirrored top layer over the top continuous electrode. An applied voltage will create a deformation in the top mirrored surface. Image taken from the Book "Adaptive optics for vision science", editor: Jason Porter.

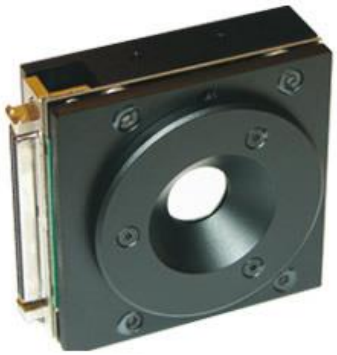

Figure 1.6. Deformable mirror 52-e from Imagine Eyes, France. It is included in the category of deformable mirror technologies shown figure 1.5c.

The measurement and correction scheme or that of inducing aberrations is shown in figure 1.7. The aberrations of the eye are measured by the SH sensor. Then the control algorithm converts these aberrations into instructions for the deformable mirror that changes its shape to correct the natural aberrations of the subject and, in certain cases, induce a different set of aberrations. The residual aberrations are then measured by the SH sensor restarting the loop.

Normally a complete correction of aberrations is achieved after 20 to 40 loops (2-3 seconds).

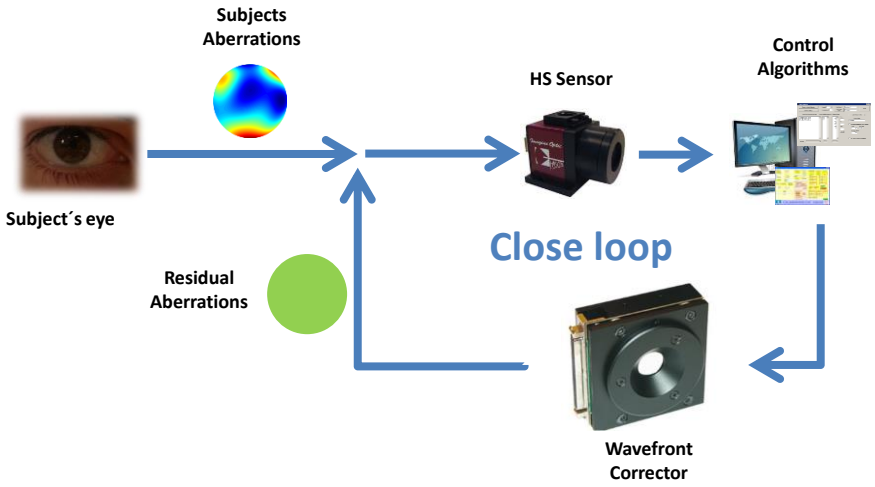

Figure 1.7. Schematic of aberration measurement and correction/induction. The main components are a deformable mirror, a HS sensor and the control algorithms.

1.4. Interaction of aberrations

The fact that Zernike polynomials are orthogonal over the unit circle allows one to modify individual modes without affecting the rest. However, mathematical independence of the modes does not mean their impact on visual performance is independent since Zernike polynomials are evaluated at the pupil plane and the visual performance is related to the optical quality present at the retinal plane. This was first noticed by Applegate et al. in 2003 for aberrations with 2 radial orders apart and having the same sign and angular frequency[17]. Cheng et al. in 2004 explored in detail the interactions between circularly symmetric aberrations where they showed how optical quality could be improved by adding certain amounts of spherical aberration to a given level of defocus [18]. Figure 1.8 shows and example of three letters (size = 5 arcmin) under 0.25 µm of defocus (left), under 0.14 µm of spherical aberration (center) and under the combination of 0.25 µm of defocus and 0.14 µm of spherical aberration (right). Of all of them the one that produces the best optical quality is the one with one with defocus and spherical aberration that also has the highest level of RMS (0.28 µm).

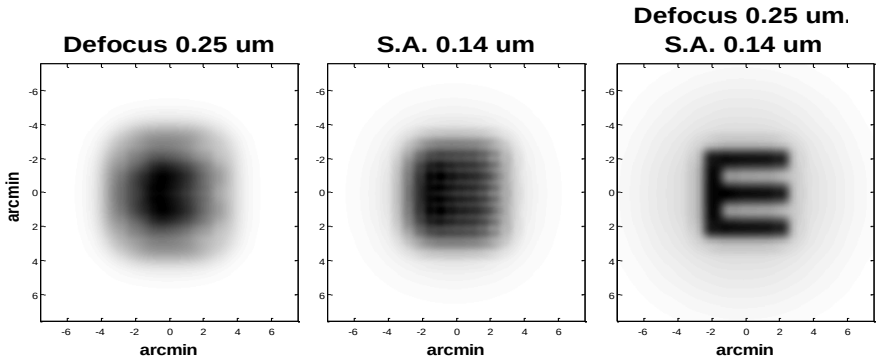

Figure 1.8. Convolved letters of 5 arcmin. Left: 0.25 μm of defocus. Center: 0.14 μm of spherical aberration. Right: combination of 0.25 μm of defocus and 0.14 μm of spherical aberration. Of all of them the one that produces the best optical quality is the one with the combination of defocus and spherical aberration that also has the highest level of RMS (0.28 μm).

These interactions are not only restricted to radially symmetrical aberrations but, as to be discussed in chapters 3 and 4, to asymmetrical modes as well. Specifically, we studied how astigmatism and coma can interact to improve the optical quality of the resultant image.

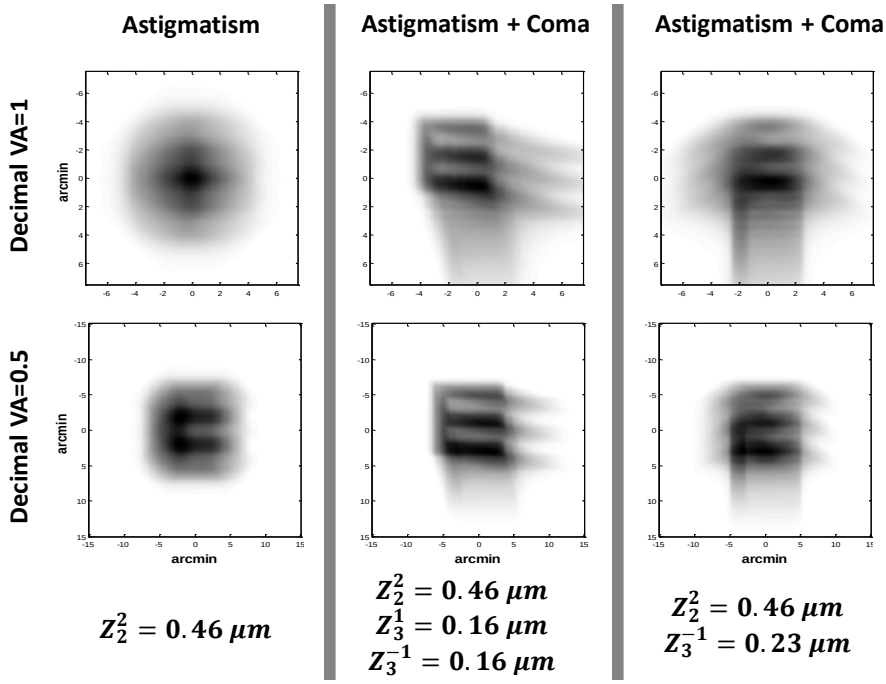

Figure 1.9. Simulated visual acuity of 5 arcmin (upper row) and 10 arcmin (lower row) based on convolution. Left panels: 0.46 μm of astigmatism at 0 degrees. Center panels: 0.46 μm of astigmatism at 0 degrees with 0.23 μm of coma at 45 degrees. Right panels: 0.46 μm of astigmatism at 0 degrees with 0.23 μm of coma at 90 degrees.

1.5. Vision under manipulated optics

Adaptive optics is an excellent tool to manipulate the optics of the subject´s eye. Early experiments using adaptive optics were aimed at exploring the limits of vision under full correction of aberrations. Liang et al. showed dramatic improvements in contrast sensitivity even at 55 cpd a spatial frequency that is close to the Nyquist limit of the eye (60 cpd)[14]. This benefit of adaptive optics correction has been reported in several studies since then[16,19-21]. In particular, results from our lab have shown that this benefit of AO correction holds over a large range of luminance levels and polarities [22]. Studies from our lab have also shown that correcting aberrations increases the perception of sharpness and even has been shown to improve the performance in everyday tasks such as face recognition [23]. On the other hand, it has been shown that inducing aberrations, in general, produce a decrease on visual function at best focus but to expand the range of acceptable vision through focus [24-27]. In chapters 3, 4 and 5 we show how selectively induced or corrected aberrations modify the visual function [28-30]. In the previous section we have shown how interactions between aberrations can critically affect retinal image quality (figures 1.8 and 1.9).

Adaptive optics is an excellent tool for testing the behavior of different multifocal patterns in a fast and non-invasive procedure. There are many studies that have evaluated the performance of presbyopic patients through focus under manipulated optics. One of the most frequent choices for increasing the depth of focus is spherical aberration [31,32]. Figure 1.10 shows letters of 10 arcmin through focus from -1.8 D to 1.8 D for three different conditions, all aberrations corrected (upper row), a pattern of spherical aberration (middle row) and a pattern with two different optical zones with coma and astigmatism of opposite signs (lower row).

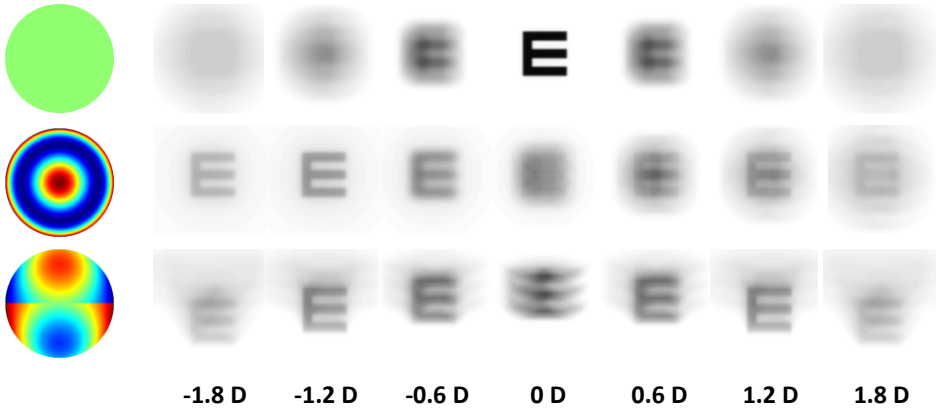

Figure 1.10. Letters of 10 arcmin through focus from -1.8 D to 1.8 D for three different conditions, all aberrations corrected (upper row), a pattern of spherical aberration (middle row) and a pattern with astigmatism and coma of opposite signs in two halves of a segmented pupil, similar to those studied in chapter 7 of this thesis (lower row). The column in the left show the phase pattern that yield the through focus performance shown by the different letters.

The condition depicted in the last row of figure 1.10 cannot be experimentally simulated with a class c system of adaptive optics technology (see figure 1.5) because the continuous-mirrored surface is not capable of simulating surface discontinuities. Liquid crystal spatial light modulators that work in a similar fashion to the type b of the AO technologies shown in figure 1.5 (but that induce changes in the index of refraction of the material rather than displacing the mirrors) allow to test solutions with steep local changes. In our lab a new system is being developed with this type of AO technology (PLUTO, HoloEye) for allowing the experimental testing of phase maps with steep changes on their profile.

1.6. Accommodation and presbyopia

The human visual system has the ability to focus light onto the retina from objects at different distances. This is possible due to a mechanism known as accommodation. The amplitude of accommodation is defined as the difference of the vergence of and object at far (0 D) and the vergence of the nearest point that the patient is able to focus. This amplitude is generally around 15 D at 10-12 years of age and starts to decline progressively reaching 0 D by the age of 55 or 60 years. By 40 years of age, the amplitude of accommodation is reduced to around 6 D, and problems with near work arise.

1.7. Presbyopia correction

Presbyopia is a condition with a prevalence of 100% for subjects older than 45 years of age. It is characterized by a loss of accommodation amplitude that prevents from focusing on near objects during extended periods of time. By the age of 45, the amplitude of accommodation already has been reduced to around 6 diopters. Therefore it is no longer possible to perform activities that require near vision for long periods of time without feeling headaches or congestion around the eyes.

Due to presbyopia, the optical power of the eye can no longer be increased. Near objects reach the eye with a vergence greater than zero and are therefore focused behind the retina. In order to correct presbyopia we need and optical aid that is capable of forming the image of a near object into the retina. Therefore the easiest solution is to place a positive lens in front of the eye (reading glasses). Figure 1.12 illustrates a presbyopic subject with a blurred image at his retinal plane and the corresponding case where presbyopic subject is corrected with a pair of reading glasses.

Unfortunately this solution does not allow sharp vision at different near working distances and also introduces blur for objects placed at far (having to remove the glasses to see far). During the next section of this chapter we will review some of the current solutions for presbyopia that aim to correct near vision at the same time that allow and easy transition to far vision.

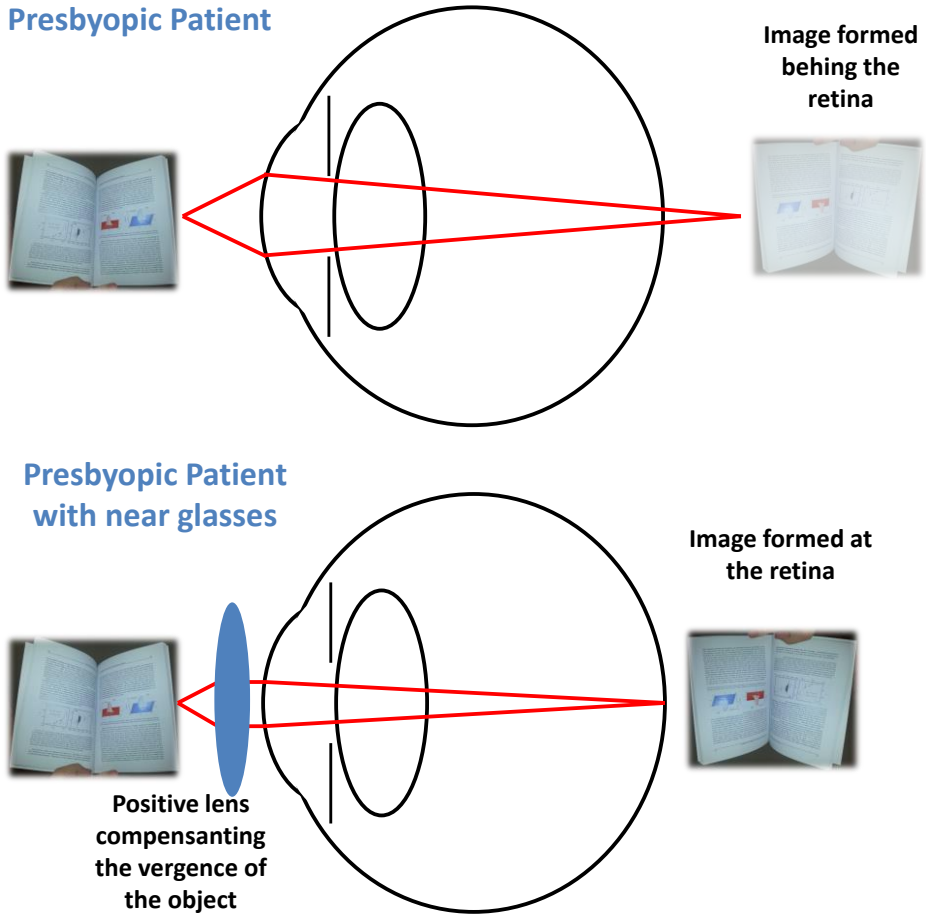

Figure 1.12. Scheme of the situation of a presbyopic patient (upper graph) and of a presbyopic patient corrected with near glasses (bottom graph).

1.8. Current solutions for presbyopia

As it is been shown in the previous section it is relatively easy to implement a partial solution for presbyopia. On the other hand, a complete solution is far from being developed. A more sophisticated method for total recovery of accommodation is lens capsule refilling[33]. Or accommodative intraocular lenses that aim to use the functional structures of the accommodative plant in presbyopic patients in order to produce changes in an intraocular lens that will in turn mimic the change in optical power that occurs during natural accommodation in non presbyopic subjects.

Currently available solutions for presbyopia are based on one of three principles: alternating vision, monovision and simultaneous vision. Some of the optical corrections available that rely on alternating vision are bifocal/progressive lenses (where changes in gaze or head position allow selection of the zone of the spectacle used to view near or far objects) [34] or translating contact lenses (where the lens, typically gas permeable, moves upwards on the eye during downward gaze during near viewing) [35]. In monovision, one eye is corrected for distance while the other for near. Monovision solutions are commonly applied in the form of corneal, intraocular lens or contact lens treatments [36]. An increasingly popular class of treatments for presbyopia relies on simultaneous vision designs where the eye is simultaneously corrected for both distance and near vision [37,38]. Bifocal solutions generally come in the form of refractive contact lenses, and diffractive or refractive intraocular lenses. Figure 1.13 shows examples of the different solutions current available for presbyopia. Alternating vision techniques include bifocal and progressive lenses (left column). Simultaneous vision can be implemented in contact or intraocular lenses and in laser guided operations (central column). Monovision techniques involve both eyes independently optimized for different distances; they are usually prescribed in the form of contact lenses, intraocular lenses or laser guided operations (right column).

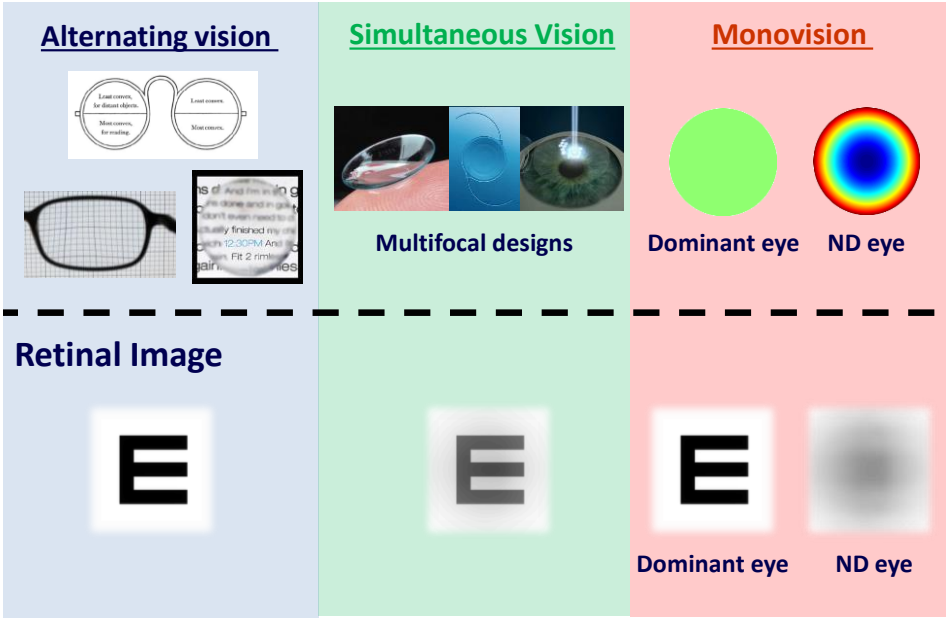

Figure 1.13. Scheme of the three principal approaches for correcting presbyopia. Alternating vision techniques include bifocal and progressive lenses (left column). Simultaneous vision can be implemented in contact or intraocular lenses and in laser guided operations (central column). Monovision techniques involve the two eyes being optimized individually for different distances; they are usually prescribed in the form of contact lenses, intraocular lenses or laser guided operations (right column). Lower row represent the optical image present at the retinal plane for each type of solution.

Simultaneous vision represents a new visual experience in which a sharp image is superimposed to a blurred replica of the same image, thus reducing the overall contrast. Our work extends upon the understanding of this type of correction since little is known about how such an image is processed by the visual system. In chapter 7, we show the correspondence of the changes in the contrast of targets imagined with a camera and the changes in the Visual Acuity reported by subjects under simultaneous vision conditions. The add-power for near vision typically ranges from 1 to 4D [39]. In chapter 7, we report how different levels of addition affect visual performance.

Also the intended optical effect of the correction according to design is combined with the particular aberrations present in the particular eye, so a given bifocal design does not produce the same optical through-focus energy distributions in all eyes. In chapter 7, the variability of fourteen different bifocal designs over a population of 100 subjects is reported.

1.9. Multifocal correction of presbyopia

We can distribute the total amount of light passing through the pupil so that fixed amounts of it will be focused at different planes lying either before or at the retinal plane. At any given moment without changing anything we could see objects located at different distances. This type of correction can be achieved with either refractive or diffractive lenses. The basic rationale of using aberrations to extend the depth of focus is shown in figure 1.14. Figure 1.15 shows the VSOTF obtained as a function of the vergence of the object for a trifocal correction (left graph), the inset represents the phase pattern of a trifocal correction where the zones have been divided angularly. Different objects that require different working distances will use mostly the quality of the image provided by the multifocal correction for that distance. Therefore, when looking at landscapes we would primarily use the red zone, for faces the green zone, for computers the blue zone, and for reading the purple area. The right part of figure 1.15 shows a schematic representation of where the different objects will be placed on each of the situations (i.e. where 25% of the energy will be in focus or close to it for reading 75% of the energy will be out of focus). Boxes on the right graph can be taken as the total amount of energy, and the part occupied but each of the graphs can be considered roughly as the portion of the total energy of use for each distance.

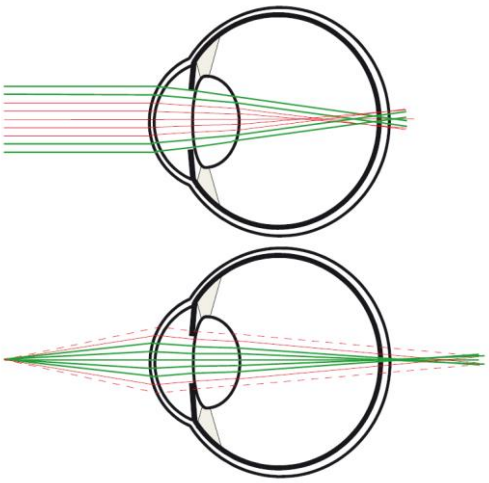

Figure 1.14 Schematic representation of an eye with spherical aberration focusing a far object (upper graph) and a near object (bottom graph). This illustration offers rough explanation of using aberrations for the extension of the depth of field. Image taken from an article of Austin Roorda in Journal of Vision [40].

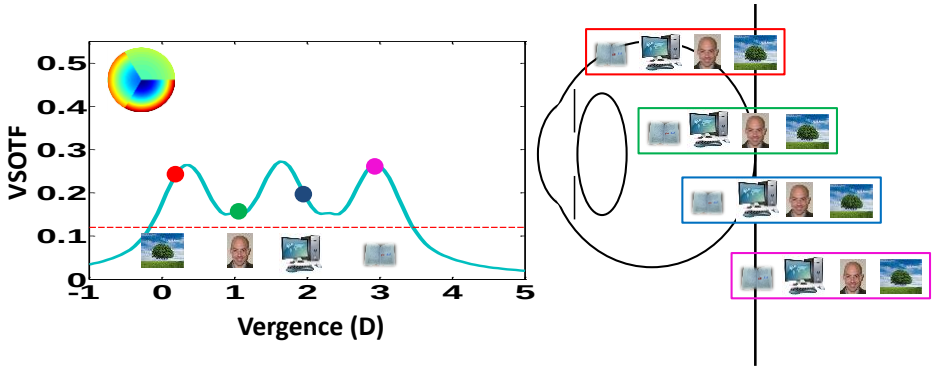

Figure 1.15. Illustrates VSOTF obtained as a function of the vergence of the object for a trifocal correction (left), the inset in the left graph represents the phase pattern of a trifocal correction where the zones have been divided angularly. Different objects that require different working distances will use mostly the quality of the image provided by the multifocal correction for that distance. On the right, a schematic representation of where the different objects will be placed for each case is shown (i.e. where at reading distance roughly 25% of the energy will be in or close to focus while the rest will be out of focus). Boxes on the right graph can be taken as the total amount of energy, and the part occupied but each of the graphs can be considered roughly as the portion of the total energy of use for each distance.

Independently of the type of solution used, there will always be part of the energy focused at the retinal plane and part of it out of focus. The focused image of the object we are looking at will be superimposed by a defocused image of the same scene. What will lead to a loss of contrast in the final optical image formed at the retinal plane. Figure 1.16 shows and illustration of the retinal image obtained with bifocal corrections with different levels of addition.

Figure 1.16. Images of E-letters formed at the retina under simultaneous vision conditions with a bifocal correction as a function of the value of the addition.

During chapters 6, 7 and 8 we will explore the visual performance obtained with bifocal/multifocal corrections.

1.10. Open questions addressed in this thesis

Interactions between aberrations without radial symmetry. A deep knowledge about the interactions between aberrations is still far for being completed and even more so when taken into account through focus performance. Astigmatism and coma do interact favorably and adding one to the other under certain conditions improves the final optical quality of the solution (see chapter 3). Also to be discussed in chapter 7, they form a good base for adding other aberrations and expand the multifocality of a correction.

Interactions between the aberrations of a new correction and the previous visual experience of the subject. Typically when prescribing a new multifocal correction the previous visual experience of the subject is not taken into account. As it is shown in chapter 4 of this thesis, when subjects have been exposed to a certain level of astigmatism adding coma does not actually improve its visual performance, revealing that the subject´s previous experience plays an important role in the outcome of a new multifocal solution.

The extent to which corrections in the optical quality of the eye with adaptive optics systems and the improvement obtained in visual performance is not clear. Previous studies suggested that the improvement in visual performance correlate linearly with the improvement of optical performance. However, as shown in chapter 5 the improvement in contrast sensitivity is lower than that predicted from optics and it is meridional dependent. Investigating contrast sensitivity under fully correcting optics at different axes will give insights in the spatial limits of vision.

Development of a new optical instrument for a fast and reliable method for testing bifocal corrections. Testing bifocal corrections in subjects is done today by testing different models of contact lenses in subjects, but the development of our new simultaneous vision simulator allows for new bifocal designs to be tested in a non-invasive, fast and reliable way. Also, new insights into bifocal simultaneous vision are allowed (see chapters 6 and 8).

Improvement of current multifocal solutions. Although the current solutions in the market for presbyopia cover a wide range, there is almost no systematic scientific information available to which one could offer the best optical performance. Our work aims to clarify which designs should be used or

avoided. The implications of this work could rapidly affect contact lens design, intraocular lens design and the ablation profiles applied to refractive surgery technics (see chapter 7).

1.11. Hypothesis

It is possible by developing new computational and experimental tools for the evaluation of the performance of the current presbyopic solutions: to gain insights in the interactions of aberrations within an optical correction, to increase the Knowledge about the optical improvement generated by AO systems and to evaluate the interaction between the multifocal optical solutions and the previous visual experience of the subject and to apply it to the development of new improved solutions for presbyopia.

1.12. Structure of the thesis

This thesis is composed by the following chapters:

Chapter 1

This chapter starts with a brief introduction about the major concepts used in this thesis (e.g. how a SH aberrometer measures the wavefront of an eye, how Zernike polynomials are used to describe a wavefront, what are the lower and higher order optical aberrations and how they can be modified with a deformable mirror). Furthermore, it is presented how accommodation works, how with age presbyopia appears and finally which are the main techniques for the correction of presbyopia. Finally the open questions addressed in this thesis for trying to improve multifocal corrections for presbyopia are presented.

Chapter 2

Various optical systems used and developed during this thesis are presented. Two different adaptive optics systems have been used, the one located at the Viobio lab at the Institute of Optics in Madrid and the one placed at the Queensland University of Technology in Brisbane in David Atchison´s lab. Also a new system envisioned and developed during this thesis is presented. It is a

simultaneous vision simulator that can in its second generation reproduce any refractive bifocal correction that we could think off. Also the basic function of a spatial light modulator is shown. After that the algorithms for the simulation of multifocal corrections and its evaluation with different metrics are presented.

Chapter 3

In this chapter we demonstrate that certain combinations of non-rotationally symmetric aberrations (e.g. coma and astigmatism) can improve retinal image quality beyond the condition with the same amount of astigmatism alone. Simulations of the retinal image quality in terms of Strehl Ratio, and measurements of visual acuity under controlled aberrations with adaptive optics are shown under various amounts of defocus, astigmatism and coma. The amount of coma producing best retinal image quality was computed and the amount was found to be different from zero in all cases (except for 0 D of astigmatism). The improvement holds over a range of >1.5 D of defocus. Measurements of VA under corrected high order aberrations, astigmatism alone (0.5 D) and astigmatism in combination with coma (0.23 μm), are presented with and without adaptive optics correction of all the other aberrations, in two subjects. Finally, we show how the combination of coma with astigmatism improved decimal VA by a factor of 1.28 (28%) and 1.47 (47%) in both subjects, over VA with astigmatism alone when all the rest of aberrations were corrected.

Chapter 4

Following the theoretical and empirical results from the previous chapter, we extended the VA test of these theoretical predictions to 20 patients. In this chapter, it is shown how adding coma (0.23 μm for 6-mm pupil) to astigmatism (0.5 D) resulted in a clear increase of VA in 6 subjects, consistently with theoretical optical predictions, while VA decreased when coma was added to astigmatism in 7 subjects. In addition, in the presence of astigmatism only, VA decreased more than 10% with respect to all aberrations corrected in 13 subjects, while VA was practically insensitive to the addition of astigmatism in 4 subjects. Finally it is described how the effects were related to the presence of natural astigmatism and whether this was habitually corrected or uncorrected. The fact that the expected performance occurs mainly in eyes

with no natural astigmatism suggested relevant neural adaptation effects in eyes normally exposed to astigmatic blur.

Chapter 5

After this initial works that included theoretical simulations and experimental measurements in subjects we wanted to get a better idea of how improvements in terms of the modulation transfer function (when optical aberrations are corrected with AO technology) will translate to visual performance in terms of the contrast sensitivity function. Since correcting the aberrations of the eye produces large increases in retinal image contrast and the corresponding improvement factors in the contrast sensitivity function had been rarely explored and the results were controversial. In this chapter, we present the CSF of 4 subjects with and without correcting monochromatic aberrations. The MTF increased on average by 8 times and meridional changes in improvement were associated to individual meridional changes in the natural MTF. CSF increased on average by 1.35 times (only for the mid and high spatial frequencies) and was lower (0.93 times) for polychromatic light. The consistently lower benefit in the CSF than in the MTF of correcting aberrations suggested a significant role for the neural transfer function in the limit of contrast perception.

Chapter 6

A prototype of an optical instrument that allows experimental simulation of pure bifocal vision is presented, validated and used to evaluate the influence of different power additions on image contrast and visual acuity. The instrument provides the eye with two superimposed images, aligned and with the same magnification, but with different defocus states. Subjects looking through the instrument are able to experience pure simultaneous vision, with adjustable refractive correction and addition power. The instrument is used to investigate the impact of the amount of addition of an ideal bifocal simultaneous vision correction, both on image contrast and on visual performance. The instrument is validated through computer simulations of the letter contrast and by equivalent optical experiments with an artificial eye (camera). Visual acuity measurements in four subjects for low and high contrast letters and different amounts of addition are presented. The largest degradation in contrast and visual acuity (~25%) occurred for additions around ~2 D, while additions of ~4 D produced lower degradation (14%). Low

additions (1– 2 D) result in lower VA than high additions (3–4 D). Simultaneous vision induces a pattern of visual performance degradation, which is well predicted by the degradation found in image quality. Neural effects, claimed to be crucial in the patients' tolerance of simultaneous vision, can therefore be compared with pure optical effects.

Chapter 7

In this chapter new multifocal phase designs aiming at expanding depth-of-focus in the presbyopic eye are presented. The designs are based on multiple (up to 50), radial or angular zones of different focus or of combined low and high order aberrations. Multifocal performance is evaluated in terms of the dioptric range for which the optical quality is above a threshold and of the area under the through-focus optical quality curves. The best designs were found for a maximum of 3-4 zone designs. Angular zone designs were significantly better than radial zone designs with identical number of zones with the same levels of addition. The optimal design (angular design with 3 zones) surpassed multifocal performance of a bifocal angular zone and of the typical design based on induced spherical aberration. It is also shown that by using combinations of low and high order aberrations, the through focus range can be extended up to 0.5 D above the best design with only defocus. These designs can be implemented in Adaptive Optics systems for experimental simulation of visual performance in subjects and transferred into multifocal contact lens, intraocular lens surfaces or presbyopic corneal laser ablation profiles. Also fourteen different bifocal patterns at three working distances far, intermediate (66 cm) and near (25 cm) are evaluated. Results are presented for simulations and for measurements in 5 subjects. In order to try experimentally the fourteen bifocal designs, a new bifocal system that allows for complete control of the pupil by using a Spatial Light Modulator was developed. Of the 14 designs tested the best performance without any other aberrations is for designs that only have 2 zones regardless of the division being horizontal or vertical (designs 1-4). All the other designs (10) show lower levels of optical performance in absence of any other optical aberrations. This advantage of 2-zone designs (Oculentis M-plus fashioned) holds when the optical aberrations of a real population of subjects (100) are taken into account. In the other hand the performance of individual subjects with each of the designs is more variable for designs of 2 zones divided horizontally or vertically than when divided radially or when more

zones are applied. The wavefronts of the best and worse subjects for 2 zone designs are clearly dominated by coma in all cases (for the three working distances). Experimental results in 5 subjects show that 2 radially segmented designs offer overall better optical properties than circularly segmented or multi-zone designs.

Chapter-2 Methods

2.1. Adaptive Optics systems for correction and induction of aberrations

In this thesis, two different adaptive optics (AO) systems have been employed. The VioBio Lab AO system is been used in work presented in chapters 3, 4 and 8. The QUT AO system was used in the work presented in chapter 5. Both systems were functional prior to work covered in this thesis. The VioBio AO had been used in different studies in the lab prior to this thesis, including the effect of correcting the aberrations on visual acuity, on the perception of natural images, and on face recognition, as well as the influence of the correction and induction of aberrations over accommodative lag[22,41,42]. In addition, the system has been used in a set of studies of neural adaptation to blur produced by astigmatism and high order aberrations and their correction and of the internal code for blur [28,29,43-46].

The QUT AO system has also been extensively used mostly centered in establishing the limits of tolerance of blur for astigmatism, defocus and higher order aberrations[25,47-50].

2.1.1 VIOBIO Lab AO-Adaptive Optics System

The VIOBIO Lab AO system can be seen in figure 2.1. The primary components of the system are a Shack-Hartmann (SH) wavefront sensor (42 x 32 microlenses, 3.6- mm effective diameter and a CCD camera (HASO 32 OEM, Imagine Eyes, France)) and an electromagnetic deformable mirror (MIRAO, Imagine Eyes, France) with 52 actuators and a 15-mm effective diameter. The measuring branch is shown in red whereas the two psychophysical channels are shown in white.

Illumination is provided by a super luminescent diode (SLD) coupled to an optical fiber (Superlum, Ireland) emitting at 827 nm. A 12 x 9 mm SVGA OLED minidisplay (LiteEye 400) is used to create high-contrast targets. The minidisplay has a nominal luminance of 100 cd/m^2, with a black level <0.2 cd/m^2 (as calibrated using a ColorCal luminance meter/ colorimeter, Cambridge Research Systems). A Badal system (mounted on a motorized

stage) compensates for spherical error. A pupil monitoring channel, consisting of a CCD camera (TELI, Toshiba) conjugate to the pupil, is inserted in the system by means of a plate beam-splitter and is collinear with the optical axis of the imaging channel.

The Hartmann–Shack system, deformable mirror and closed-loop correction are controlled with custom software in C++ specifically designed for the studies shown in chapters 3 and 4. This software will be explained in detail in the next section of this chapter. The program controls the generation and error measurement of the mirror states and the Badal system. It also controls a subroutine to perform the VA measurements programmed in Matlab.

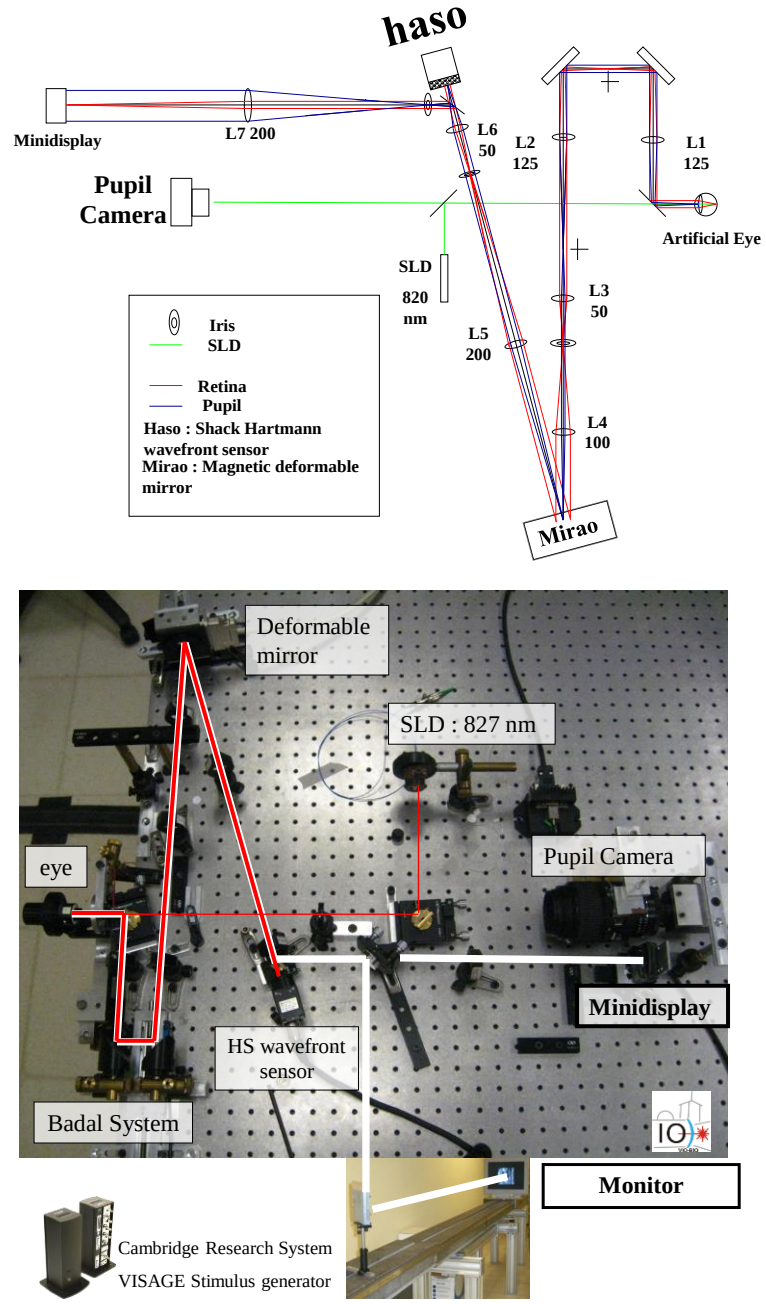

Figure 2.1. Set-up of the VIOBIO Lab Adaptive Optics system (upper graph scheme, lower graph image) which main elements are an Imagine eyes deformable mirror 52-e and a Hartman shack wavefront sensor. The lower image has two different psychophysical channels labeled in white. For the purposes of this thesis only the psychophysical channel with the minidisplay was used.

2.1.2 Software implementations for experimental control

Customized software was developed for controlling our adaptive optics system (C++ based). This software allows a fast and reliable control of the experiment performing 12 measuring/correction iterations per second. Figure 2.2 shows the final control panel of the software used for the works presented in chapters 3 and 4. Parts of the software implemented specifically for this works are outlined in red. This software allows introducing any amount and direction of coma and astigmatism desired. It also has the capability to communicate with Matlab for synchronizing the measurements of optical quality with the visual acuity tests performed on the subjects.

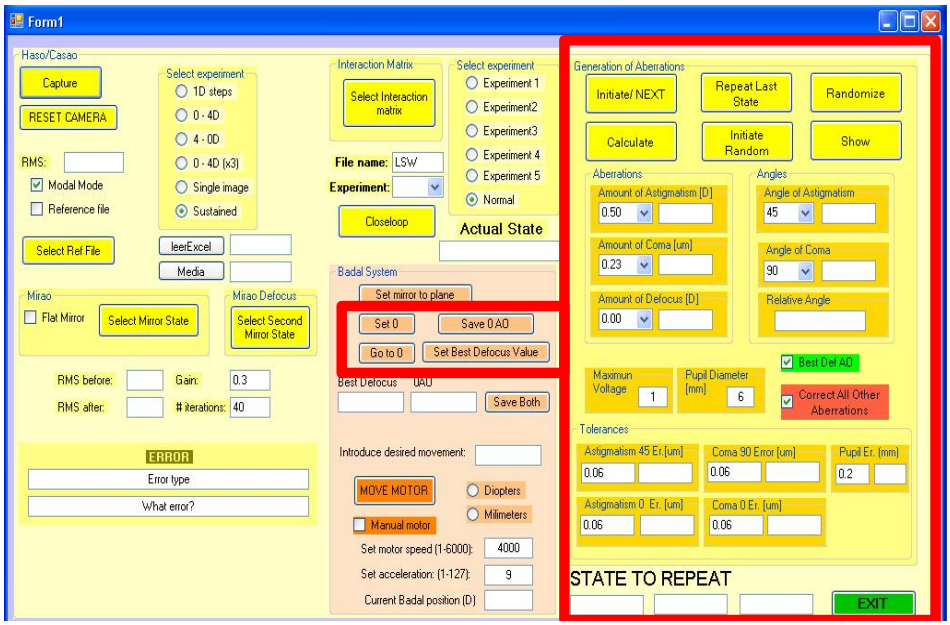

Figure 2.2. Control panel of the VIOBIO lab adaptive optics system. Outlined in red are features developed specifically for the studies shown in chapters 3 and 4.

Another software was also implemented for calibrating purposes, aiming at studying experimentally the optical effect of modifying the aberrations on an image, independently of neural effects. These routines allowed the simultaneous control of the AO system (including the Badal system), a Visage system (Cambridge Research Systems, UK) for the presentation of images and a scientific CCD camera (Retiga 1300, 16 bits; Qimaging, Surrey, BC, Canada) with a 100- mm - f/3.5 camera lens (Cosina, Nakano, Nagano Prefecture,

Japan) which acted as an the "retina" of an artificial eye. This system allowed automatizing the presentation of images in the screen, the creation of different mirror states and the capture of images through these modified optics for different Badal positions. An image of this software's control panel can be seen in figure 2.3.

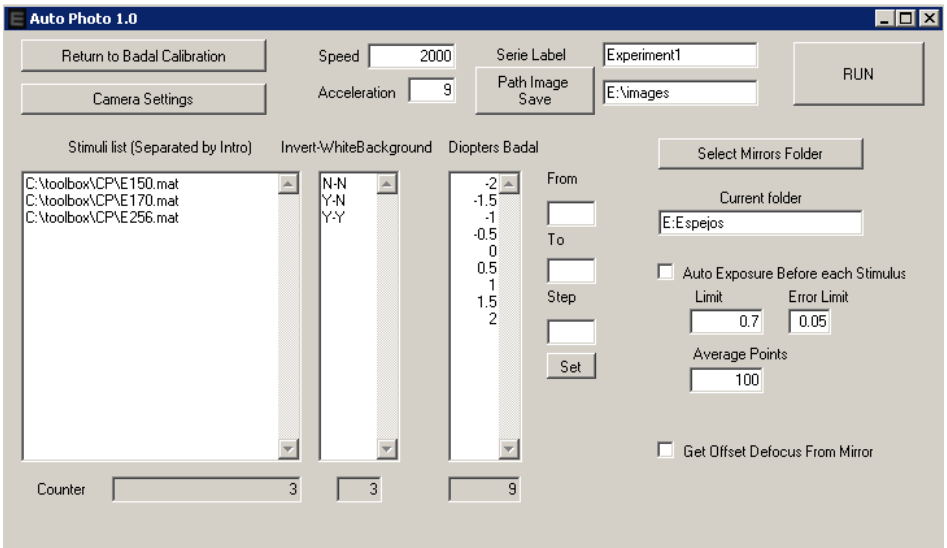

Figure 2.3. Control panel of the software developed for controlling the AO system, the Visage software displaying images and the Retiga 1300 for the registration of images.

The artificial eye consisted of the mentioned digital CCD camera and a photographic objective lens (Cosina 100 mm f/3.5). The artificial eye was mounted on a 3-D micrometer stage at the exit pupil of the system, and aligned with its optical axis. Best focus was obtained by achieving maximum contrast for 5 cpd sinusoidal images displayed on the CRT and projected on the CCD through the optical system and the camera lens, while varying the Badal optometer in 0.05 D steps. The AO mirror was set to correct all the aberrations of the optical system and that of the camera lens. The RMS of the residual aberrations was always less than 0.03 µm for a 6-mm pupil diameter.

Images of the sinusoidal gratings at nine different spatial frequencies (2.5, 5, 10, 15, 20, 25, 30, 35 and 40 cpd) projected on the CRT monitor were obtained on the CCD camera of the artificial eye for two different conditions: (1) Images of degraded gratings (achieved by convolving with the PSF obtained from real subjects' aberrations at best focus) for best AO-correction at zero focus; (2) Images of maximum contrast gratings for a mirror state inducing the

aberrations of the subject. In this latter condition, the Badal optometer was set to the defocus position that maximized the VSOTF for each set of aberrations. The Michelson contrast of the images captured by the CCD camera in each condition was calculated after removing the background, and used to estimate the MTF of the optical system, and to compare the contrast degradation produced by real aberrations (generated on the mirror) or by convolution with the same set of aberrations. Figure 2.4 compares the experimental and computationally simulated MTF for different aberration patterns (corresponding to 4 real subjects) reproduced by the AO mirror.

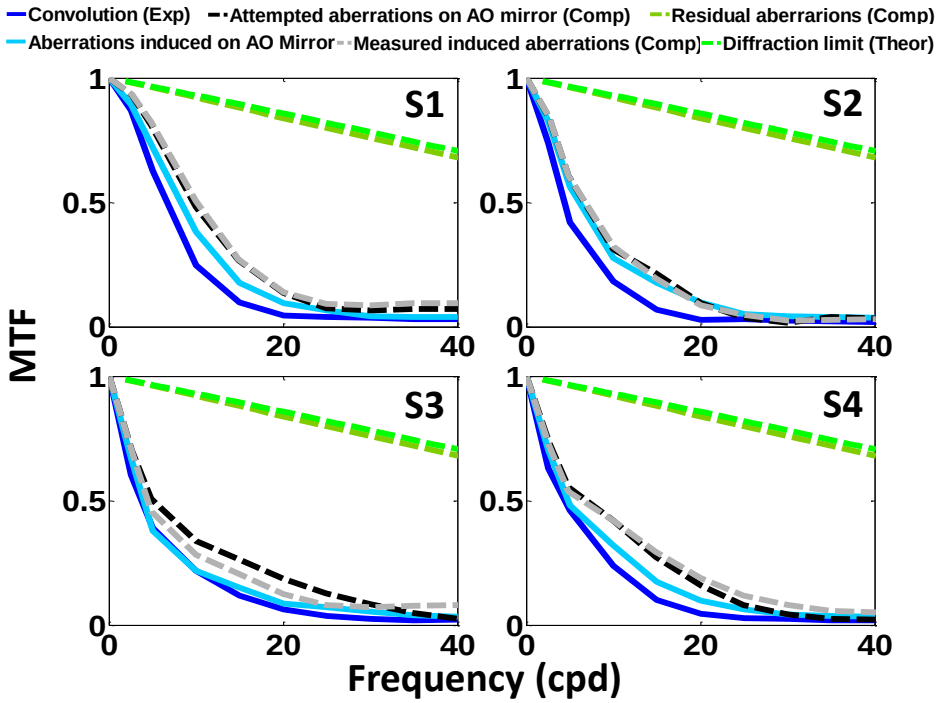

Figure 2.4 Computed (dashed lines) and experimental (solid lines) MTFs for different aberration patterns (corresponding to the 4 subjects shown in section 1.2.1). MTFs from the Michelson contrast of high contrast sinusoidal fringes projected through the AO mirror inducing aberrations (light blue lines). MTFs from the Michelson contrast of sinusoidal fringes convolved by the same set of aberrations, under full AO correction of aberrations (dark blue lines). Theoretical MTFs for the corresponding measured aberrations (gray dashed lines). Theoretical MTFs for the aberrations actually set in the AO mirror (black dashed lines). Diffraction-limited MTF (light green dashed lines). MTFs for the residuals of the full AO correction (dark green dashed line). Data are for 6 mm pupils.

2.1.3 QUT AO-Adaptive Optics System

The study presented in chapter 5 was conducted in Prof. David Atchison´s lab at the Queensland University of Technology at the end of 2010. A custom-developed AO system was used in the study to correct and induce selected aberrations. The system has been described in detail in several publications [30,47,48]. For the study of this thesis the OLED display was replaced by a projector (Epson EMP 1810 multi-media projector) and a high resolution rear projection screen (Novix Systems, Praxino rear projection screen) placed at a distance of 3 m. In brief, the main components of the system are a SH wavefront sensor (composed by 42 x 32 microlenses of which 415 were used to measure our 5.2-mm pupils, with 15-mm effective diameter and a CCD camera; HASO 32 OEM, Imagine Eyes, France) and an electromagnetic deformable mirror (MIRAO 52d, Imagine Eyes, France). The desired mirror states were achieved in closed-loop. Visual stimuli were presented by the gamma-corrected projector on the rear projection screen, viewed through the AO mirror, and a Badal system. The stimuli were Gabor patches (standard deviation: 0.66 deg). The generation of stimuli was controlled by a Cambridge Research Systems VSG card. The mean luminance at the pupil plane was 50 cd/m^2 and the total magnification of the system was x 0.5. A schematic representation of the system and a photo are presented in figure 2.5.

QUT Lab Adaptive Optics System

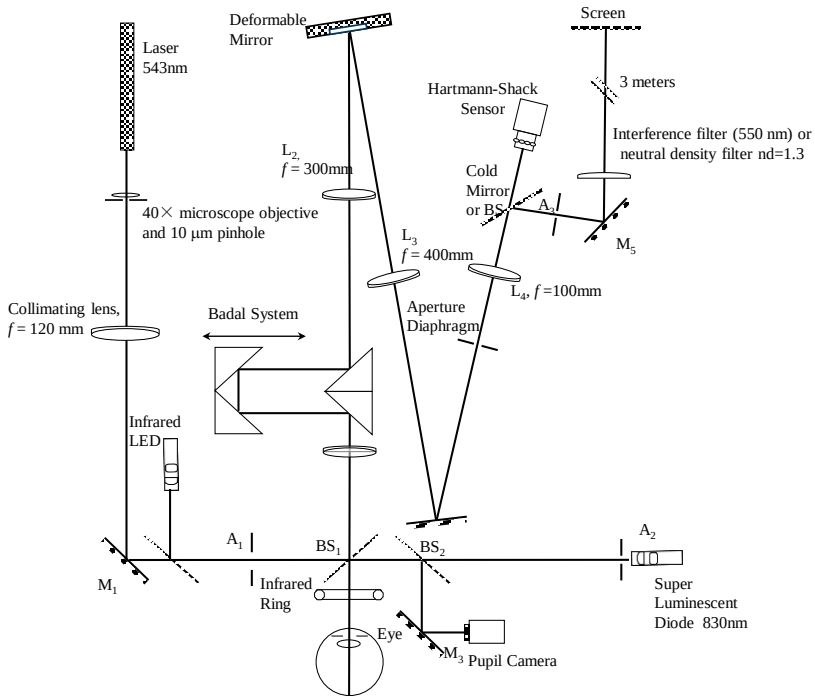

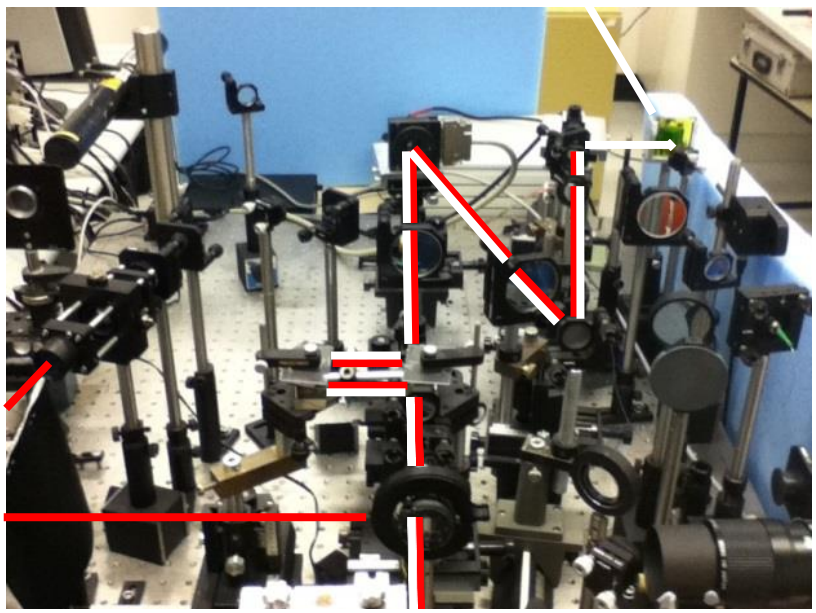

Figure 2.5. Schematic diagram of the QUT lab adaptive optics system (upper graph) and an accompanying photo. The lower image has two a psychophysical channel labeled in white anda measuring channel labeled in red.

2.2. Simultaneous Vision System

2.2.1 Simultaneous Vision System 1.0

Deformable-mirror based AO systems are excellent tools for correcting and manipulating optical aberrations, but the continuous mirror surface is not capable of reproducing discontinuities in the wavefront. This is relevant because many of the current solutions for presbyopia rely on dividing the pupil into multiple zones whether it would be to achieve multifocality via diffractive kinoforms or simply varying the power across the pupil. Therefore a simultaneous vision system capable of introducing discontinuities in the wavefront was designed and implemented during the course of this thesis [51]. Figure 2.6 shows and schematic representation and a photo of the first version of the system used for the work presented in chapter 6.

A schematic illustration of how this system manages to reproduce simultaneous vision in comparison with the one provided by a bifocal contact lens is shown in figure 2.7. For far vision, the bifocal contact lens produces a sharp image of the far object, superimposed to a defocused near vision image (Fig. 2.7.A). For near vision, the bifocal contact lens produces a sharp image of the near object, superimposed to a defocused far vision image (Fig. 2.7.B). Conversely, the simultaneous vision simulator produces a myopic defocus (positive dioptric correction, which mimics a near addition) by channel 2, and a far sharp image in channel 1, allowing testing of the impact of a near addition on far vision (Fig. 2.7.C). Also, a hyperopic defocus (negative dioptric correction) in channel 2 allows testing the impact of a defocused far image (Fig. 2.7.D).

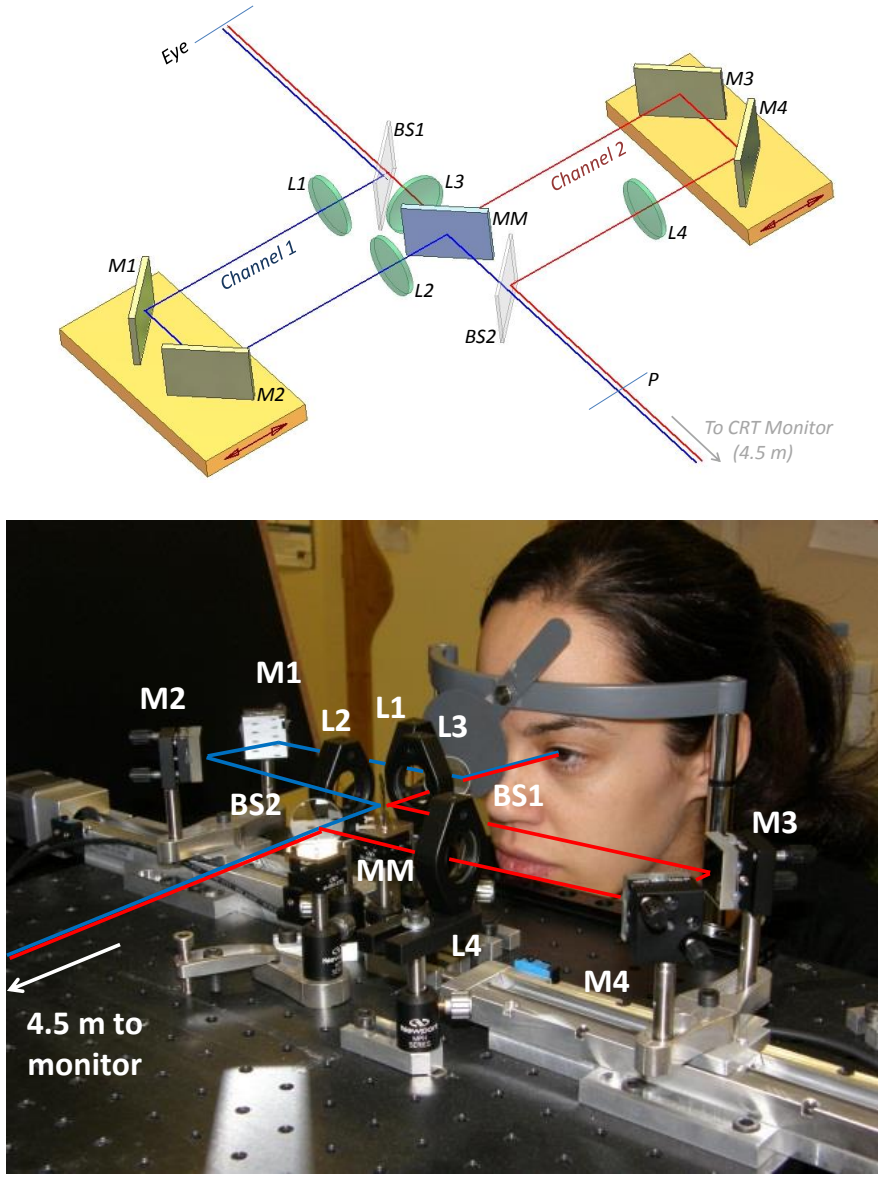

Figure 2.6 First version of the simultaneous vision system. Schematic diagram of the Simultaneous Vision System (upper graph) and a photo of the system (lower graph). Light from a CRT monitor is separated into two channels by means of a beamsplitter (BS2) and recombined by means of a double mirror (MM) and a second beamsplitter (BS1). Each channel consists of an independent Badal Optometer (composed by two lenses of 150 mm focal lengths and two mirrors mounted on a motorized moving stage). Channel 1 (blue line) is typically focused at far (subject's distance prescription) and Channel 2 (red line) moves to simulate near additions. An artificial pupil (P) limits the natural pupil size (4 mm in this study). The two channels (illustrated with red and blue lines slightly separated) are perfectly coincident in the real set-up between the monitor and BS2, and between BS2 and the eye.

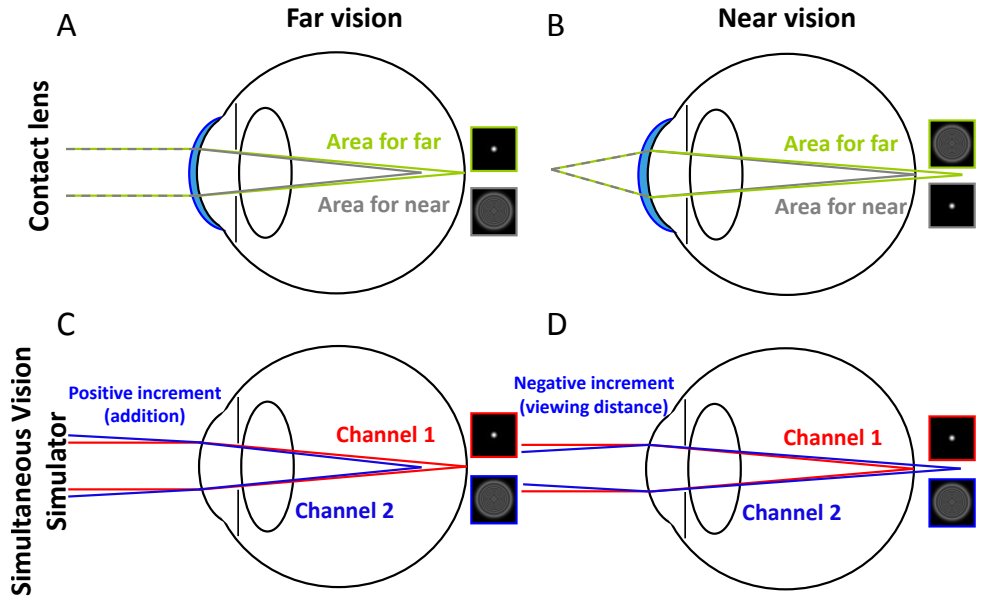

Figure 2.7. Schematic diagram of the near and far vision conditions produced by a bifocal intraocular (A, B) and those simulated in our study (C, D). PSFs and surrounding boxes represent the image projected in the retina by the rays with the corresponding color/line style.

2.2.2 Software implementations for experimental control of the simultaneous vision system

Dedicated software was developed to automatically control the system for experiments on subjects, as well as for validations using an artificial eye provided with a CCD as a retina, similar to that described in de Gracia et al. [52]. The software controls the Badal systems, the Visage system for the presentation of targets and a scientific CCD camera. An image of the control panel of the program is shown in figure 2.8.

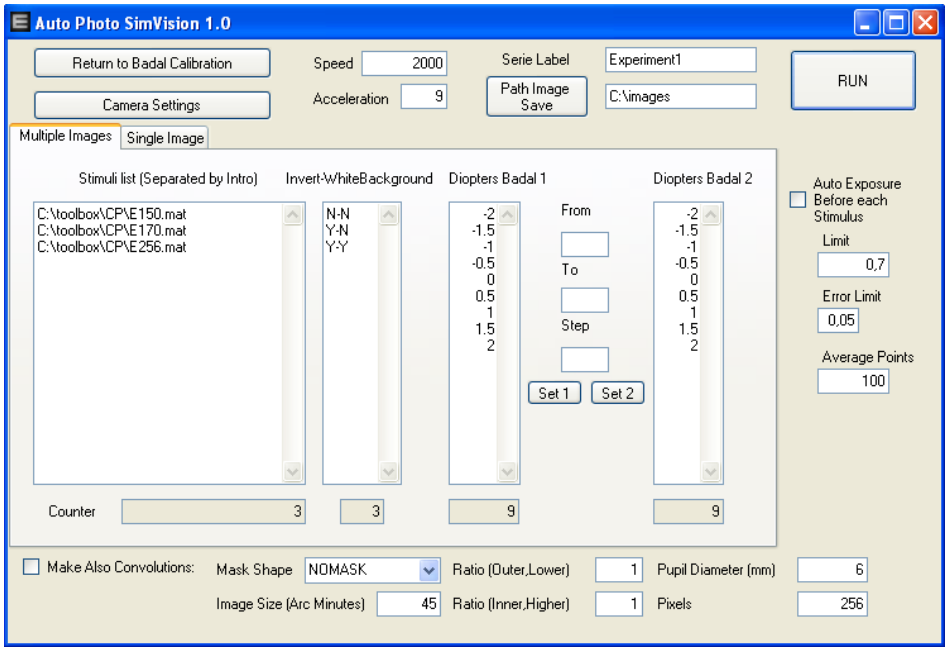

Figure 2.8. Control panel of the software to operate the simultaneous vision system. It allows for automating the capture of images of different targets through the system with different levels of defocus introduced by the two badal systems.

The calibrations performed compared the loss of contrast produced in convolved targets under simultaneous vision with the loss of contrast obtained experimentally in images taken through the system under the same conditions. The results are discussed in chapter 6. For illustrative purposes one condition of the calibrations is shown in figure 2.9. Computations of contrast through convolved images and images taken through the system show a great level of agreement.

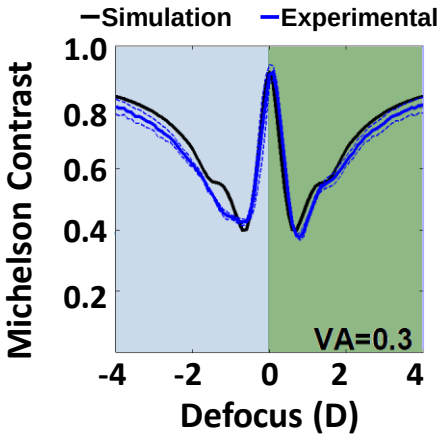

Figure 2.9. Comparison of the Michelson contrast obtained with computer simulations (black lines) and with the artificial imaging system (blue lines) as a function of the amount of addition. For a letter size corresponding to a VA of 0.3. Positive defocus (shaded green) represents far vision in focus in presence of a near defocused image (due to the addition). Negative defocus (shaded blue) represents near vision in focus (at different distances) in presence of a far defocused image. Data are for 4-mm pupils.

2.2.3 Simultaneous Vision System 2.0

Many of the current solutions for presbyopia rely in the division of the pupil for their use at different distances. The initial version of the simultaneous vision system did not allow selecting different areas of the pupil for different additions but rather used the whole pupil for both corrections (similar to diffractive designs). Therefore in order to reproduce refractive designs in which different areas of the pupil are used for different distances 3 new elements where introduced into the system: a linear polarizer to polarize the incident light, an spatial light modulator (SLM) that has the ability to change the polarization of the incident light and a polarizing cube beam splitter (PCBS, replacing BS_1) that will selectively reflect or let the light pass through it depending on the angle of polarization of the incoming beam. A scheme of the functioning of the system is shown in figure 2.10, a 3-D representation of the system is shown in figure 2.11.

The model of SLM used is a LC 2012 transmisive. The LC 2012 SLM is based on a transmissive Liquid Crystal (LC) microdisplay with 1024 x 768 pixel resolution with a pixel pitch of 36 µm and a fill factor of 58%. The active area is 36.9 x 27.6 mm. The SLM provides a phase shift of 2 π at 532 nm and around 1 π at

800 nm. The microdisplay and drive electronics are packaged into a compact box for easy integration into optical setups. The device is delivered with a mounting ring which fits for standard laboratory posts / holders. The LC 2012 is addressed using a standard HDMI interface and advanced calibration can be performed using an USB interface. It has an intensity ratio of 1000:1 @ 633 nm with coherent light.

Source

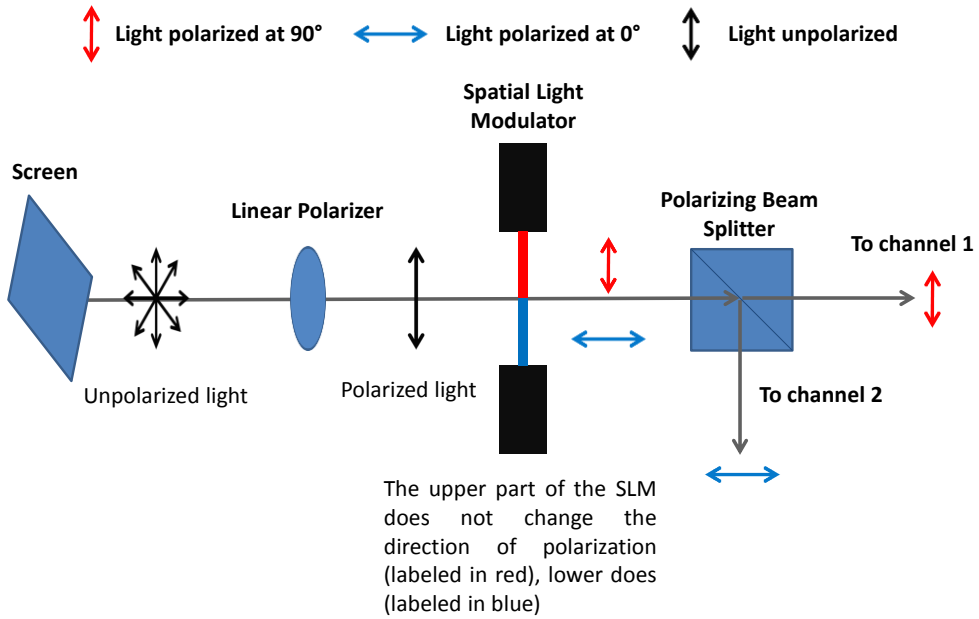

Figure 2.10. Illustration of the operation of the simultaneous vision system using polarized light. The incoming unpolarized incident light coming from the screen is polarized by the linear polarizer. Then the spatial light modulator changes the polarization of the light by 90 degrees in the blue area and does not affects to the polarization of the light in the red area. When both lights (horizontal and vertical polarized) reach the polarizing beam splitter are divided by their direction of polarization sending light through 2 different paths. The light polarized in the vertical direction goes through channel 1 and the one polarized in the horizontal direction goes through channel 2. On each channel a badal system will introduce the desired level of defocus after which both channel will be recombined and projected into the eye.

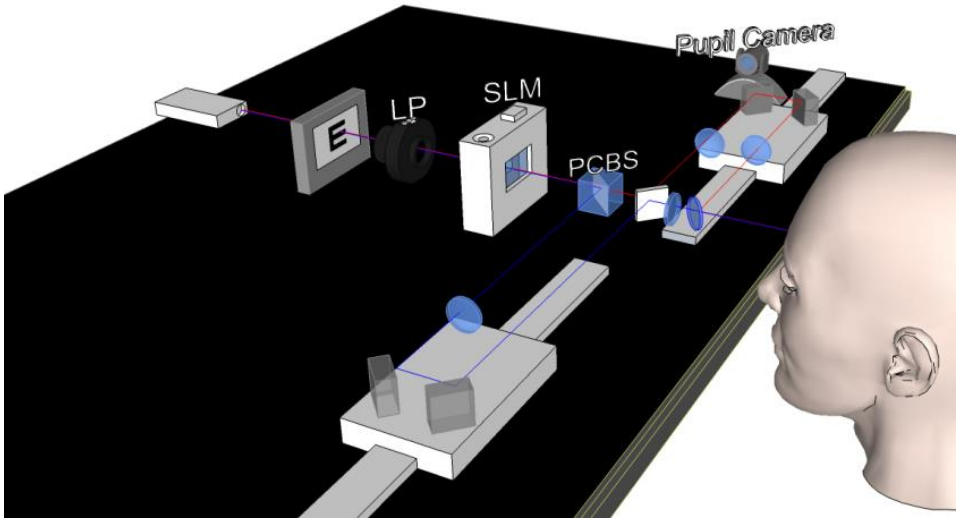

Figure 2.11. 3D representation of the simultaneous vision system. Light is divided by the action of a linear polarizer (LP), a spatial light modulator (SLM) and of a polarizing cube beam splitter (PCBS) in two different channels marked as red and blue.

For illustrating purposes we show 3 of the pupil patterns evaluated in chapter 7 imaged at a pupil plane of the system (Figure 2.12). The top row represents a 2-zone concentric design. The middle row represents a four zone angularly divided design and the bottom row represents an 8-zone bifocal design where radial and angular divisions have been performed. Images obtained of the bifocal patterns by blocking either channel 2 or channel 1 are given in the left and center columns with the right column representing when both channels are visible. It is important to notice that all the designs are bifocal since there are only two different channels which are the limiting factor for introducing different levels of defocus. So regardless of the number of areas of the design, one value of defocus is assigned to all the dark areas (e.g. addition value) and another to the bright areas (e.g. far correction).

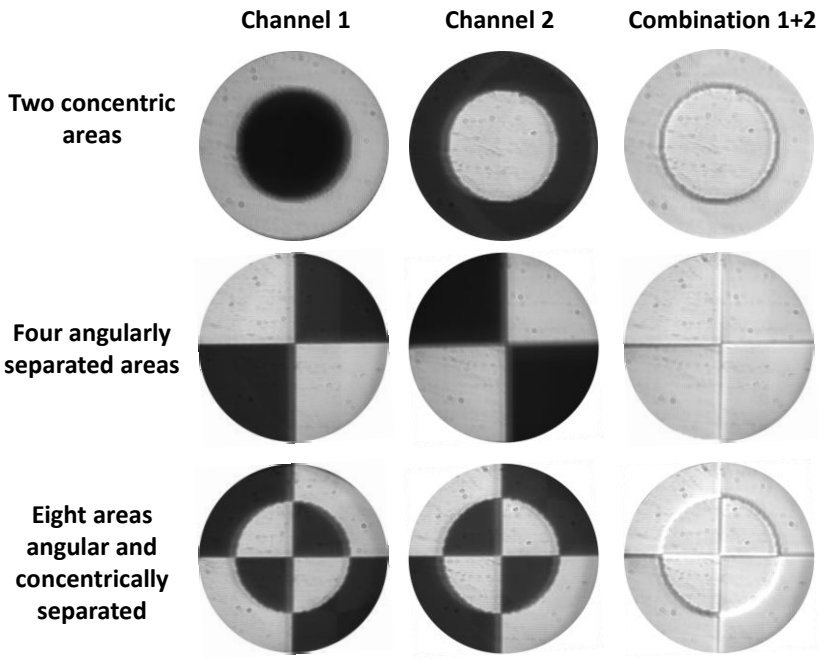

Figure 2.12. Pupil patterns imaged at the pupil plane of the system. Each row shows a different pupil pattern: 2-zone concentric design (upper row), 4-zone angularly divided design (middle row) and 8-zone concentric design (bottom row). Images obtained of the bifocal pattern by blocking channel 2, channel 1 and with both channels combined are shown from left to right.

2.3. Optical quality metrics

We quantified the optical quality of the eye under manipulated optics using Fourier Optics. The same routines were used in computer simulations as well as to characterize the experimental performance. In general the optical quality metrics are derived from the Point Spread Function (PSF) and the Modulation Transfer Function (MTF) [9], which can be defined from the wave aberration of a subject by calculating the generalized pupil [53]:

$$PupilG = Pupil * exp^{\frac{2\pi i W}{\lambda}} \qquad (2)$$

Where Pupil is a circle defining the aperture of the eye, W is the wavefront of the subject (equation 1) and λ is the wavelength used for the calculations.

For obtaining the irradiance PSF:

$$PSF = |FT(PupilG)|^2 \quad (3)$$

The Optical Transfer Function (OTF):

$$OTF = FT(PSF) \quad (4)$$

And to obtain the Modulation MTF:

$$MTF = |OTF| \quad (5)$$

For the purposes of this thesis, these functions were calculated assuming no pupil apodization and monochromatic light (λ=532 nm).

The following optical quality metrics have been used in this thesis:

Strehl ratio

Calculated as the ratio of the peaks of a PSF limited by the subject´s aberrations by the diffraction limited PSF. This metric has been used in the studies presented in chapter 3.

Visual Strehl:

As shown by Marsack et al. it is the best metric to try to predict the visual performance of a subject from his aberrations [9]. This metric has been used in the studies presented in chapters 7 and 8 as defined in equation 6 [54]:

$$VSOTF = \frac{\int_{-\infty}^{\infty}\int_{-\infty}^{\infty} CSF_N(f_x, f_y) * \left|\mathrm{Re}\{OTF(f_x, f_y)\}\right| \, df_x df_y}{\int_{-\infty}^{\infty}\int_{-\infty}^{\infty} CSF_N(f_x, f_y) * \{OTF(f_x, f_y)\} \, df_x df_y} \quad (6)$$

Where the integration is done for all the frequencies, the optical transfer function (OTF) is the Fourier transform of the PSF and the CSF is the Contrast Sensitivity Function of a standard subject. This metric will be used in the studies presented in chapters 7 and 8.

2.3.1 Evaluation of the depth of focus

For evaluating the depth of focus in chapter 7 of this thesis we have repeated the VSOTF calculations for a wide range of defocus values, keeping other aberrations fixed. Figure 2.13 shows an example of the typical through focus calculation of the VSOTF for two different patterns (spherical aberration and a pattern divided in two sub-zones with different amounts of coma and astigmatism). The green line represents an accepted threshold of acceptable vision[18,31].

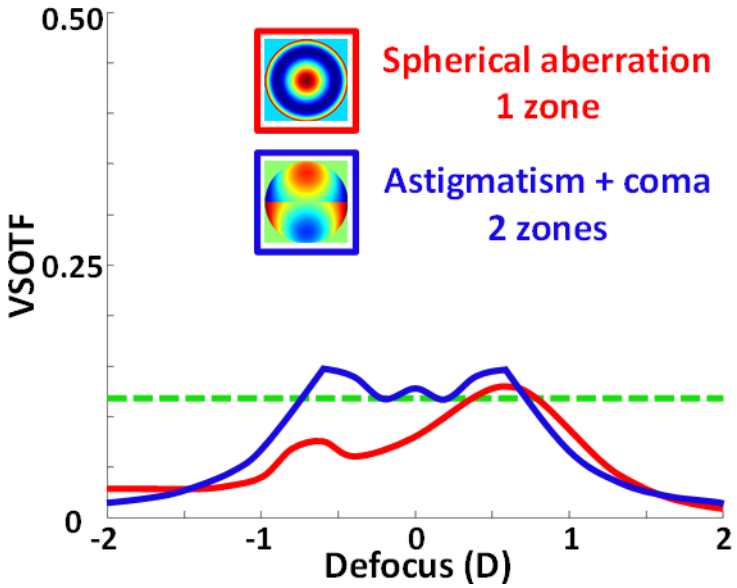

Figure 2.13. Behavior through focus of a two-zone divided pupil with astigmatism and coma in comparison of the one obtained for spherical aberration.

2.4. Psychophysical Measurements in Subjects

2.4.1 Visual Acuity Measurements

Subjects were asked to identify the orientation of a tumbling E letter (right, left, up, or down) using a keyboard. Each run consisted on 50 trials presented during 0.5 seconds with no feedback to the subject. A QUEST algorithm was programmed in Psychtoolbox [55] to select the size of each stimulus and optimize the estimation of the spatial resolution threshold. Experiments were done for black E letters on a white background.

Measurements performed for the experiments shown in chapters 3 and 4 introduced astigmatism at 45º what helped to minimize differences in blur for each of the four letter orientations. The letters were displayed on the minidisplay shown in figure 2.1.

The letters used for the measurement of VA in chapter 6 were presented using a CRT monitor controlled by a Visage instrument (Cambridge Research Systems).

2.4.2 Contrast Sensitivity Measurements

CSFs presented in chapter 5 were measured for six spatial frequencies (1.9, 3.8, 7.6, 15.2, 22.7 and 30.3 c/deg) and four orientations (0, 45, 90, 135 deg) with a staircase (2 down/ 1 up) four Alternative Forced Choice procedure (4 orientations for a fixed frequency) in steps of 0.05 log contrast. Measurements started between 0.2 and 0.4 log units above threshold and were considered finished after 7 reversals were completed, and the threshold was determined from the average of the last 6 reversals. The stimulus was presented after an auditory tone during 0.5 s. Each measurement was repeated 3 times, and deemed satisfactory if the standard deviation of the trials was less than 0.2 log units; most standard deviations were less than 0.1 log units. The stimuli were Gabor patches (standard deviation: 0.66 deg). The generation of stimuli was controlled by a Cambridge Research Systems VSG card. The mean luminance at the pupil plane was 50 cd/m^2 and the total magnification of the system was ×0.5. Measurements with and without AO-correction of aberrations were randomized. For each spatial frequency, four simultaneous staircase procedures were interleaved (one for each orientation). Aberrations were corrected across a 5.2-mm pupil. An artificial stop projected to the eye provided a 5-mm pupil for viewing the visual display.

Aberrations were measured immediately before and after a CSF measurement. A closed loop correction was generated immediately before and after the CSF measurements for the AO condition.

Monochromatic CSFs measurements were performed by placing an interference filter (peak transmission 550 nm; FWHM 10 nm). Polychromatic CSF measurements were performed for the extended spectral range of the projector lamp (EPSON EMP1810). In order to achieve equal luminance values

at the pupil plane in the polychromatic conditions the interference filter was replaced by a neutral density filter (ND 1.3).

Each complete CSF measurement took about 4 hours (including all frequencies, angles, and 3 repetitions). Measurements were conducted for monochromatic and polychromatic light (2 subjects); AO and non-AO corrected (all 4 subjects), and astigmatism corrected (2 subjects). Subjects were allowed to take breaks during the session. A complete set of data per subject was collected in between 2 and 5 sessions. Before the actual runs, a training session was conducted (with only one frequency) in order to familiarize the subjects with the protocols and tasks.

2.4.3 Perceived image quality measurements

The experimental measurements presented in chapter 7 consisted in the presentation of 105 pairs of images (each of the 14 phase patterns compared with all the others included itself). The phase patterns were presented randomly on each subject. The sequence for one trial was: load the first pupil pattern into the spatial light modulator, presentation of the image (1.5 s), gray screen (0.5 s), load the second pattern, presentation of the image (1.5 s), gray screen and wait until subject responses. This sequence was repeated 105 times for presenting all possible combinations of pairs during a single trial. Given that one sequence lasted around 15 minutes 2 breaks where taken (around the presentation of the pair numbers 35 and 70). This sequence was repeated thrice for each condition. Subjects performed these trials for far, intermediate and near vision conditions. When testing far vision badal 1 was set to 0 and badal 2 to +3 D when testing intermediate vision badal 1 was set to -1.5 D and badal 2 to +1.5D and when near vision was tested badal one was set to -3 and badal 2 to 0 D. The mean luminance of the experiments was 9 cd/m^2. The pupil size was limited to 4 mm by an artificial pupil positioned at the SLM. Measurements in one subject lasted around 3 hours.

Chapter-3 Simulated optics under combined astigmatism and coma: Preliminary experiments

This chapter is based on the paper by de Gracia et al.: “Combining coma with astigmatism can improve retinal image over astigmatism alone”. Vision Research 50, 2008-2014 (2010).

The coauthors of this study were Carlos Dorronsoro, Enrique Gambra, Gildas Marin, Martha Hernández and Susana Marcos.

The author of this thesis performed the simulations to find the best combinations possible between coma and astigmatism, programmed new software for the experimental measurements in the Adaptive Optics system, designed the experiments, run the experiments and analyzed the results.

As a result of this work new interactions between coma and astigmatism that improved the optical quality over the one obtained with either one alone were found. Also above average extension of the depth of focus by combining astigmatism and coma was found. These findings will be used as the foundations for part of the work presented in chapter 7.

3.1. Introduction

As elaborated previously the availability of wavefront sensors and the renewed interest in understanding the sources and effects of aberrations on optical quality and vision, have motivated studies aiming at understanding the interactions between aberrations. As shown in the introduction. several studies have demonstrated the interactions between low and high order aberrations (HOA) [56,57]. In particular, adding spherical aberration to defocus can improve retinal quality over defocus alone, indicating that cancelling defocus in the wave aberration Zernike polynomial expansion does not necessarily produce the best optical quality. As a consequence, the contribution of spherical aberration to the refraction needs to be considered [8,18]. Favorable interactions between other high order aberrations must also be present. McLellan et al. showed that the actual combination of high order aberrations found in eyes produced typically a better Modulation Transfer Function (MTF) than most combinations of equal amounts of aberrations and random signs [58]. Chromatic and monochromatic aberrations seem also to interact favorably: the relative degradation produced by longitudinal and transverse chromatic aberration of the eye on the MTF at short wavelengths with respect to the MTF at higher wavelengths is much higher in diffraction-limited eyes than in eyes with natural monochromatic aberrations [59,60].

Besides defocus, astigmatism is one of the most frequent, and important aberrations of the eye [61], followed by coma [62-64]. Apart from the natural astigmatism and coma that can be present in an eye on-axis, astigmatism and coma increases off-axis [65-67]. Certain pathologies increase progressively corneal astigmatism and coma (e.g. keratoconus) [68]. Ophthalmic lenses may induce astigmatism and coma [69]. Some surgical procedures induce astigmatism, such as the corneal incision in cataract surgery [70].

While the management of astigmatism is in many cases straightforward with cylindrical or toric lenses, the understanding of potential interactive effects of astigmatism and coma is crucial. In many situations, the correction must come with complex optical designs (i.e. lenses aiming at reducing off-axis aberrations; progressive lenses, etc.). In other cases (i.e. cataract surgery) surgeons may play with the incision location to maximize optical quality. Furthermore, the use of aberrometry for the measurement of astigmatism

(Z_2^{-2} and Z_2^2) may not be optimal if interactions of coma and astigmatism are present.

In this chapter we test the potential interactive effects of astigmatism (Z_2^{-2} and Z_2^2) and coma ($Z_3^{-1}$and Z_3^1) using computer simulations of retinal image quality and measurements of VA in subjects under controlled aberrations. We will demonstrate that optical/visual quality in the presence of astigmatism can be improved by adding coma (and vice versa).

3.2. Methods

3.2.1 Optical quality computer simulations

Point Spread Functions (PSFs) were computed for different combinations of astigmatism, coma and defocus using standard Fourier optics. The Strehl Ratio (SR) was used as an optical quality metric. Two dimensional maps of SR for fixed amounts of astigmatism and coma were generated, as a function of the orientation of astigmatism and coma ranging between 0 and 90º (at 3º steps).

SR was computed for astigmatism ranging from 0 to 1.50 D (1.38 µm) at 0.05 D steps and angles ranging from 0º to 90º. For a fixed amount of astigmatism, the amount of coma (and relative angle) that optimized SR was estimated. Coma values ranging from 0 to 1 µm were tested (at 0.02 µm steps). The simulations were done for different amounts of defocus, typically ranging from -1 to 1 D (at 0.02 D steps). Unless otherwise noted, the computations were performed for 6-mm pupil diameters, and λ = 555 nm. Simulations were performed setting all High order aberrations (HOA) to zero, and repeated for the natural HOA of two subjects (see experimental measurements below), where coma and astigmatism were replaced by those of the conditions under test.

3.2.2 Experimental measurements

Measurements of Visual Acuity (VA) were performed on two subjects for different combinations of coma, astigmatism and defocus. The aberrations were manipulated using an adaptive optics system.

3.2.3 Experimental set up

We used an adaptive optics system developed at the Visual Optics and Biophotonics Laboratory (Instituto de Optica, CSIC, Madrid) and described in detail in previous publications and in the introduction of this thesis [22,42].

3.2.4 Subjects

The experiments were performed in the right eye of two male subjects. Subject CDD was 37 years old, with a refraction of +1.5 D sphere. Subject ANC was 30 years old and emmetrope. Both subjects had an ophthalmological evaluation before performing the experiments. Accommodation was paralyzed and the pupil was dilated with 1% tropicamide. Subjects signed a consent form approved by the institutional review boards after they had been informed on the nature of the study and possible consequences. All protocols met the tenets of the Declaration of Helsinki.

3.2.5 Experimental Protocol

Visual acuity (VA) was measured in two subjects for astigmatism alone (0.5 D), with and without coma, and with and without the HOA of the subject.

The measurements were repeated for different amounts of defocus: -0.6, -0.2, 0, 0.2, and 0.6 D, with respect to the best subjective focus (which may change across conditions). All defocus conditions were achieved by moving the badal system. Spherical refraction was compensated by means of the Badal system and the induction in all the experiments was introduced with the Badal system. The experiments were performed under dilated pupils, with an artificial pupil of 6-mm placed in a plane conjugate to the pupil in the psychophysical channel.

A total of 5 series of through-focus VA measurements were performed on each subject in different conditions: (1) 0.5 D of astigmatism, all HOA corrected. (2) A combination of 0.5 D of astigmatism and 0.23 µm of coma (best combination predicted by simulations in absence of HOA), all other HOA corrected. (3) 0.5 D of astigmatism, 0 µm of coma and all the rest of HOA set to their natural values. (4) Natural aberrations replacing the natural astigmatism by 0.5 D and the natural coma by 0.23 µm. (5) Natural aberrations replacing the natural

astigmatism by 0.5 D and the natural coma by the best coma parameters predicted for each subject's aberrations.

The angle of both astigmatism and coma was 45º (relative angle 0º), except in condition (5), where both angles (of astigmatism and coma) where the ones providing the best predicted optical combination with each subject's aberrations.

Besides the through-focus series, two control measurements were performed in focus: All natural aberrations corrected and all natural aberrations uncorrected.

The tests were conducted in two different sessions. The first session involved the conditions with all aberrations corrected and the second one involved the cases in which natural aberrations were present. Conditions within each session were randomly tested.

Decimal VA was measured using a four alternative choice procedure with high-contrast tumbling Snellen E letters as shown in the Methods section. The VA measurement was deemed satisfactory if the standard deviation of at least the 8 last trials (from a sequence of 50 trials) was less than 0.06 arcmin. Otherwise the VA measurement was considered incorrect and repeated. The effective luminance of the minidisplay for the subject was 25 cd/m^2. This value was estimated taking into account the light losses in the system.

The mirror state was achieved after a closed-loop of 40 iterations. Experiments were performed under a static state of the mirror, but the wave aberrations were periodically monitored to ensure that the deviations from the desired wave aberration pattern was achieved and used during the measurement. The aberrations of the eye + mirror were measured just before and after each VA run. If the amount of coma or astigmatism differed from the expected value by more than 0.10 µm (on average the discrepancy was 0.04 µm), the closed-loop operation to achieve the desired mirror state was performed again and the VA measurement repeated. The centration of the pupil was monitored just before, in the middle and after the VA run.

In summary, the procedure sequence of the experiment for each condition was: 1) refractive correction with the Badal system; 2) measurement of ocular aberrations with the Hartmann-Shack sensor; 3) closed-loop to set the mirror

status (aberration correction + specific astigmatism/coma combination); 4) subjective focus setting with the badal system; 5) repeat steps 2 and 3; 6) Measurement of eye+mirror aberrations; 7) Measurement of VA; 8) Measurement of eye+mirror aberrations.

3.3. Results

3.3.1 Optical quality simulations

The different combinations of astigmatism and coma produce significant changes in Strehl Ratio (SR), which depend on the relative angle between both, and the amount of defocus. Fig. 3.1 shows 2-D SR maps for fixed amounts of astigmatism and coma, at different angles. Each panel represents a different amount of defocus (from -0.5 to 0.5 D). The rest of the HOA aberrations are assumed to be zero. The symmetry of the maps allows reducing the description in terms of relative angle, and each sequence of images can be summarized into one single 2-D plot. In Fig. 3.2 SR is represented as a function of relative angle and defocus. We observe optimal combinations of relative angle and defocus that maximize optical quality. Alternatively for a fixed amount of astigmatism, one can find the amount of coma that maximizes optical quality through focus. Fig. 3.3 shows the SR through-focus for 0.5 D of astigmatism, and different amounts of coma. Fig. 3.3A represents SR for a relative angle of 0º, which is the relative angle that produces the highest SR value (see Fig. 3.2). Each line on Fig. 3.3A corresponds to the central horizontal section of a map such as that shown in Fig. 3.2. Fig. 3.3B represents the maximum SR at each defocus position, at the best relative angle.

We found that for a significant range of coma (0.15 to 0.35 μm) and for a relatively wide range of focus (>1.5 D), adding coma to astigmatism improves the optical performance over astigmatism alone (shown in solid black line). The same results stand for negative values of coma, being the SR values equal for any pair of ± μm of coma.

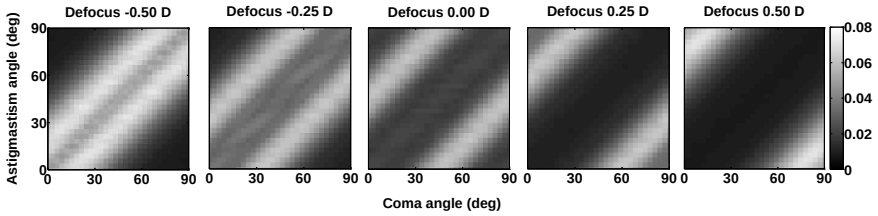

Figure 3.1. Strehl Ratio maps for combinations of 0.5D of astigmatism with 0.23 μm of coma, as a function of angle of coma and astigmatism. Each panel represents a different amount of defocus, ranging from -0.5 D to 0.5 D in steps of 0.25 D. The vertical axis represents angle of astigmatism. The horizontal axis represents angle of coma.

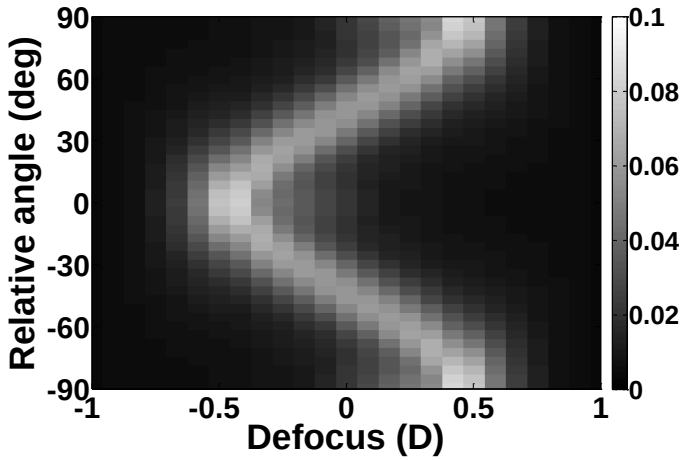

Figure 3.2. Strehl Ratio for combinations of 0.5 D of astigmatism and 0.23 μm of coma at different defocus positions and relative angles. This map summarizes an entire sequence of maps like those shown in Fig. 1.

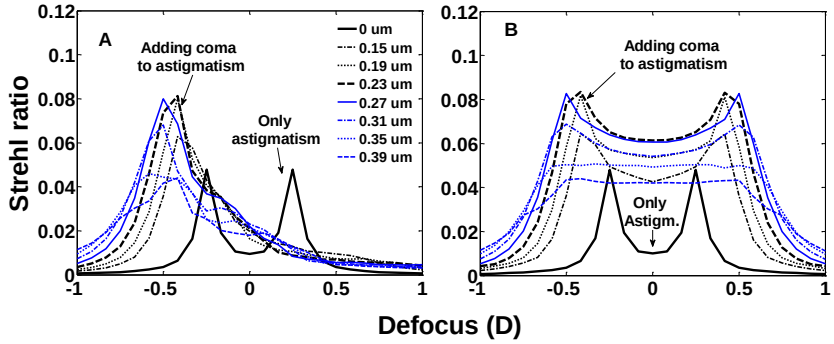

Figure 3.3. Strehl ratio for combinations of 0.5 D of astigmatism and different amounts of coma, ranging from 0 to 0.39 μm. (A) For a fixed relative angle of 0º. (B) For a varying relative angle giving the optimal SR at each defocus. Pupil 6 mm.

The same calculations were performed for a total of 31 amounts of astigmatism ranging from 0 to 1.5 D (at 0.05 D steps), and for two different pupil diameters (4 and 6 mm). Two dimensional maps of optical quality as a function of coma versus astigmatism were obtained (Fig. 3.4), for two pupil sizes, 4 mm in A and 6 mm in B. The area under the through-focus SR curves between -0.5 and +0.5 D was chosen as optical quality metric. The dashed red lines show the amount of coma for each amount of astigmatism that maximizes the metric. Combinations between the blue dotted line and the x-axis provide better performance than astigmatism alone (x-axis).

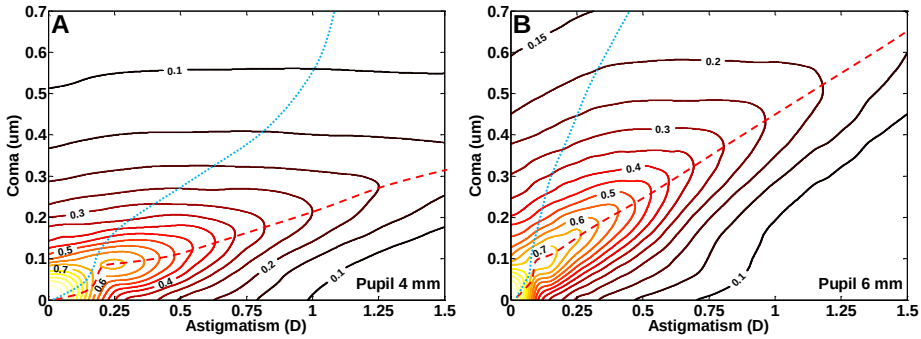

Figure 3.4. Two dimensional maps of optical quality as a function of coma versus astigmatism. The height at each point of the map represents the value of the optical quality metric (area under the through-focus SR curves between -0.5 and +0.5 D), normalized to the diffraction limited condition (coma and astigmatism set to 0). The red dashed line represents the optimal combinations of coma and astigmatism that maximizes the area under the Strehl Ratio. Combinations below the blue dotted line provide better performance than astigmatism alone.

Fig. 3.4 shows again that there is a wide range of values of coma that improves optical quality in the presence of astigmatism (i.e. for 1 D of astigmatism and a 4 mm-pupil, any value of coma up to 0.5 µm). Optimal combinations of coma and astigmatism (dashed red lines in Fig. 3.4) can be fitted by linear regressions. The following expressions are linear regressions to the data (R^2 >0.98) and can be used to approximately obtain the optimal amount of coma (or astigmatism) to maximize Strehl Ratio for a given amount of astigmatism (or coma):

Astigmatism (D) = 0.404 · Coma (µm) + 0.040, for a 6-mm pupil

Astigmatism (D) = 0.204 ·Coma (µm) + 0.013, for a 4-mm pupil

When astigmatism is expressed in μm, the slope of the linear fit and therefore the amount of coma that maximizes the metric is approximately ½ of the astigmatism-value for both pupils (slopes of 0.44 and 0.49 for 4-mm and 6-mm pupils respectively).

The simulations above assumed an eye in which only astigmatism and coma were present. We also performed computer simulations of Strehl Ratio using wave aberrations of real eyes (from the two subjects that participated in the experiment, described below). The presence of other HOA breaks the symmetries of Fig. 3.1, and the description in terms of relative angle is no longer valid. In our subjects, the best combination is provided by an astigmatism angle of 9º and a coma angle of 84º (corresponding to a relative angle of 75º) for subject ANC, and an astigmatism angle of 11º and a coma angle of 63º (relative angle 48º) for subject CDD. Fig. 3.5 represents the through-focus SR functions for different combinations of astigmatism (0.5 D) and coma (from 0 to 0.61 μm), as in Fig. 3.3, but in presence of the rest of the natural HOA, for the two subjects (ANC, 3.3A, 3.3B and 3.3C and CDD, 3.3D, 3.3E, 3.3F). The optical quality with the fixed angles providing the best combination for each subject are shown in Fig. 3.5A and 3.5D. Figures 3.5B and 3.5E show the SR with the best combination of angles at each defocus position. Figures 3.5C and 3.5D represent the SR values for fixed angles of astigmatism and coma of 45º, i.e. the ones providing best optical quality in the absence of other HOA.

The improvement of astigmatism by adding coma is still present. For subject ANC, the combination of 0.5 D of astigmatism with 0.11 μm of coma increases performance by a factor of 1.13 (13%), over astigmatism alone, but the defocus range over which this occurs is narrower than in the absence of other HOA (Fig. 3.3). Furthermore Fig. 3.5B shows on average higher SR values than Fig. 3.3B, indicating that natural aberrations+astigmatism+coma can lead to better optical performance than astigmatism+coma+HOA corrected. For subject CDD, the combination of 0.5 D of astigmatism with 0.51 μm of coma increases SR by a factor of 2.44 (144%). In the presence of HOA, the amount of coma that maximizes SR changes across individuals. For subject ANC, the condition producing the highest SR is 0.2 D of defocus and 0.11 μm of coma (at 84º, with astigmatism at 9º). For subject CDD, the condition producing the highest SR is 0.6 D of defocus and 0.51 μm of coma (at 63º with astigmatism at 11º).

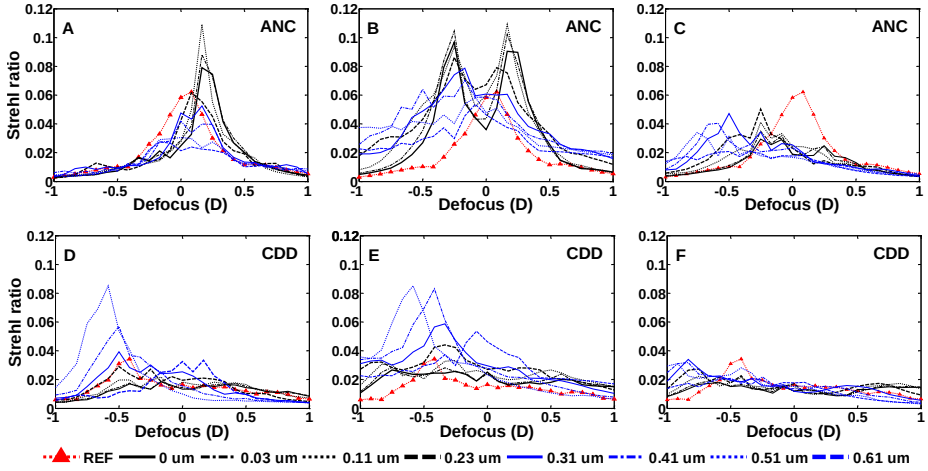

Figure 3.5. Through focus Strehl Ratio with real aberrations (Subject ANC, upper panels, CDD lower panels), in the presence of astigmatism (0.5 D) combined with different amounts of coma. Panels (A) and (D) represent the SR values for a fixed relative angle (75º for ANC and 48º for CDD, see text for details). Panels (B) and (E) represent the best SR values for the best optical angles at each defocus position. Panels (C) and (F) represent the SR values for fixed angles of astigmatism and coma of 45º. The red dotted line (triangles - REF) represents the through-focus SR for the subject´s own natural aberrations.

3.3.2 Optical aberrations induction and correction

ANC had a natural astigmatism of -0.02 D at 160º, a natural coma of 0.10 µm at 60º, and a RMS_{HOA} of 0.214 µm for a 6-mm pupil diameter. CDD had a natural astigmatism of -0.17 D (at 144º), a natural coma of 0.15 µm at 30º and a RMS_{HOA} of 0.454 µm (for 6-mm pupils). The ocular HOA of the subjects were corrected down to 0.072 and 0.048 µm respectively (0 D defocus). The induced combinations of astigmatism and coma deviated from the desired state typically less than 1% (RMS wavefront error, as measured with an artificial eye), and on average 0.04 µm when measured on the subjects' eye.

3.3.3 VA measurements

Fig. 3.6 shows through-focus measurements of Decimal VA for a combination of 0.5 D of astigmatism and 0.23 µm of coma, and relative angle of 0º, for the rest of HOA corrected for both subjects. This combination of astigmatism and coma was shown to provide optimal improvement of optical quality in the simulations (with corrected HOA). Decimal VA with astigmatism alone and VA with natural aberrations (at best focus) are also shown as a reference. In the

absence of HOA, both subjects show a dramatic improvement of VA when coma is added to astigmatism over at least a 0.5 D interval. When all aberrations are corrected VA is around 1.4. Adding 0.5 D of astigmatism reduces VA to about 0.8. However, adding 0.23 µm of coma increases VA by a factor of 1.25 for ANC and by a factor of 1.33 for CDD in the best focus conditions over the VA with astigmatism alone.

Fig. 3.7 shows thru-focus VA results on the same subjects with natural HOA, for the same amounts of coma and astigmatism, and relative angle than the measurements shown in Fig. 3.6.

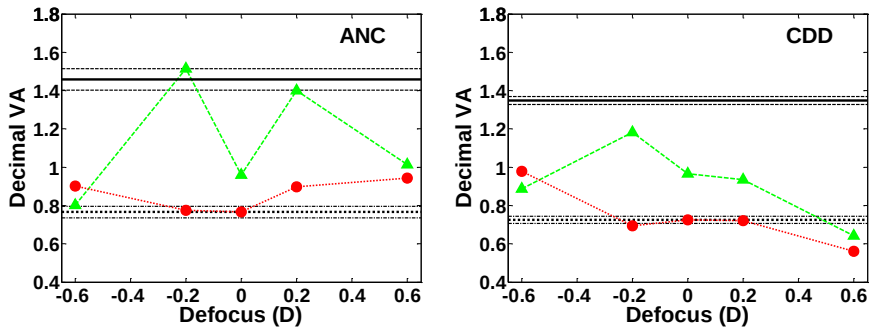

Figure 3.6. Through focus VA for corrected HOA. The green line (triangles) represents VA measurements with a combination of 0.5 D of astigmatism and 0.23 µm of coma, while the red line (circles) VA measurements for 0.5 D of astigmatism. The black solid line represents VA in focus for all aberrations corrected (dashed lines on both sides represent the standard deviation of the measurement). Black-dotted line represents VA in focus with only 0.5 D of astigmatism (doted-dashed black lines represent its standard deviation values).

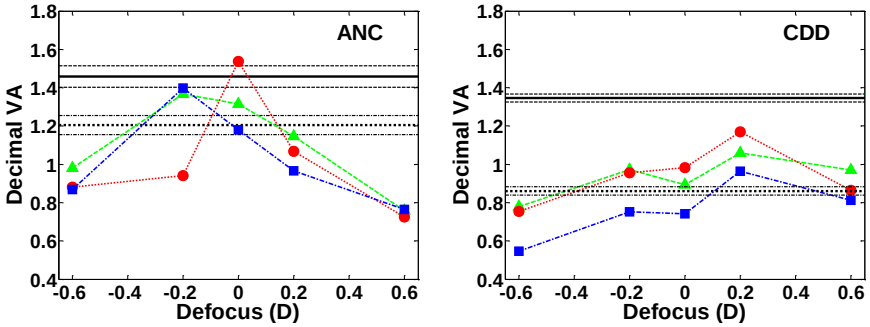

Figure 3.7. Through-focus decimal VA for natural HOA. The green line (triangles) represents VA measurements with 0.5 D of astigmatism and 0.23 µm of coma; the red line (circles) represents VA measurements with 0.5 D of astigmatism; the blue line (squares) represents the VA obtained under the best condition obtained on the simulations for each subject with natural aberrations and 0.5 D of astigmatism (astigmatism angle 9º and coma 0.51 µm at 63º for CDD; astigmatism angle 11º and coma 0.11 µm at 84º for ANC). The black solid line represents VA in focus for all aberrations corrected, (dashed lines on both sides represent the standard deviation of the measurement). Black-dotted line represents VA in focus for natural aberrations (doted-dashed black lines represent its standard deviation values).

VA was also tested under the best possible combination of astigmatism (0.5 D) and coma, (magnitudes and angles) as predicted by the simulations in the presence of the natural HOA of the subjects. Blue line (squares) represents VA values obtained under these optimized conditions.

For ANC, VA for the best combination is 1.40 ± 0.07, for CDD VA for the best combination is 0.96 ± 0.03, not showing improvement over the condition of astigmatism alone.

3.4. Discussion

We found that adding coma to astigmatism can improve Visual Acuity over the condition where only astigmatism is present. Simulations reveal that Strehl Ratio can be improved by 40% or more when adding coma to 0.5 D of astigmatism. For a 6-mm pupil the improvement hold for a range of at least 1 D of defocus and 0.20 µm of coma. When the natural aberrations were present, this improvement is very dependent on the subject's own aberrations, but there are specific amounts of coma and angles of coma and astigmatism that produce an improvement.

Previous works reported that combinations of certain types of aberrations (in particular symmetric aberrations such as spherical aberration and defocus)

can produce higher optical quality than those aberrations individually [17]. We have demonstrated that the effects happen both optically (measured in terms of Strehl Ratio) and visually (in terms of high contrast Visual Acuity) for asymmetric aberrations such as coma and astigmatism.

Adaptive Optics has allowed us to manipulate the optics of the eye, and measure visual performance after introduction of desired combinations of coma and astigmatism (either under correction or in the presence of natural aberrations).This approach allows the simulation of aberration patterns which may be adopted in the design of lenses or the simulation of induced aberrations by certain pathologies or surgeries that increase the amounts of aberrations and coma. By using adaptive optics it is possible to quantify not only the optical effects of aberrations over vision that are also present in convolved images but it is also possible to measure the neural effects occurring in later stages of the image processing in human vision. The results have important implications in the management of astigmatism correction and the evaluation of the optical aberrations induced by lenses (e.g. as progressive spectacle lenses, contact lenses or intraocular lenses) and pathologies (e.g. keratoconus) or surgeries (e.g. refractive surgery, cataract surgery).

Our data show that in the presence of astigmatism, having certain amounts of coma improves optical and visual performance very substantially. Alternatively, the presence of coma can be attenuated by astigmatism. In the absence of other HOA the effect is very robust. Other metrics of optical quality where computed: VSOTF [9,54] and $rMTF_{515}$ [71]. Both of them showed a similar trend and confirmed the beneficial effect of adding coma to astigmatism.

The effect is reduced in the presence of other natural aberrations. The range of conditions in which the improvement is produced by adding coma to astigmatism when natural aberrations are present is more restricted, and larger differences between the optical prediction and the VA might occur if slight discrepancies from the optimal conditions are present.

In our study we focused on fixed amounts of astigmatism and coma, which were varied experimentally with adaptive optics. We found that specific combinations of these aberrations produced optical and visual improvements. An interesting question is whether these optimal

combinations may occur naturally. A study by McLellan et al. suggests that this may happen, at least in terms of signs (relative orientation of coma and astigmatism, among others), as the MTF generated by random combinations of signs of the Zernike terms were in general more degraded than that from the natural aberrations of the eye (McLellan et al. 2006). Our results suggest favorable or protective effects of other HOA against astigmatism. In both subjects VA with astigmatism and HOA (see Fig. 3.7) tends to be higher than VA with astigmatism alone (see Fig. 3.6).

We have found a relatively good correspondence between the effects revealed by SR and VA when all the natural aberrations are corrected in these two subjects. Additional simulations with residual aberrations predicted lower SR improvement rates than those assuming perfect correction (as considered in the simulations). In addition, it is expected that the SR metric does not capture all the effects as it refers only to contrast degradation, and not phase, which is likely relevant in the presence of asymmetric aberrations. On the other hand VA is affected by neural factors which cannot be captured optically. The difference in VA (see Fig. 3.6) between subjects under identical optical conditions arises from differences in neural stages of the visual process. Furthermore, neural adaptation may play a role in subjects with significant amounts of natural astigmatism [72]. Therefore, previous visual experience can be of crucial relevance when experiencing the benefits of the combination of coma and astigmatism on vision. In the next chapter we will extent the measurements to 20 subjects and we will evaluate their performance according to their level of natural astigmatism.

Chapter-4 Visual acuity under combined astigmatism and coma: Optical and neural adaptation effects

This chapter is based on the paper by de Gracia et al.: “Visual acuity under combined astigmatism and coma: Optical and neural adaptation effects” *Journal of Vision* **11**, (2011a).

The coauthors of this study were Carlos Dorronsoro, Gildas Marin, Martha Hernández and Susana Marcos.

The author of this thesis performed the simulations to find the best combinations possible between coma and astigmatism, programmed new software for the experimental measurements in the Adaptive Optics system, designed and run the experiments and analyzed the results.

The results of this chapter show that there is a strong correlation between the improvements obtained with the combination of coma and astigmatism and the previous visual experience of the subject. Astigmatic subjects performed better under the presence of astigmatism than emmetropic subjects. Also astigmatic subjects benefit less from the addition of coma to astigmatism than emmetropic subjects.

4.1. Introduction

Interactions between symmetric low and HOA have been studied computationally and experimentally [56,57]. As already mentioned, previous studies have shown that spherical aberration and defocus can interact favorably to achieve better image quality than either one alone [17]. Also the expansion of the depth of focus with spherical aberration of 4^{th} and combinations of 4^{th} and 6^{th} order has been studied profusely [31,32]. Favorable interactions between HOA seem to occur in the human eye, as artificial combinations of similar amounts of Zernike but random signs produce lower MTFs than the actual Zernike set [58]. As a general rule adding aberrations decrease VA at best focus while improves the depth of focus. Therefore, to identify specific combinations of aberrations that increase the DOF while minimize the decrease of VA at best focus can help to improve multifocal solutions.

In the previous chapter we have shown possible favorable interactions of astigmatism and coma[28]. We found that optical quality in the presence of astigmatism can be very significantly improved by adding coma. For example, Strehl ratio (SR) increased by a factor of 1.7 by adding 0.23 μm of coma to 0.5 D of astigmatism, over Strehl ratio for 0.5 D of astigmatism alone for a pupil of 6 mm. Improved VA when astigmatism and coma were combined was demonstrated on two subjects who did not have significant amounts of natural astigmatism.

In this chapter, we will test whether the theoretical optical improvement achieved with certain combinations of coma and astigmatism results in a systematic increase of visual performance. Experimental measurements were performed in a group of 20 young normal patients, with various amounts of spherical and cylindrical refraction, with no *a priori* selection of their refractive profiles. We found that astigmatic subjects, particularly subjects where astigmatism was not habitually corrected, did not improve visual acuity when astigmatism was added, in contrast to the optical predictions. The fact that subjects with identical optical properties exhibit very different relative responses is suggestive of adaptation effects, to astigmatic blur in particular. Adaptation to the blur induced by low and HOA has been suggested before. Several studies report improved visual performance in myopes after periods of adaptation to defocus [73,74]. This

phenomenon has been also reported in emmetropic subjects after periods of induced defocus [75]. Changes in the perception of blur after brief periods of adaption to blurred or artificially sharpened images have also been demonstrated [76]. In a recent study, we have shown angular selective adaptation to astigmatic blur after brief periods of adaptation to images blurred by horizontal or vertical astigmatism [72].

In this chapter we test the interactions of astigmatism, coma and defocus in a group of 20 subjects. The subjects included three refractive profiles (non-astigmatic emmetropes, astigmatic patients which were habitually corrected by spectacles, and uncorrected astigmatic subjects). A *post-hoc* analysis of the data showed that the differences in the response were associated to the presence/absence of astigmatism, and whether this was habitually corrected. We hypothesized that prior adaptation to astigmatism is responsible for the discrepancy from the optical predictions of the benefits of adding coma to astigmatism.

4.2. Methods

4.2.1 Experimental set up

A custom-developed Adaptive Optics system was used in the study to induce the desired patterns of astigmatism and coma, while the natural low and higher order aberrations were corrected. The system has been described in detail in previous publications [22,28] and in the introduction of this thesis. In brief, the main components of the system are a Hartmann–Shack wavefront sensor (composed by 32 × 32 microlenses, with 15 mm effective diameter and a CCD camera; HASO 32 OEM, Imagine Eyes, France) and an electromagnetic deformable mirror (MIRAO, Imagine Eyes, France). The desired mirror states were achieved by a closed-loop operation. Dedicated routines have been developed specifically for this study, allowing a full automatization of the process, so that after the mirror state is created, no further interaction from the experimenter is required.

Visual stimuli were presented on a minidisplay (12 mm × 9 mm SVGA OLED minidisplay, LiteEye 400), viewed through the AO mirror, and a Badal system.

VA was measured using a 4-alternative forced choice procedure with tumbling E letters, and a QUEST procedure programmed in psychotoolbox[55].

4.2.2 Optical Predictions

We have shown previously that, under certain conditions, adding coma to astigmatism improves optical quality over astigmatism alone. We calculated the SR values for amounts of coma ranging from 0 to 1 μm, astigmatism from 0 to 1.5 D, and defocus from -1 to 1 D respectively, for 2 different pupil diameters (4 and 6 mm). We predicted a peak improvement in SR by a factor of 1.7 when adding 0.23 μm of coma to 0.5 D of astigmatism, in an otherwise fully corrected eye (for 6-mm pupils). Improvement of SR by adding coma to 0.5 D of astigmatism was found for a range of 0.85 D of defocus, for coma values ranging from 0.15 to 0.35 μm of coma, and a range of 60° of relative angle (from 0 to 60)[28].

4.2.3 Experimental protocols

To further explore possible interactions between coma, astigmatism and defocus. VA was measured under a total of 18 conditions in 20 subjects. The conditions were selected according to the predictions from computer simulations, which identified the amounts and orientations of coma which interacted favorably with 0.5 D of astigmatism at 45° [28]. A set of conditions varying the amount of coma, relative angle of coma and astigmatism and defocus were tested. In all cases natural astigmatism and HOA of the subject were corrected, and the desired combinations of astigmatism and coma were induced. In particular we tested VA for the following conditions: (1) Across defocus experiment: 0.5 D of astigmatism at 45°. 0.23 μm coma, a relative angle of 0°, and defocus varying from -0.6 D to 0.6 D (amount of defocus tested: -0.6, -0.2, 0, 0.2, 0.6); (2) Across coma experiment: 0.5 D of astigmatism at 45°, variable coma (from 0.11 to 0.41 μm in 0.06-μm steps), and a relative angle of 0°; (3) Across relative angle experiment: 0.5 D of astigmatism, coma (0.11, 0.23 and 0.35 μm), and relative angles of 0°, 45° and 90°. In addition, VA was measured also for 2 control conditions, with all low and HOA corrected and with all low and HOA corrected and 0.5 D of astigmatism at 45°. The order in which the different conditions were tested was randomized. The series of measurements of conditions 1, 2 and 3 represent the experiments labeled as 1, 2 and 3 respectively.

All the experiments were performed under dilated pupils (by tropicamide 1%), with an artificial pupil of 6-mm placed in a plane conjugate to the pupil in the psychophysical channel. Wave aberrations were fitted by 7^{th} order Zernike polynomials. We used the OSA convention for ordering and normalization of Zernike coefficients.

Each VA measurement consisted on 50 trials, each one presented during 0.5 seconds. Subjects had to determine the orientation of the letter E (pointing up, down, left or right). The introduction of astigmatism at 45° in most of the VA measurements, along with the fact that Z^2_{-2} is introduced by the mirror at the circle of least confusion, (equivalent spectacle prescription: +0.25 -0.50 x 45°) helps to minimize differences between the four possible letter orientations. There was no feedback to the subjects. As a control parameter to decide the validity of the VA measurement, at least 8 of the last 25 trials must have a standard deviation under 0.06 arcmin. If the measurement did not meet this criterion it was discarded and repeated. Taking into account the light losses in the system, the effective luminance of the minidisplay at the pupil plane was 25 cd/m^2.

The steps of an experimental session were, sequentially: 1) focus setting; 2) measurement of ocular aberrations with the Hartmann-Shack sensor; 3) closed-loop for natural aberration correction; 4) set of mirror status (aberration correction + specific astigmatism / coma combination); 5) measurement of eye + mirror aberrations; 6) measurement of VA; 7) measurement of eye + mirror aberrations. The sequence was repeated for each condition tested.

The focus setting was determined using a Maltese cross as a fixation target. The focus setting was determined for each subject under a mirror state that induced 0.5 D of astigmatism at 45° and 0.23 μm of coma at a relative angle of 0°, for all measurements except for the condition where all aberrations corrected. For this condition, the focus setting was obtained for the state of the mirror producing best correction of astigmatism and HOA.

4.2.4 Subjects

Twenty subjects participated in the study, with ages ranging from 23 to 42 years (29.1 ± 5.1). Spherical errors ranging from -5.75 D to +1.75 D (mean: -0.73 ±1.72). Astigmatism ranged from 0 to 1.5 D. All patients followed an

ophthalmological evaluation before performing the experiments. Subjects signed a consent form approved by the institutional review boards after they had been informed on the nature of the study and possible consequences. All protocols met the tenets of the Declaration of Helsinki. Table 4.1 shows the profile of the patients; the subjective prescription and whether they were habitually corrected. There were no significant differences in the wave aberration magnitude and distribution of the HOA across groups.

Subject #	Sph (D)	Astig. (D)	Angle (Degrees)	EYE	Age (Years)	Habitual astigmatic correction	Group
1	0	0	--	Right	30	NO	1
2	1.5	0	--	Right	37	NO	1
3	-1.5	0	--	Right	25	NO	1
4	0	0	--	Right	25	NO	1
5	0	0	--	Left	26	NO	1
6	0	0	--	Right	29	NO	1
7	-5.75	0	--	Left	39	NO	1
8	-1.25	0	--	Right	27	NO	1
9	-0.75	0	--	Right	23	NO	1
10	0.75	0	--	Left	31	NO	1
11	-3	-0.5	180	Right	26	YES	2
12	-4	-1	175	Right	27	YES	2
13	-1.5	-1.5	150	Left	28	YES	2
14	-1.75	-0.5	70	Right	25	YES	2
15	-0.75	-0.75	75	Right	25	YES	2
16	0. 5	-0.25	110	Right	30	NO	3
17	0.25	-0.5	50	Right	42	NO	3
18	-0.5	-0.5	135	Right	33	NO	3
19	1.75	-0.5	30	Right	28	NO	3
20	0.5	-0.5	125	Right	25	NO	3

Table 4.1. Group 1: No natural astigmatism n=10. Group 2: natural astigmatism habitually corrected (0.50-1.50 D) n=5. Group 3: natural astigmatism habitually uncorrected (0.25-0.50 D) n=5.

The type of astigmatism differed across groups. Compound myopic astigmatism was predominant in the group of habitually corrected astigmats (5/5). Hyperopic astigmatism was predominant in Habitually non-corrected astigmats (3/5). One subject showed compound mixed astigmatism (#17) and one subject showed compound myopic astigmatism (#18). None of the Habitually non-corrected astigmats except for subject #19 wore any prescription. Subject 19 is habitually corrected from 1.25 D of hyperopic defocus (residual prescription: +0.5 -0.5 x 30). Habitually corrected astigmats were habitually corrected for their sphero-cylindrical errors. It is commonly assumed that non-corrected hyperopic astigmats can shift their best focus by means of accommodation, and therefore may experience images blurred along different orientations throughout the Sturm interval for distance vision. Figure 4.1 illustrates the range of PSFs (not taking into account HOA) available to the habitually uncorrected astigmats. For far vision, subject #17 and subject #18. may experience a more limited range of orientations in their PSFs than the hyperopic astigmats.

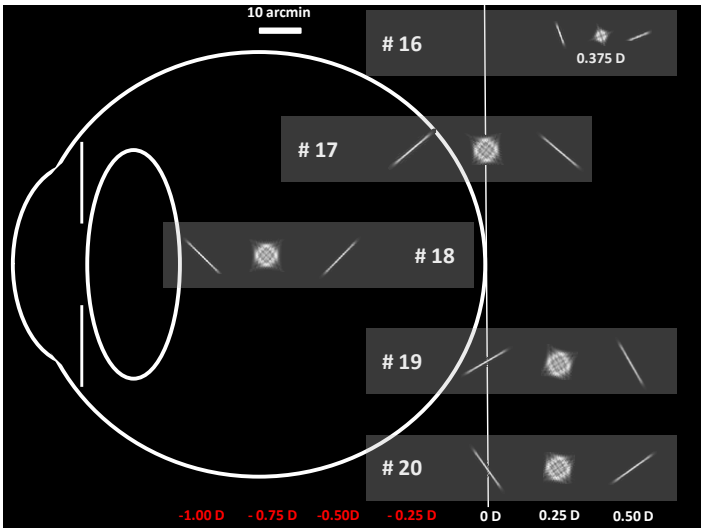

Figure 4.1. PSFs for habitually non-corrected astigmatic subjects. The numbers under each PSF indicate the defocus required to place the image onto the retina. A schematic eye (not in scale) is included for reference in the background. PSFs available for distance vision are labeled in white. The vertical line represents the retinal plane for all subjects. The scale bar only applies to the size of the PSFs.

4.2.5 Data analysis

VA was compared across conditions and groups both in absolute and relative terms. The visual benefit of adding coma to astigmatism was expressed as the ratio between VA (for a given combination of astigmatism, coma and defocus) and VA in the presence of astigmatism only:

$$Visual\ Benefit = \frac{VA(Astigmatism + Coma)}{VA\ (0.5\ D\ of\ astigmatism)} \qquad (4.1)$$

The visual degradation produced by inducing astigmatism to fully corrected eye was defined as:

$$Visual\ Degradation = \frac{VA(All\ aberrations\ corrected)}{VA\ (0.5\ D\ of\ astigmatism)} \qquad (4.2)$$

Statistical comparisons of the visual performance across groups were performed using a linear mixed model, with the VA as the dependent variable, group as a factor, and the different conditions as repeated measurements. Bonferroni definition of confidence intervals was used.

4.2.6 Aberration correction and induction

Astigmatism and HOA were fully corrected and/or selectively induced (astigmatism and coma) by the mirror. The mirror states were measured just before and after each VA measurement. The achieved state was compared with the attempted state, and a maximum discrepancy of 0.10 µm in the astigmatism or coma terms was allowed. If the mirror state did not fulfill these requirements the measurement was discarded and repeated. Figure 4.2 shows an example of correction and induction of aberration on one subject (#2). The top row shows the natural wave aberration pattern for the subject (excluding tilt and defocus (A) and after AO-correction (B). The bottom row shows the attempted wave aberration pattern, a combination of 0.5 D of astigmatism at 45° and 0.23 µm of coma at a relative angle of 0° (C), the achieved pattern (after AO- correction of the natural aberrations and induction of the desired pattern (D) and the error (E). The examples show a high compliance in the correction and induction of aberrations. HOA were successfully corrected in all subjects, with the residual RMS being lower than

0.11 µm (including errors in all HOA and astigmatism). Figure 4.3 shows the residual RMS error for all subjects when inducing a wave aberration pattern of 0.5 D of astigmatism at 45° and 0.23 µm of coma at a relative angle of 0°. The difference between the attempted and achieved aberration patterns (for combinations of astigmatism and coma) did not vary significantly across groups. For example, for a combination of astigmatism of 0.5 D at 45° and coma of 0.23 µm, with a relative angle of 0° (as that shown in example of Fig. 4.3), the residual RMS error after correction of astigmatism and HOA was on average 0.082 for non-astigmats, 0.071 for habitually corrected and 0.058 for habitually non-corrected astigmats . The residual RMS difference was found to be 0.024 µm larger in non-astigmats than in habitually non-corrected astigmats . Residual errors for the three groups are within a range from 10 to 15% of the ideal RMS attempted.

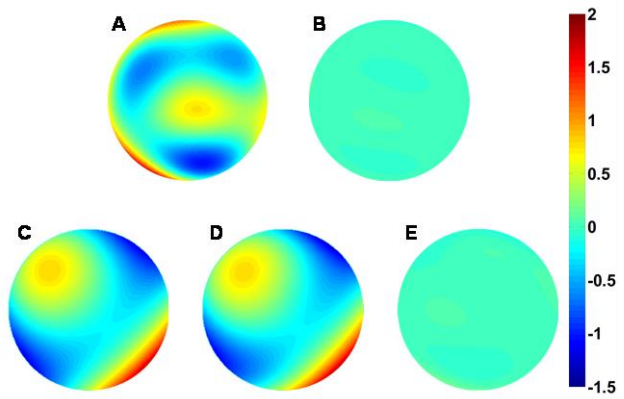

Figure 4.2. Upper row: A. Natural wave aberration of Subject # 2 (excluding tilt and defocus RMS = 0.45 µm); B. Wave aberration after AO correction (RMS = 0.020 µm). Bottom row: C. Wave aberration for a mirror state attempting a combination of 0.23 µm of Coma and 0.5 D of Astigmatism both at 45°; D. Achieved wave aberration pattern; and E. Difference map between ideal and achieved (RMS = 0.030 µm). Pupil diameter: 6 mm.

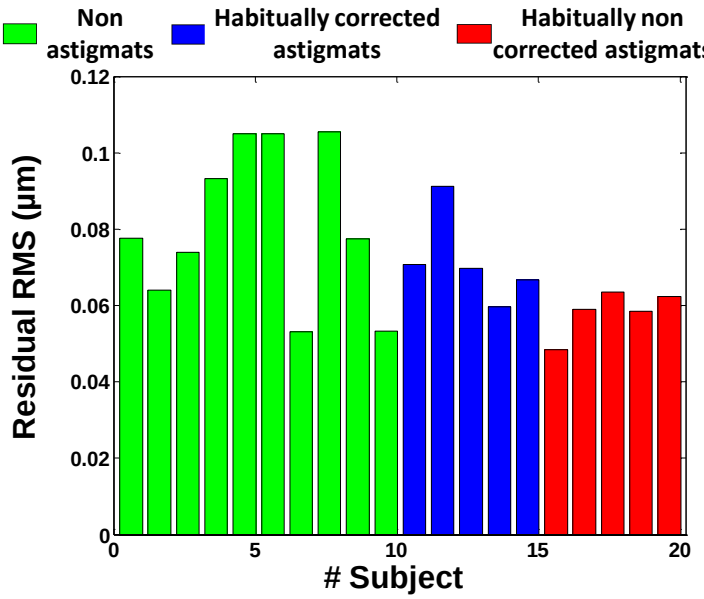

Figure 4.3. RMS of the difference achieved-attempted map (for a combination of 0.5 D of astigmatism and 0.23 um of coma, at a relative angle of 0 deg) in all subjects. Green bars represent non-astigmats subjects, blue bars represent habitually corrected subjects and red bars represent habitually uncorrected ones. Pupil diameter=6 mm.

4.3. Results

4.3.1 Visual acuity with combined astigmatism and coma

Figure 4.4 shows the visual benefit of adding coma to astigmatism over astigmatism alone (equation 4.1) in all three experiments (across defocus, across coma and across relative angle). Data are averaged across all subjects in each group. Optical predictions (in terms of Strehl Ratio) anticipate a benefit across defocus for a range of 0.85 D, for amounts of coma between 0.15 and 0.35 µm and for a range of relative angles between coma and astigmatism of 60° (0°-60°)[28]. Very consistently across experiments, the non-astigmatic group shows improved VA when coma and astigmatism are combined. The group with habitually corrected astigmatism does not show a clear benefit by adding coma to astigmatism, while for the habitually non-corrected astigmatic group, VA is decreased when adding coma. Altogether non-astigmatic subjects show a very similar trend to that expected from

optical simulations. VA improved in a range of 0.7 D of defocus, in the tested range of coma (0.11 to 0.41 µm), and for a range of relative angle of 60°. However, in the other two groups the visual findings differ from optical predictions. While all experiments were performed under identical optical conditions for all subjects, the presence of natural astigmatism seems to be associated with the lack of correspondence between visual benefit and optical benefit. The disagreement is high in subjects that are habitually exposed to astigmatism (group 3). We explored the correlation between the predicted optical benefit (in terms of SR) and the measured visual benefit (in terms of VA), for all the tested optical conditions. We found significant correlations for non astigmatic subjects (r=0.67, p=0.008) and habitually corrected astigmats (r=0.59, p=0.027). There was no correlation between optical predictions and visual measurements in habitually un-corrected astigmats (r=0.44, p=0.12).

Figure 4.5 shows the visual benefit (averaged values across experiments 1, 2 and 3 for each subject) as a function of the amount of natural astigmatism. Subjects from each group are identified by different colors. Most non-astigmatic subjects experience a visual benefit by adding coma and astigmatism (up to x1.4). Visual benefit for habitually corrected astigmats is close to 1, whereas for habitually un-corrected astigmats is less than 0.8.

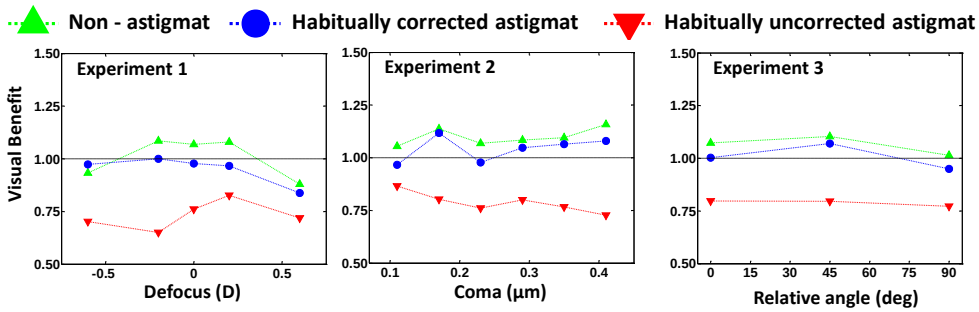

Figure 4.4. Averaged values of Visual Benefit of adding coma to astigmatism for the 3 groups, (non-astigmatic, in green triangles; habitually corrected astigmatic subject in blue circles; habitually non-corrected astigmatic subject in red triangles); Experiment 1: Combined astigmatism (0.5 D) and coma (0.23 µm), as a function of defocus. Experiment 2: Combined astigmatism (0.5 D) with various amounts of coma. Experiment 3: Combined astigmatism and coma (average of various amounts) as a function of relative angle. Error bars stand for half standard deviations.

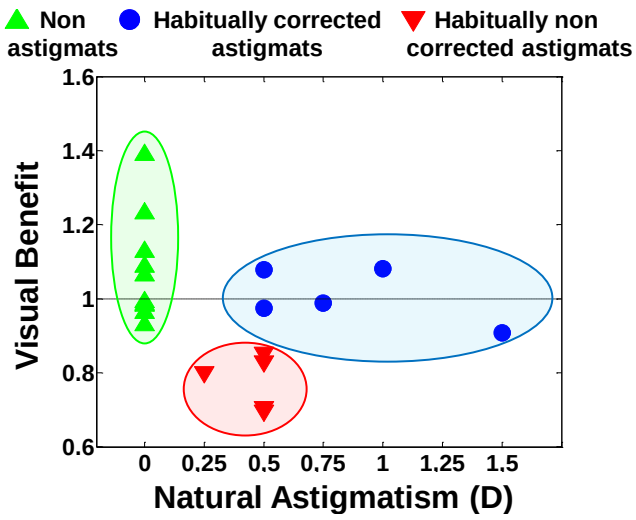

Figure 4.5. Visual benefit of adding coma to astigmatism over astigmatism alone averaged across experiments 1, 2 and 3 for each subject, as a function of the amount of natural astigmatism. Non astigmats are represented by green triangles, habitually corrected astigmats by blue circles and habitually non corrected astigmats by red triangles.

We found the difference across groups to be very robust, regardless the axis of astigmatism of the eye. However, we explored potential relationships between the angle of the natural astigmatism of the subjects and the visual acuity for fully corrected optics, astigmatism alone (0.5 D at 45°), and combined astigmatism (0.5 D at 45°) and coma (0.23 µm at 45°). Figure 4.6 shows absolute decimal VA, under three different conditions: 1-Full correction of aberrations, 2- 0.5 D of astigmatism and 3- Combined coma and astigmatism (from experiment 1: 0.23 µm of coma, 0.5 D of astigmatism at 45° and a relative angle of 0°). Natural astigmatism is plotted in the range of 0° to 90° (as the non-habitually corrected astigmats experience retinal images in the two orientations).

We found that when the axis of natural astigmatism was aligned with the axis of the induced astigmatism, the effects are significantly stronger. Best performance in the presence of astigmatism only (0.5 D of astigmatism at 45°) is achieved by habitually non-corrected subjects with natural astigmatism axis close to 45° or 135° (Subjects 17, 18, 19 and 20). In those subjects decimal VA in the presence of astigmatism is almost as high as their VA when all aberrations are corrected (ratio between VA with 0.5D of astigmatism and with all aberrations corrected: 0.97). The lack of visual

improvement when adding coma to astigmatism appears rather un-affected by the natural axis of astigmatism.

Figure 4.7 shows the Visual Benefit (equation 4.1) of adding coma to astigmatism alone, averaged per group, for each experiment (across defocus, across coma and across relative angles, 7A) and average across experiments (7B). Non astigmatic subjects experience an increase in VA when adding coma (visual benefit of 1.07, on average), habitually corrected astigmatic subjects do not experience an increase in VA (visual benefit of 0.99, on average) whereas habitually non-corrected astigmatic subjects show a decrease in VA when coma is added (visual benefit of 0.79, on average). Differences between non-astigmats and habitually non-corrected astigmats, and between habitually corrected-astigmats and habitually non-corrected astigmats are statistically significant in all cases.

4.3.2 Deleterious effect of astigmatism on visual acuity across groups

Differences across groups were also found in VA with astigmatism alone, and VA with all aberrations corrected. Habitually non-corrected astigmatic subjects showed relatively higher VA when all aberrations are corrected, and remarkably appeared to be insensitive to the addition of 0.5D of astigmatism, as opposed to the non-astigmatic subjects, and the habitually corrected astigmatic subjects, who experienced a significant decrease in VA when astigmatism was induced.

Figure 4.6 shows that the effect (little impact of induced astigmatism on VA) is larger when the axis of the natural astigmatism is parallel or perpendicular to that of the induced astigmatism (45° in this experiment), in habitually un-corrected astigmatism. We compared decimal VA across groups in the absence of low and high order aberrations (Figure 4.7A) and after induction of astigmatism (0.5 D at 45°, Figure 4.7B). Figure 4.7C shows the relative decrease (visual degradation) of inducing astigmatism. Fully corrected VA was not statistically significantly across groups. However, in the presence of astigmatism, VA was statistically significantly higher in habitually non-corrected astigmatic subjects than in non-astigmatic subjects ($p<0.01$) and than in habitually corrected astigmatic subjects ($p<0.05$). Inducing 0.5 D of astigmatism in non-astigmatic subjects produced a decrease in VA by 23%

and in habitually corrected astigmatic subjects by 21%, whereas in habitually non-corrected astigmatic subjects the decrease is only 5%.

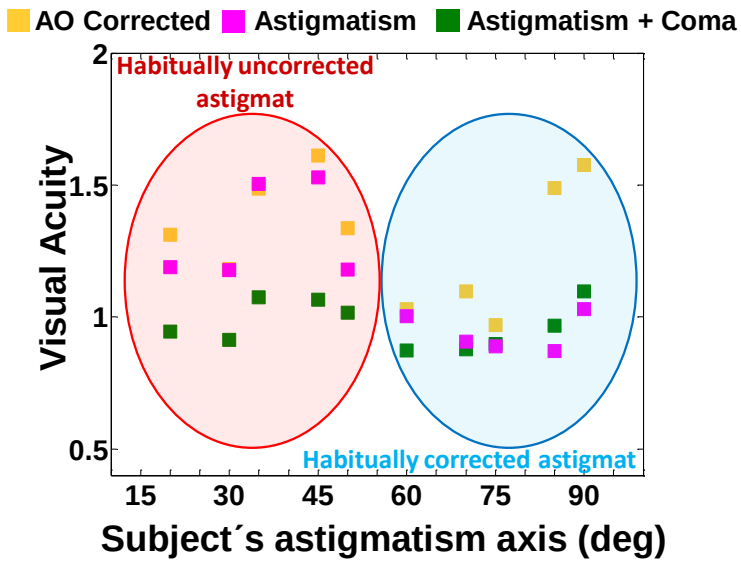

Figure 4.6. VA in all astigmatic subjects (habitually corrected and habitually non-corrected) as a function of the axis of their natural astigmatism (from 0 to 90°), for all aberrations corrected, yellow squares; combination of coma and astigmatism (average from experiments 1 and 2), green squares, and or 0.5 D of astigmatism, magenta squares.

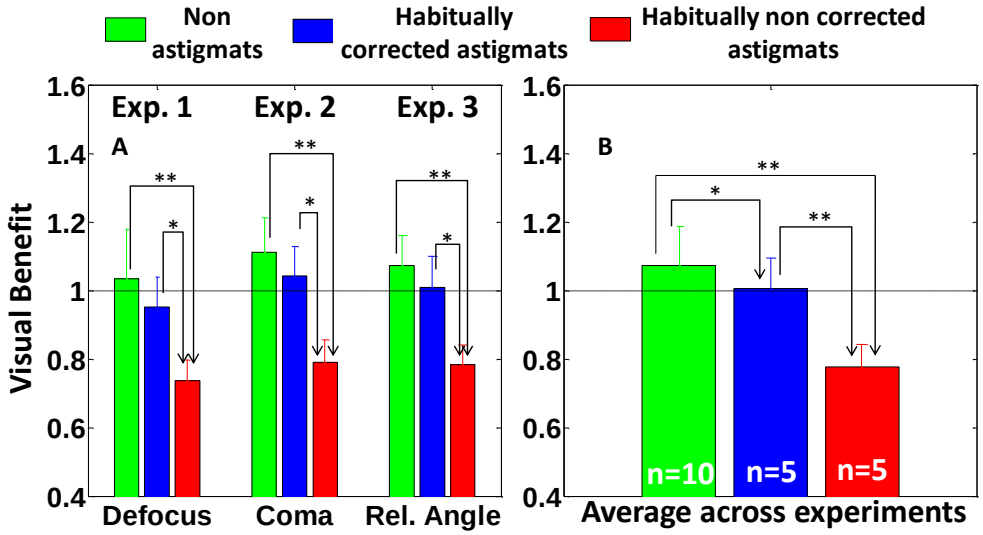

Figure 4.7. Visual Benefit of combining astigmatism with coma for the three groups. A For the three experiments; B Averaged across experiments. Error bars stand for half standard deviations; ** stands for $p<0.001$ and * stands for $p<0.05$.

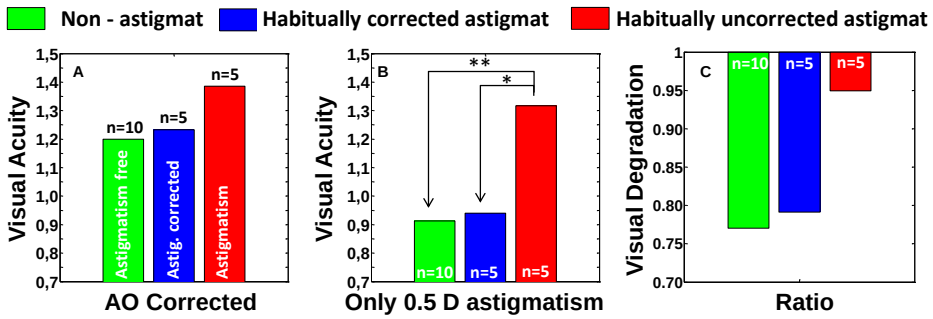

Figure 4.8. A. Decimal VA when all aberrations are corrected. B Decimal VA, for 0.5 D of astigmatism only. C Visual degration (Ratio of data from A and B) when 0.5 D of astigmatism is added. Data are averaged across subjects in each group; ** stands for<0.001 and * for p<0.05.

4.4. Discussion

In the previous chapter we had shown that optical interactions between astigmatism and coma can result in an improvement in optical quality[28]. We predicted that adding amounts of coma between 0.15 and 0.35 µm to 0.5 D could lead to an increase in peak Strehl Ratio values, in the absence of other HOA, with a peak improvement of 27% for 0.23 µm of coma. The optical predictions were illustrated by improvements in VA in two subjects. In the present chapter we extended the initial sample to 20 subjects, and found that not all subjects improved as predicted by the optical simulations. In fact, we found that despite all subjects being measured under identical optical conditions, the visual improvement produced by adding coma to astigmatism seems to be highly dependent on the presence of natural astigmatism, and whether this is habitually corrected or not. We have shown that non-astigmatic subjects generally improve VA (by a factor of 1.11) when coma (ranging from 0.11 to 0.35 µm, experiment 2) is added to 0.5 D of astigmatism (data from Experiment 2), while naturally astigmatic subjects do not experience the predicted improvement. Habitually non-corrected astigmats actually experienced a decrease in VA when adding coma to astigmatism (by a factor of 0.79). In these experiments (as in the computer simulations), the natural aberrations of the eye were corrected, and identical aberration patterns were produced in all subjects, therefore the different visual performance found across groups must arise from a neural

component. The strong influence of the presence of natural astigmatism (and whether this is habitually corrected or not) on the response is suggestive of prior neural adaption to astigmatism. The high tolerance to the induction of astigmatism in subjects with habitually non-corrected astigmatism may be indicative of an adaptation to astigmatism in these patients (and this being disrupted by the addition of coma).

Very interestingly, habitually non-corrected astigmatic subjects show a high tolerance to astigmatism despite the fact that blur induced by astigmatism is troublesome[47]. This effect could result from neural adaptation to astigmatism, which would mitigate its deleterious effects on vision[77]. Performance adaptation to defocus blur has been reported before resulting into an improvement of VA[73,75,78]. Also, we have recently reported shifts in the perceived non astigmatic-defocused image after a brief period of adaptation to astigmatism, indicating that the perceptual adaptation to blur can be selective to the orientation of the blur.

Habitually non-corrected astigmats can easily change the state of accommodation along the Sturm interval, and are not necessarily adapted to blur in a particular orientation. Depending on the characteristics of the target and the availability of the different focal lines a different value of accommodation may be chosen to provide the best visual performance[79]. The presence of astigmatic blur seems to provide blurred images in the two orientations (see figure 4.1).

We found larger effects in habitually non-corrected astigmats with the angle of natural astigmatism closer to 45 and 135° but our experiments were not designed to match the angle of the induced astigmatism to the angle of astigmatism of the subject (in all cases, the astigmatism was induced at 45°). Ongoing experiments in our lab will try to further clarify this point by angle-specific tests that will take into account the angle of the natural astigmatism of the subject.

Also, in our sample, habitually non-corrected astigmats show high VA under full correction of all low and higher order aberrations, indicating no sign of meridional amblyopia resulting from uncorrected astigmatism. This fact is not entirely surprising since amounts of astigmatism leading to meridional amblyopia are usually higher than 1 D, and amblyopia has a higher

prevalence in subjects with both meridians myopic, rather than hyperopic astigmats [80,81].

Our results show different responses between habitually corrected and habitually non-corrected astigmatic subjects. Habitually corrected astigmatic subjects tend to experience less benefits of adding coma to astigmatism than non-astigmatic subjects, but they definitely show lower tolerance to the induction of astigmatism than habitually non-corrected astigmatic subjects. An interesting question is whether a period of astigmatic correction would alter the response (both in terms of benefit of coma addition, and tolerance to astigmatism) of the habitually non-corrected subjects. The question is relevant for a deeper understanding of the relationships between optical and visual performance (and in this particular study the implications of coma and astigmatism interactions), but also of important practical significance, as many contact lens wearers have their astigmatism typically left uncorrected [82]. In fact, the adaptation to an astigmatic prescription has been largely debated in the clinical literature[83], and it has been reported that adaptation to changes from one astigmatic prescription to another may be limited and highly dependent of age[84]. An intriguing open question is whether these adaptation effects, in case they occur, require short periods of time, as shown in the shift of the perceived focused image by Sawides et al.[72], longer periods, up to 2 hours of adaptation, as for the improvement in VA for defocus blur[75], or even longer periods to become fully adapted to a new prescription. The study of the time-course of adaptation mechanisms to astigmatism (or its correction) is an interesting open question, which has been addressed in our lab, following the results of this thesis [46].

Most of the works aiming at evaluating the visual function measure the VA of a subject. Measurements of VA are much faster but do not produce as much information as measuring the contrast sensitivity function (CSF). By measuring the CSF information at different frequencies and meridians can be obtained. In the next chapter we will evaluate the improvement obtained in terms of CSF when correcting the aberrations with an AO system.

Chapter-5 Contrast Sensitivity benefit of adaptive optics correction

This chapter is based on the paper by de Gracia et al.: “Contrast Sensitivity benefit of adaptive optics correction” *Journal of Vision* **11**, (2011b).

The coauthors of this study were Susana Marcos, Ankit Mathur and David Atchison.

The author of this thesis performed the simulations of the contrast sensitivity function presented in the paper, designed and run the experiments and analyzed the results.

As a result of this work differences between the expected improvements of the adaptive optics corrections and the improvement in contrast sensitivity were identified. Also the lower CSF at oblique orientations after correction of the optical aberrations despite the isotropic AO-corrected MTF confirms the neural origin of the oblique-effect.

5.1. Introduction

The advent of laser systems and interferometry in the 1960s allowed determination of the neural contrast sensitivity function by bypassing the optics of the eye [85]. Recently adaptive optics has allowed the projection of any type of stimulus to the retina under corrected optical aberrations. Several studies have studied the visual benefit of correcting high order aberrations on visual acuity [19,22,86] and other visual tasks such as familiar face recognition [23]. An improvement in visual performance is observed in the majority of the cases, although to which extent the visual system exploits the increase of optical quality is not fully clear. Despite the expected direct improvement of the Contrast Sensitivity Function (CSF) by improvement of the Modulation Transfer Function (MTF) upon correction of optical aberrations, this has been relatively little explored, and the relationship between the improvement in the MTF and the corresponding improvement in the CSF is somewhat controversial. In their seminal work, Liang and Williams showed a maximum increase in the CSF by a factor of 6 for 27.5 c/deg, although comparisons between MTF and CSF improvements were not reported [14]. In another work Yoon et al. showed improvements of CSF up to a factor of 3 in one subject and up to 5 in another when the improvements predicted by the MTF calculations were up to a factor of 20 [19]. A recent study compared the improvement in the CSF and MTF for different age groups with correction of optical aberrations, and found that although the CSF values were lower for older observers they did benefit more from the AO correction than younger observers [87]. They found optical benefits of up to a factor of 2 for a spatial frequency of 18 c/deg, slightly lower than the visual benefit that they found in the CSF (factor of 2.5 for the same spatial frequency of 18 c/deg). On the other hand, another study reported similar increases (by up to a factor of 8) both in the CSF and the MTF, although it appears that both the CSF and MTF improvements were not defined similarly [88]. However, most of the studies reported a much higher AO/no AO ratio for the MTF than for the CSF [19,25]. Yoon et al. attributed the differences to imprecision in the AO corrections [19].

On the other hand the CSF measured after correction of aberrations should not exceed the neural transfer function. Campbell and Green measured this function by direct projection of interference fringes on the retina. The reported ratio of the standard CSF (under natural viewing) and the CSF

measured bypassing the optics of the eye (neural CSF) ranged from 1 for spatial frequencies lower than 5 c/deg to 5 at 40 c/deg (for 5.8-mm pupils). These values would represent an upper limit to the improvement of CSF expected when correcting the optical aberrations of the eye.

Classical studies showed differences in the CSF thresholds at different orientations. Typically the horizontal CSF exceeds the vertical CSF, and the CSF is lowest for oblique orientations. This phenomenon has been known as the "oblique effect" [89,90]. These psychophysical measurements have a good correspondence with the preferred neuron selectivity to different orientations shown by neurons in the visual cortex [91]. Interestingly, it has been shown that perceptual learning can improve the orientation selectivity of neurons in the primary visual cortex effectively promoting spatial interactions and resulting in an increase in contrast sensitivity, suggesting that not only optical and physiological factors, but also neuronal plasticity of the visual cortex in adults play a role in perceptual contrast sensitivity [92,93]. On the other hand a recent study of Murray et al. postulates that optical factors could contribute to this oblique effect [88].

In this study we will explore the limits of the visual improvement due to the optical improvements on the image projected on the retina by measuring the CSF in monochromatic and polychromatic conditions under natural aberrations and after AO correction for a wide range of angles and frequencies.

5.2. Methods

5.2.1 Adaptive Optics set-up

A custom-developed Adaptive Optics system was used in the study to correct and induced selected aberrations. The system has been described in detail in previous publications [47,48] and in the chapter of methods of this thesis.

5.2.2 Subjects

Four subjects aged 28 to 56 years were tested. Subjects S1 and S2 were two of the authors and experienced observers in psychophysical trials. Subjects

S3 and S4 were naïve and unacquainted with the purpose of the study. Table 5.1 shows the refractive profile of the subjects.

Subject #	Age	Defocus (D)	Astigmatism (D)	Angle (°)
S1	56	-2.25	-0.25	50
S2	28	0.25	-0.25	170
S3	28	0	0	~
S4	29	0	-0.25	90

Table 5.1. Age and refractions of the subjects of the study.

5.2.3 Experimental protocol

Subjects were instilled with one drop of 1% cyclopentolate 20 minutes before the experiment started, with one additional drop applied every 90 minutes

Before the CSF measurements, the focus setting for each condition (all aberrations corrected; natural aberrations; natural aberrations with astigmatic correction) was determined. The subjects were asked to find the best focus while viewing a Maltese cross target, by moving a Badal system. The setting was repeated 5 times, and the average taken as the correcting focus setting.

CSFs were measured for six spatial frequencies (1.9, 3.8, 7.6, 15.2, 22.7 and 30.3 c/deg) and four orientations (0, 45, 90, 135 deg) with a staircase (2 down/ 1 up) four Alternative Forced Choice procedure (4 orientations for a fixed frequency) in steps of 0.05 log contrast as previously explained in section 2.4.3. Measurements started between 0.2 and 0.4 log units above threshold and were considered finished after 7 reversals were completed, and the threshold was determined from the average of the last 6 reversals. The stimulus was presented after an auditory tone during 0.5 s. Each measurement was repeated 3 times, and deemed satisfactory if the standard deviation of the trials was less than 0.2 log units; most standard deviation was less than 0.1 log units. Measurements with and without AO-correction of aberrations were randomized. For each spatial frequency, four simultaneous staircase procedures were interleaved (one for each orientation). Aberrations were corrected across a 5.2-mm pupil. An artificial stop projected to the eye provided a 5-mm pupil for viewing the visual display.

Aberrations were measured immediately before and after a CSF measurement. A closed loop correction was generated immediately before and after the CSF measurements for the AO condition.

Monochromatic CSFs measurements were performed by placing an interference filter (peak transmission 550 nm; FWHM 10 nm). Polychromatic CSF measurements were performed for the extended spectral range of the projector lamp (EPSON EMP1810). In order to achieve equal luminance values at the pupil plane in the polychromatic conditions the interference filter was replaced by a neutral density filter (ND 1.3).

Each complete CSF measurement took about 4 hours (including all frequencies, angles, and 3 repetitions). Measurements were conducted for monochromatic and polychromatic light (2 subjects); AO and non-AO corrected (all 4 subjects), and astigmatism corrected (2 subjects). Subjects were allowed to take breaks during the session. A complete set of data per subject was collected in between 2 and 5 sessions. Before the actual runs, a training session was conducted (with only one frequency) in order to familiarize the subjects with the protocols and tasks.

5.2.4 Wave aberrations and MTF calculations

Wave aberrations were fitted by 7^{th} order Zernike polynomials. The coefficients were measured for a 5.2 mm pupil and then re-scaled for a 5-mm pupil. The MTF calculations were performed using standard Fourier optics in Matlab (Mathworks, Naticks, MA) from the wave aberrations, for 5.0-mm circular pupils and 550-nm wavelength. The defocus term was set to 0 for the AO-corrected aberrations, and to the value corresponding to the defocus setting shift (with respect to the AO-condition) for any other condition. For the MTF calculations, the average of the Zernike coefficients measured before and after a set of CSF measurement was used.

5.3. Results

5.3.1 Measurement and correction of ocular aberrations

Insets in Figure 5.1 show the wave aberrations (natural and AO-corrected) for the four subjects of the study. Tilts and defocus were set to zero for representation. The RMS of the 4 subjects decreased after correction of their aberrations to an average a 20% of the natural RMS. Figure 5.1 shows the corresponding RMS values for natural and AO-corrected wave aberrations (5-mm pupils) and the percentage of correction.

The wave aberrations and RMS values shown in Figure 5.1 correspond to averages of 36 common measurements to all subjects during the experiment (6 frequencies, with 3 repetitions of each trial before and after each trial). RMS standard deviations (for repeated measurements of the same condition throughout the session range from 0.05 to 0.07 μm.

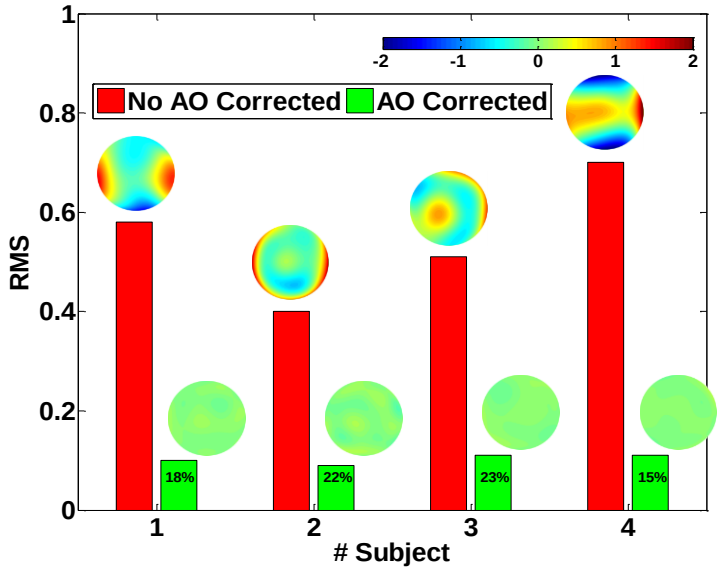

Figure 5.1. RMS values of the four subjects, with natural aberrations (red) and after AO-correction (green). Insets over each bar show the average wavefront of all 36 measurements for the monochromatic condition. The colorbar shows the common scale of all wavefronts. The percentages represent the level of correction with respect to the natural aberrations of the subjects.

5.3.2 MTF and CSF measurements

Figure 5.2 shows 2-D MTFs and Figure 5.3 shows 2-D CSFs for the 4 subjects with their natural aberrations (no AO) and after the correction of their high order aberrations and astigmatism. The MTFs were computed from the wave aberrations at the same focus as for the CSFs measurements. The CSFs are interpolations for measurements at the selected spatial frequencies and orientations. With correction of astigmatism and HOA, there is an increase in the symmetry of the MTF, increase in contrast, and a clear extension of the spatial frequency range. The oblique effect (less sensitivity at 45 and 135 deg) in the CSF is apparent both in the uncorrected and AO-corrected CSFs. There is a slight extension in the CSF spatial frequency range with correction.

The levels of optical correction of our subjects (S1 , S2, S3 and S4) achieved 80%, 63%, 81% and 87% MTF-values with respect to the diffraction limited MTF (values averaged across angles and between 1.9 and 30.3 c/deg).

The MTFs at 0 and 90 deg orientations are higher by 10% than the MTF at 45 and 135 deg, for natural aberrations However, the difference between horizontal/vertical and oblique meridians decreases to 1% when all aberrations are corrected. However, the CSF is higher at 0/90 deg than at 45/135 deg both for natural aberrations (by 10%) and after correction of aberrations (by 8%). These data are averaged across subjects and spatial frequencies (from 1.9 to 30.3 c/deg range for the MTF; and all the measured spatial frequencies of the CSF).

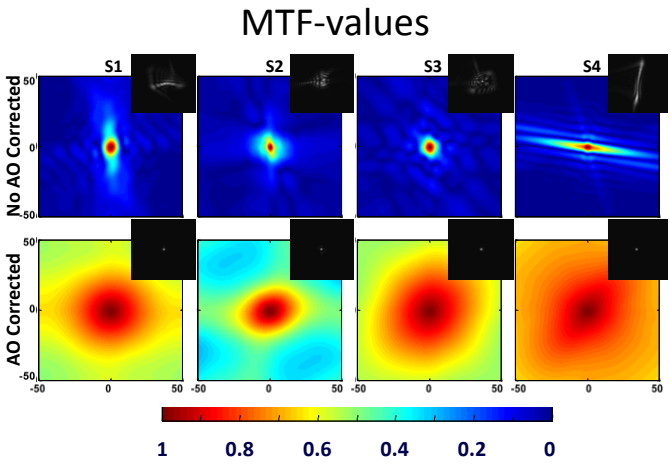

Figure 5.2. 2-D MTFs for the four subjects of the study. Upper row: under natural aberrations. Lower row: under AO-correction of astigmatism and HOA, and their corresponding PSFs (insets). Data are for best subjective focus in each condition. MTFs are represented up to ±50 c/deg. PSF window size= 50 μm.

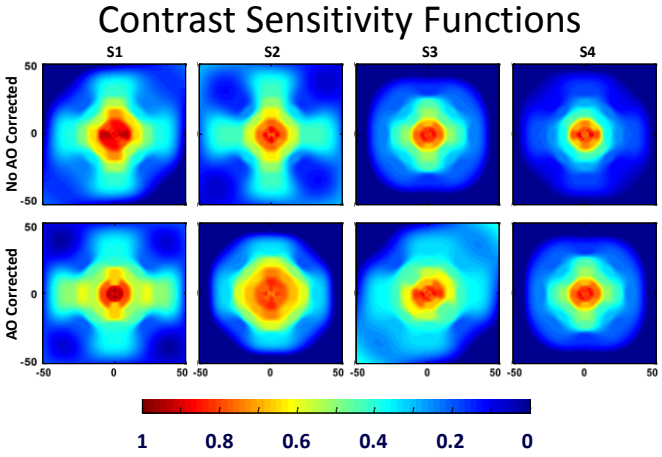

Figure 5.3. 2-D CSFs (linear interpolations) for the four subjects. Upper row: under natural aberrations. Lower row: under AO-correction of HOA, for best subjective focus in each condition. CSFs are represented up to ±50 c/deg.

Each subject-data (AO and No AO) has been normalized by its maximum that could have been obtained for AO or No AO corrected conditions.

5.3.3 MTF and CSF improvements with AO-correction as a function of spatial frequency

Figure 5.4 shows the improvement with AO-correction in the MTF (MTF_{AO}/MTF_{NoAO}) and in the CSF (CSF_{AO}/ CSF_{NoAO}) as a function of spatial frequency, and a comparison of the MTF and CSF ratios (with the y-axis appropriately scaled to make them comparable). The MTF improves on average by a factor of 8, and the CSF on average by a factor of 1.15. The improvement in the MTF increases steadily with spatial frequency (from ×1.1 at 1.9 c/deg to ×15 at 30.2 c/deg). The CSF increases only for spatial frequencies higher than 7.6 c/deg, e.g. by ×1.52 at 22.7 c/deg). For intermediate spatial frequencies, the improvement in the CSF and MTF correlate well (although they differ by a factor of 7), but not for the lowest and highest spatial frequencies.

5.3.4 MTF and CSF improvements with AO-correction as a function of orientation

Figure 5.5 shows the improvements with AO-correction in the MTF (MTF_{AO}/MTF_{NoAO}) and (CSF_{AO}/CSF_{NoAO}) as a function of orientation, and a comparison of the MTF and CSF ratios (with the y-axis appropriately scaled to make them comparable). Data are averaged across central frequencies (15.2 and 22.7 c/deg) and subjects. On average, there is a relatively good match between the most improved meridians (45 and 135 deg) and least improved (0 and 90 deg) in both the MTF and CSF.

At the individual level, although the improvement in the oblique orientations are higher than at 0/90 deg orientation, the AO-corrected CSFs are lower than in the oblique meridians than at 0/90 deg.

Figure 5.6 shows radial profiles of figures 5.2 and 5.3 for the individual subjects. In these graphs it can be seen how the values at 0 and 90 degrees are higher than those obtain at 45 and 135 degrees for the condition of natural aberrations both in MTF (10%) and CSF (10%) values, and how this difference is still present on the CSF values (8%) for the AO condition but is not present anymore in MTF values (1%).

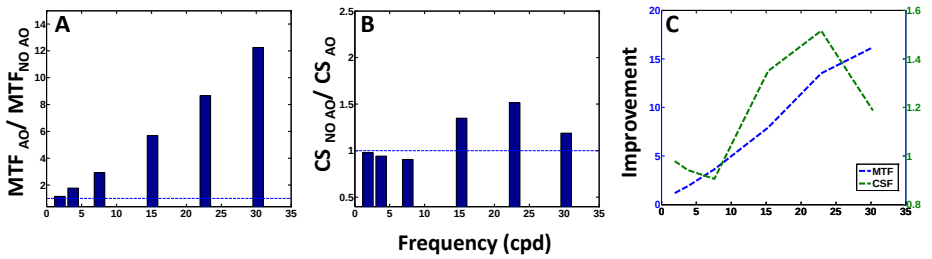

Figure 5.4. MTF AO/No AO ratios (A) and CSF AO/No AO ratios (B) as a function of spatial frequency, averaged across orientations and subjects, and comparative ratios (C).

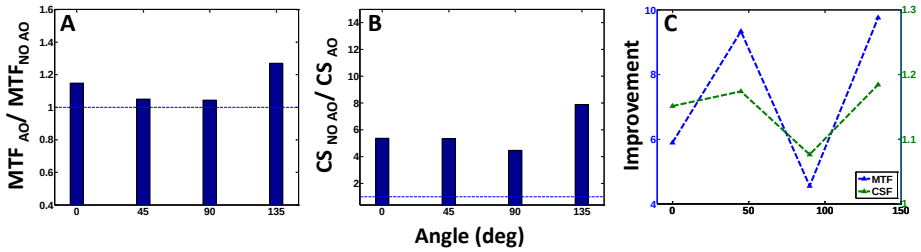

Figure 5.5 MTF AO/No AO ratios (A) and CSF AO/No AO ratios (B) averaged across mid-spatial frequencies (15.2 and 22.7 c/deg) and subjects. (C) Comparative ratios are averaged across all frequencies and subjects.

5.3.5 CSF improvements in polychromatic conditions

Figure 5.7 compares the improvements in monochromatic and on polychromatic CSFs, as a function of spatial frequency and angles. The average improvement in polychromatic light is consistently lower for all subjects and angles (averaged across frequencies, and for most of the spatial frequencies (averaged across angles) than under monochromatic conditions (ratio of improvements mono/poly 1.2±0.2).

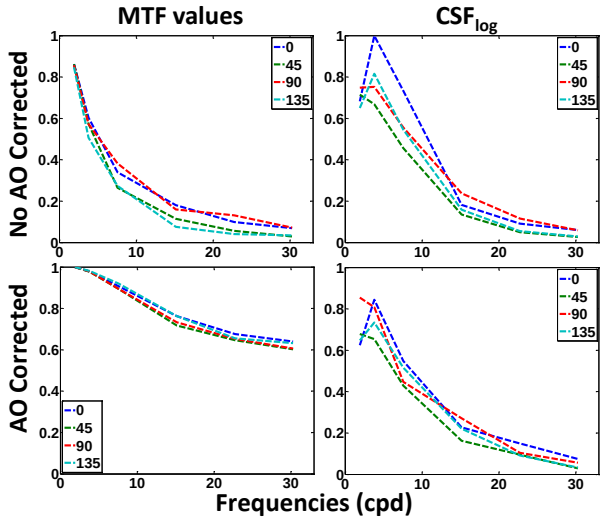

Figure 5.6. MTF (right column) and CSF (left column) cross-sections (at 0, 45, 90 and 135 deg meridians) for AO-corrected aberrations (upper row) and natural aberrations (lower row), for all subjects.

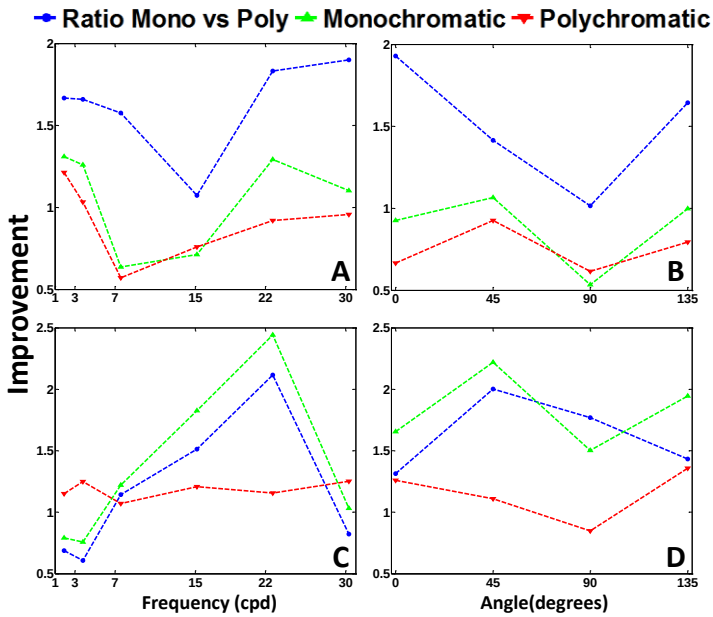

Figure 5.7. CSF AO/CSF no AO for monochromatic (green line) and polychromatic (red line) light for subjects 1 (top) and 2 (bottom), averaged across angles as a function of the frequency (left column) and averaged across central frequencies (7.6, 15.2, 22.7 c/deg) as a function of the angle (right column).

5.4. Discussion

We have shown improvements in contrast sensitivity upon correction of HOA. However, despite a large increase in the modulation transfer function (by a factor of 8 at intermediate spatial frequencies), the corresponding improvement in the contrast sensitivity function (by a factor of 1.4 is minor), for 5-mm pupils. The AO-corrected MTF is close to diffraction limit (within 80% on average across subjects), with the difference likely arising from residual aberrations. The lack of correspondence between the improvement in the MTF and CSF has been reported by some, but not all studies. Yoon & Williams reported an improvement in the CSF by ×6 in one subject and ×3 in another subject, for 6-mm pupils, where the expected improvement in the MTF was ×20 times [19]. They attributed the lower apparent performance in the CSF than in the MTF to a single set of optical aberrations (measured at the beginning of the session) in the calculation of the MTF. We minimized this potential source of error by using the average of set of Zernike coefficients measured at various times during the measurements. Other studies suggested a good correspondence between the optical and perceptual contrast increases. Murray et al. used a metric expressed in dB for the CSF improvement (which implied multiplication by a factor of 20) but not for the CSF, and found a correlation between the improvement in the CSF and the MTF for spatial frequencies of 12 and 16 c/deg and 6-mm pupils, with a slope near 1 [88]. On the other hand, another study reported optical improvements ranging from 1 to 3 times for spatial frequencies ranging from 1 to 18, which were comparable, or in fact slightly lower than the improvements found in the CSF, for 6-mm pupils [87]. It is not clear to which extent their optical computations (which involved convolutions of the Gabor targets with the estimated MTFs) differed from direct calculations of the MTFs. Most of the studies focused on low and intermediate spatial frequencies. The lack of improvement in the CSF for low spatial frequencies is consistently found in all studies. Yoon et al. also reported relative less improvement for the highest spatial frequencies [19], as we also found in the current study.

An excellent match between the CSF ratio and in MTF ratio following a change in the optics have been widely reported, when the change consisted

of an optical degradation, such as defocus [94-96] or an increase in the optical aberrations, i.e. induced by LASIK surgery [97]. A decrease in the MTF therefore seems to produce a similar decrease in the CSF. However, the results of our study (as that of Yoon and Williams, 2002) suggest that an increase in the MTF (producing almost diffraction-limited retinal image) does not produce a similar increase in the CSF. The limits imposed by the neural CSF are likely the reason for this moderate improvement in the CSF, as the CSF_noAO cannot exceed neural limits.

Campbell and Green found that the ratio between the CSF measured with interference fringes and the one obtained through the natural optics of the eye was almost one for low frequencies and went up to ×5 at 40 c/deg (for 5.8-mm pupils) [85]. These results are consistent with the CSF AO-corrected/CSF natural ratios of our study (up to a ×4 for 5-mm pupils) and those found by Yoon and Williams (up to ×5 for 6-mm pupils) [19].

Our results are consistent with the well-accepted neural origin of the oblique effect. The lower CSFs at 45 and 135 deg (relative to 0 and 90 deg) also occurs under AO-correction of aberrations, despite rather symmetric AO-corrected MTFs. On the other hand, the fact that the AO/no AO ratios show similar dependencies with meridian (Figure 5.6) is indicative of some optical contribution to the oblique-effect under natural aberrations, as in these subjects the natural MTF is on average higher at 0 and 90 deg than at 45 and 135 deg. Interestingly, all our subjects showed better optics at 0/90 deg than 45/135 deg. Whether the higher neural specialization in the visual cortex at 0/90 deg arises from a typically better optical quality at this orientation is still an open question [88,98,99] . Alternatively, our data (particularly in Subject 4) are suggestive of visual adaptation mechanisms that overcome some of the optical losses at specific orientations. S4 shows a highly anisotropic MTF (horizontal meridian shows MTF values 2.58 times higher than the vertical), whereas the CSF tends to be much more symmetric (0.83). While a shift in the defocus (by 0.20 μm) would have led to a more symmetric MTF, at the circle of least confusion, repeated measurements on this subject confirmed the subjective focus preference of this subject at the selected defocus setting (used in the MTF computations and CSF measurements). A potential explanation to the apparent better visual performance at the optically degraded astigmatism is adaptation to astigmatism. In a recent study we

have shown a relative insensibility to astigmatism in habitually non-corrected astigmats which led to a better visual acuity than that predicted optically, and better than the visual acuity of non-astigmats with equivalent induced astigmatism [29]. These results are consistent with an early study where the notches of the CSF in the presence of astigmatism can be relatively well predicted by the optics (we have performed the MTF calculations for the set of coefficients of Zernike of S1 with second order aberrations fixed to 0 and adding 0.5 µm of astigmatism and the first notch in MTF correspond to the notch found for subject HS between 7 and 10 c/deg), as in that study astigmatism was induced, and not naturally present in the subjects (Apkarian et al. 1987). Interestingly in that study, the sensitivity loss produced by astigmatism occurred in a relatively narrow spatial frequency band (5 c/deg) that we could have missed in the frequencies tested. We measured the CSF under correction of astigmatism in 2 of the subjects of the study with significant natural astigmatism (S1 and S2), while leaving the HOA uncorrected. We did not find significant differences with respect to the CSF measured under natural aberrations (ratio=1.01), suggesting an adaptation to their natural astigmatism in these subjects.

As expected, the benefit of AO correction on the CSF was less in polychromatic than in monochromatic light. Chromatic aberrations have a more deleterious effects on the optics in the absence of HOA than under natural aberrations [59], and the expected MTF AO/noAO is lower in polychromatic light.

5.5. Conclusions

We compared the optical improvement of correcting high order aberrations and astigmatism using adaptive optics with the visual improvement in contrast sensitivity. The results of this chapter allow concluding that the optical benefit (in the MTF) exceeds the visual benefit (in the CSF) by a factor of 5. The improvement in the CSF by near diffraction-limited optics appears to be limited by neural contrast sensitivity and although the trend of the CSF results under AO correction is well described by the MTF, the magnitude of the impact of the correction is overestimated. The largest benefit in the CSF

occurs at intermediate spatial frequencies and as expected the benefit of aberration correction in the CSF decreases in polychromatic light.

The relatively lower CSF at 45/135 deg after correction of the optical aberrations (despite the isotropic AO-corrected MTF) confirms the neural origin of the oblique-effect. The tendency for a better optical quality at 0/90 deg might suggest an optical role in the neuronal meridional selectivity in the visual cortex. The lack of meridional correspondence in the MTF and CSF in subjects with natural astigmatism suggests spatial adaptation to astigmatism in these subjects.

CSF measurements performed in this chapter allowed to evaluate neural aspects of vision that where not possible to evaluate with the VA measurements shown in chapters 3 and 4.

Chapter-6 Experimental simulation of simultaneous vision

This chapter is based on the paper by de Gracia et al.: “Experimental simulation of simultaneous vision” Investigative Ophthalmology & Visual Science 54, 415-422, (2013).

The coauthors of this study were Carlos Dorronsoro, Álvaro Sánchez González, Lucie Sawides and Susana Marcos.

The author of this thesis designed and implemented the simultaneous vision system, programmed part of the software to control it, designed and run the experiments and analyzed the results.

The results shown in this chapter present a good correlation between optical quality measurements and the visual acuity performance of the subjects under simultaneous vision conditions.

The correspondence found sets the base for explaining how a simultaneous image is processed by the eye and the brain.

6.1. Introduction

Adaptive optics (AO) systems are useful to manipulate the aberrations to which a subject is exposed [19,22,28,40,47,100] as already shown in the introduction and in chapters 3 and 4. Many of the laboratory based AO visual simulators rely on deformable mirrors that can only modify relatively low amounts of high order aberrations (i.e. spherical aberration), limiting the ability to introduce phase patterns with discontinuities or reproduce bifocal patterns. AO systems based on Spatial Light Modulators [101,102] show much higher spatial resolution, allowing in principle steep slope changes in the wavefront, although they may be subject to additional limitations (i.e. chromatic effects) [103,104], and are still relatively pricey.

Although none of the current available solutions for presbyopia (the age-related loss of crystalline lens accommodation) restores the full dynamic capability of the young eye to change its refractive power upon an accommodative stimulus, there are multiple treatments that attempt to provide functionality for both near and far vision to the presbyopic patients as shown in the introduction chapter.

Simultaneous vision represents a new visual experience in which a sharp image is superimposed to a blurred replica of the same image, thus reducing the overall contrast. This situation occurs both when a bifocal/trifocal… solution is used or when the DOF is been increased while trying to preserve the visual performance at best focus by using different combinations of aberrations as shown in chapters 3 and 4.

The intended optical effect of the correction (driven by its design) is combined with the particular aberration pattern of the eye, so a given bifocal design does not produce the same optical through-focus energy distributions in all eyes. On top of the multiple designs, the near addition typically ranges from 1 to 4D [39].

Not all patients tolerate the contrast reduction induced by simultaneous vision. It is often argued that only those patients who learn how to automatically process the image, ignoring or suppressing the image components which are not in focus, adapt to simultaneous vision solutions. These mechanisms for adaptation remain to be elucidated, but are supposed

to rely on specialized and sophisticated (while automatic) neural processes that restore the physically degraded images to overcome their optical quality limitations.

To date, it is not clear if the lack of adaptation to multifocal vision has a physical or a neural origin, or whether they are combined. As shown in chapter 3, 4 and 5 the neural post processing has a key role in the final visual performance of the subject. A better understanding of optical and neural interactions in simultaneous vision bifocal corrections is critical to improve lens prescription.

To date, most studies of the outcomes of bifocal corrections compare visual clinical outcomes in patients prescribed with lenses available in the market [26,105-107]. Also, systematic evaluations of many of the available lenses are normally performed on bench (lacking from the optical, and of course, the neural complexity of a patient) [108-110].

In this chapter we present a study using the new simultaneous vision instrument described in section 2.2 of the methods chapter [51] that allows the experimental simulation of a pure simultaneous vision correction by combining two channels, one focused at near and the other focused at far. The system allows for experimental simulation of idealized bifocal corrections, i.e. isolated from factors inherent to the specifics of real corrections (i.e. lens flexure and fitting in a bifocal contact lens, tilt or decentration of a bifocal IOL), yet in the presence of the subject's own aberrations and neural response. The system allows investigation of fundamental questions associated with simultaneous vision, with a relevant practical interest.

In particular, this chapter addresses the impact of the amount of addition power on image quality and on visual performance with a simultaneous vision correction in an experimental setting. The additions used in this study ranged from 0 to 4 D, within the range of additions generally available in commercially available bifocal designs. To our knowledge, this is the first systematic study of the impact of the amount of addition on contrast degradation and Visual Acuity (VA). Using the new developed Simultaneous Vision Experimental Simulator, the study will respond to the following specific questions: what is more deleterious for vision: a large addition which

creates a low contrast defocused superimposed retinal image, or a small addition which introduces a smaller amount of defocus but two very close images superimposed? Is there an optimal (or a particularly suboptimal) addition? If found, are those specific to the subject, or relatively similar across different subjects?

6.2. Methods

6.2.1 Optical System

A compact instrument has been developed with two collinear channels that allow simultaneous projection of two overlapping images on the retina. A complete description of the system is shown in section 2.2 of the methods section.

For the purposes of the current study, Channel 1 was used to correct distance refraction, providing a sharp image in best focus. Channel 2 was moved to create superimposed hyperopic or myopic defocused images, while keeping Channel 1 fixed. As a result of the Badal optometer configurations, all powers refer to the pupil plane, not the spectacle plane. Fig. 6.1 compares the simultaneous vision as achieved with, for example, a diffractive bifocal intraocular or contact lens (top panels) with that produced with the Simultaneous Vision Simulator (lower panels). The bifocal lens produces a sharp image for far vision, superimposed to a defocused near vision image, in far vision (Fig. 6.1A) and a sharp image for near vision, superimposed to a defocused far vision, in near vision (Fig. 6.1B). Conversely, the Simultaneous Vision Simulator produces a myopic defocus (positive dioptric correction, which mimics a near addition) by Channel 2, and a far sharp image in Channel 1, allowing testing of the impact of a near addition on far vision (Fig. 6.1C). Also, a hyperopic defocus (negative dioptric correction) in Channel 2 allows testing the impact of a defocused far image (Fig. 6.1D). For the purposes of this study, best focus in either channel is referred as 0 D, and the addition is therefore defined as the refraction difference between Channel 1 and Channel 2.

6.2.2 Simulations

The optical degradation produced by pure bifocal vision was computationally simulated. These simulations provide a reference for the subsequent experimental testing of the system by means of an artificial imaging system, to establish predictions on pure optical bases. Defocused images were generated using standard Fourier Optics techniques [53]. The Point Spread Function (PSF) for the corresponding levels of defocus was generated, and the simulated image targets (of different sizes and contrast) were obtained by convolution of the original targets with the corresponding PSFs using custom-developed routines written in Matlab (Mathworks, Natick, MA, USA). Pure bifocal images were simulated by adding two images, one in focus and the other out of focus (i.e. the addition of two images one in focus 0 and the other defocused by 4 D will represent a bifocal simultaneous vision image with an addition of 4 D). The superimposed images were normalized dividing by 2. For the purposes of this simulation one of the added images was always in focus while the other varied in defocus from -4 to 4 D in 0.1 D steps. Simulations were performed for different letter sizes (5 to 50 arcmin) and 10 levels of contrast (white background, and letter luminance luminance level ranging from 0 to 0.9 times the white level). The Michelson Contrast (MC) inside the E-letter of the resulting superimposed images was then calculated.

6.2.3 Experimental measurements on an imaging system

The contrast loss in the simultaneous images was experimentally measured through the system, to evaluate the pure optical degradation. These experiments also served to test the system alignment and configuration (in the absence of the subject's aberrations) and were compared to computer simulations (above) and to visual performance in patients (below). Images through both channels were projected on an artificial imaging system consisting on a scientific CCD camera described in the methods chapter. The stimuli (presented on the CRT monitor and projected on the artificial imaging system's CCD through both channels) were Snellen E targets, similar to those in the computer simulations. Channel 1 was focused at far, and additions were achieved by moving the focus of Channel 2 from -4 to 4 D in 0.1 D

steps. Targets of different sizes (5 to 50 arcmin) and contrasts (black background, and white letters ranging from 0 to 0.9 times the white level of the monitor) were used. Monofocal control conditions were also tested, with high contrast (white on black) letters. Contrast degradation was estimated by computing the Michelson contrast inside the letter.

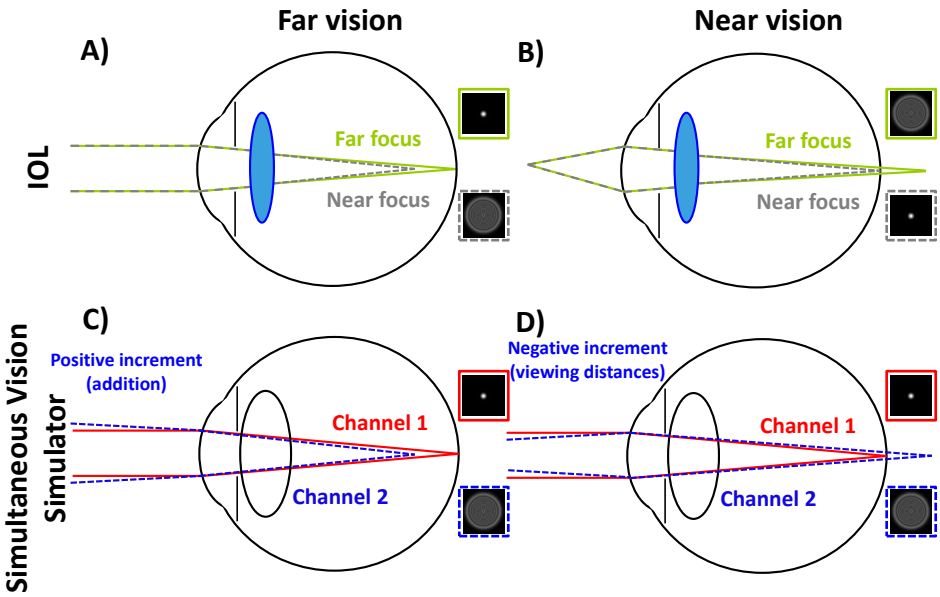

Figure 6.1. Schematic diagram of the near and far vision conditions produced by a bifocal intraocular (A, B) and those simulated in our study (C, D). PSFs and surrounding boxes represent the image projected in the retina by the rays with the corresponding color/line style.

6.2.4 Subjects

Four subjects aged 28 to 42 years (±34.5 years) participated in the study. All subjects were experienced observers, trained in different psychophysical tasks. Subjects S1 and S2 were emmetropes, and subjects S3 and S4 were myopic of -3 and -5.5 D, respectively. Both myopic subjects performed the experiments wearing their usual monofocal contact lenses correcting their far vision. All subjects had followed an ophthalmological evaluation before performing the experiments. Accommodation was paralyzed to simulate presbyopia (and to dilate the pupil) with periodic instillation of drops of 1% tropicamide. Subjects signed a consent form approved by the institutional review boards after they had been informed on the nature of the study and

possible consequences. All protocols met the tenets of the Declaration of Helsinki.

6.2.5 Experimental measurements in subjects

While keeping Channel 1 adjusted for subjective best focus at far, VA was measured for different amounts of defocus increments (i.e. additions) in Channel 2 ranging from -4 to 4 D. Measurements were performed in 0.5 D steps between -2 and +2 D of addition, and in 1-D steps between ±2 and ±4 D. Measurements with positive defocus increments in Channel 2 represent far vision with different near additions superimposed, while measurements with negative defocus increments in Channel 2 represent near vision in focus, in the presence of a defocused far image. A control condition was also tested by blocking Channel 1, therefore testing vision in a monofocal condition, from -2 D to 2 D (0.5 D steps) in Channel 2.

VA measurements were performed for high-contrast (HC, MC=1) and low contrast (LC, MC=0.33) targets, with white backgrounds. VA was measured using tumbling Snellen E letters in a four alternative forced choice procedure (2AFC) programmed in the Psychphysics Toolbox in Matlab [55]. The procedure was followed until 16 reversals were performed, or 50 letters were presented. The average of the 6 last reversals was taken as the subject's VA for that condition. A total of 39 measurements of VA were performed, 15 for each one of the bifocal conditions (HC, LC) and 9 for the monofocal condition. Measurements in one subject lasted typically between 4 and 5 hours.

The subject adjusted his/her best focus while looking at an empty black square (45 arcmin, also used as fixation stimuli in between VA letters) in monofocal conditions (through one channel at a time).

6.3. Results

6.3.1 Image contrast with simultaneous vision from simulations and experimental measurements

Measurements of image contrast degradation on a diffraction-limited imaging system acting as an artificial eye allowed us to test purely optical factors, in the absence of aberrations or neural factors. Figure 6.2 shows the normalized contrast of the targets imaged on the CCD of the artificial imaging system through both channels simultaneously, as a function of defocus in Channel 2 (blue lines), as well as the contrast of the computer simulated targets (black lines). The curves shown in each panel represent data for targets of different sizes (equivalent to decimal VA ranging from 0 to 1). Blue dashed lines represent the standard deviation of normalized contrast values obtained for different initial contrasts on the images captured on the CCD ($\pm$0.01 on average). As expected, the curves from both simulations and experiments on the artificial imaging system were highly symmetric. The slight asymmetry observed in the experimental curves may arise from some minor aberrations in the experimental system.

As the relative impact of the optical aberrations of the system varied across letter sizes, the experimental values of contrast shown in Figure 6.2 were divided by a factor (ranging from 0.67 for a letter size equivalent to VA=1.0 to 0.98 for a letter size equivalent to VA=0.1) to match the contrast in monofocal conditions (Addition=0 in the simulation and experiment). While for the largest letter tested (VA=0.1) the experiment and simulations yielded similar contrast degradation, discrepancies in the absolute contrast degradation increased when decreasing the letter size, likely as a result of the contrast loss introduced by residual aberrations in the system.

In both experimental and simulated bifocal images, the contrast loss varied with the amount of addition. The maximum contrast was obtained in all cases for monofocal vision (zero addition). The minimum contrast was obtained for values of addition ranging between 0.5 and 2 D depending on the letter size, while contrast increased for the largest amounts of addition. The contrast had a notch of maximum degradation (23 % with respect to the

target contrast, on average across letter sizes) in the 0.5-2 D addition ranges (depending on the letter size), while contrast degradation was less than 15 % (on average) in the 2.5-4 D addition range.

In all cases, contrast decreases rapidly when adding defocus (addition) in Channel 2. After reaching a peak in degradation, the image contrast is partially recovered, as it increases with higher defocus values. This analysis allows estimating sets of additions producing the largest contrast degradation for each letter size, as shown in Figure 6.3 for simulations and experiments. The range of additions that produced the largest image degradation followed a similar trend in simulations and experiments: between 1.8 D (for the largest letter tested: 50 arcmin, VA=0.1) and 0.3 D (for letters <10 arcmin, or VA>0.5) for the experimental images, and between 2.1 and 0.3 D for the simulated images.

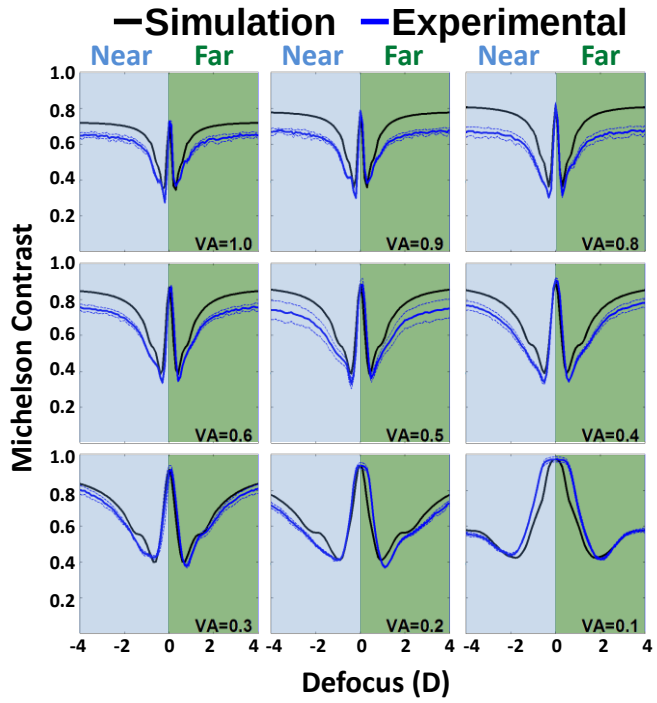

Figure 6.2. Comparison of the Michelson contrast obtained with computer simulations (black lines) and with the artificial imaging system (blue lines) as a function of the amount of addition. Each panel represents a different letter size (expressed in terms of the corresponding VA). Positive defocus (shaded green) represents far vision in focus in presence of a near defocused image (due to the addition). Negative defocus (shaded blue) represents near vision in focus (at different distances) in presence of a far defocused image. Data are for 4-mm pupils.

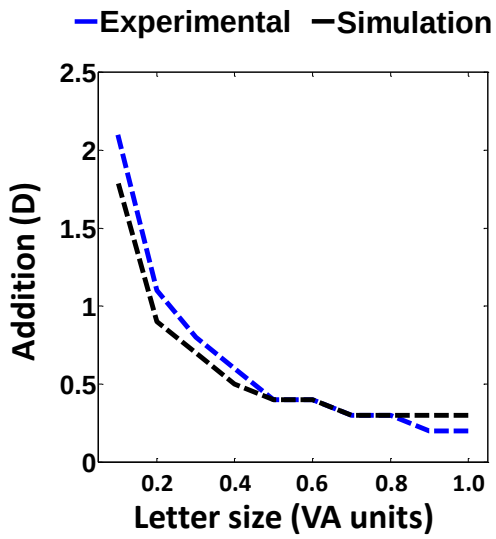

Figure 6.3. Additions that produced the maximum contrast reduction, as a function of letter size. Letter size is represented in VA units from 0.1 to 1 (equivalent to 50-5 arcmin).

6.3.2 Simultaneous vision in subjects

Figure 6.4 shows the individual measurements of VA for the four subjects of the study in three different conditions: High contrast (HC) and low contrast (LC) VA for bifocal vision and different additions (for Channel 1 focused at far, and at different focus positions in Channel 2); and HC VA for monofocal vision (Blocking Channel 1, and for different focus positions in Channel 2). The 0 to +4 D addition range (shaded green) represents bifocal vision with far vision in focus and different near additions. On the other hand the -4 to 0 D addition range (shaded blue) represents bifocal vision, with near vision in focus and the different additions representing different viewing distances. In this case, the blurred superimposed image is focused behind the retina. The monofocal condition represents a standard through-focus VA curve, for reference. Unlike the data obtained in the imaging system acting as an artificial eye, in general, the curves are less symmetric for positive and negative defocus, likely due to the presence of aberrations in the eye. Performance with LC stimuli tends to parallel, in most subjects, that for HC stimuli. Monofocal VA decreases steadily with defocus, as expected. In bifocal vision VA decreases rapidly for small additions, typically reaches a minimum, and improves for larger additions. Bifocal VA in focus (with

different superimposed additions) largely exceeds monofocal vision in the presence of equivalent amounts of defocus for most of the defocus range in all subjects.

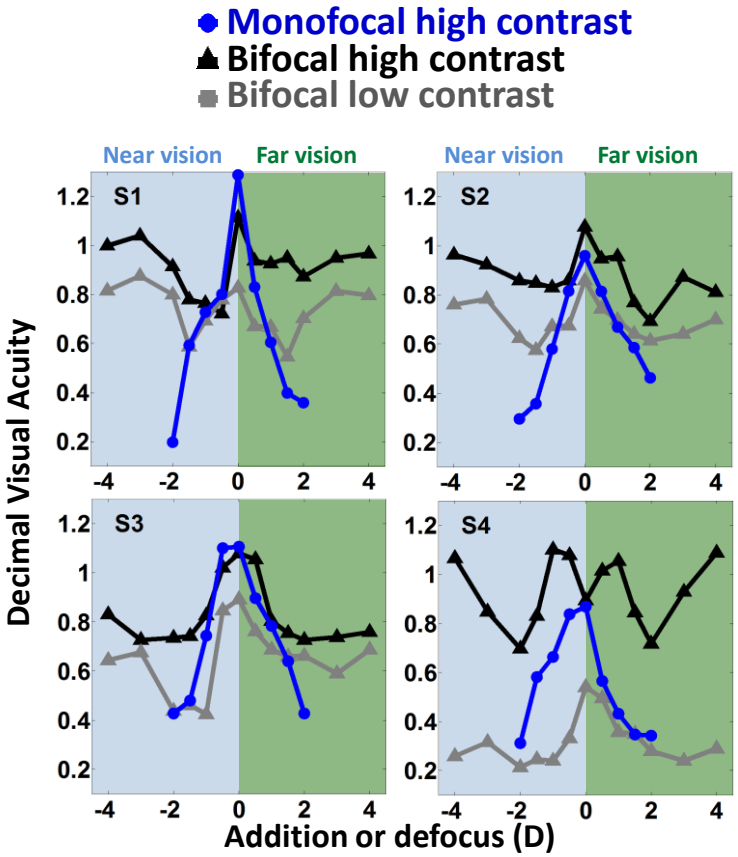

Figure 6.4. VA for different defocus increments in channel 2 (representing additions for bifocal images, and defocus for monofocal images): Bifocal HC VA curves (black line and symbols); Bifocal LC VA (gray line and symbols); monofocal through-focus HC VA (blue line and symbols). Each panel represents data for a different subject (S1 to S4). The 0 to +4 D addition range (shaded green) represents bifocal far vision with different near additions. The -4 and 0 D focus range (shaded blue) represents bifocal near vision at different distances. See text for a detailed explanation.

Figure 6.5 shows equivalent VA curves vs addition (for simultaneous vision) or defocus (for monofocal vision), averaged across subjects. At 0 D monofocal and bifocal VAs are very close, despite the luminance in the bifocal condition being double (as it combines light from two channels) than the monofocal condition. This is expected, as the dependence of VA with luminance for this luminance range (25-50 cd/m2) is minor, compared to that at lower luminances [22]. Monofocal VA decreased systematically with defocus (from 1.05 at 0 D to 0.35±0.04 at ±2D, on average). For simultaneous vision, VA decreased when increasing addition with a minimum of 0.66±0.06 at 1.69±0.25 D (averaged for HC and LC across subjects), and then increased for higher additions (0.78±0.06 for an addition of 3.75±0.23 D). While, on average, VA for monofocal vision decreased below 0.7 for defocus higher than 0.5 D, VA with bifocal corrections remained above 72 % of the VA obtained under monofocal conditions for all the addition range (0 ±4 D). Low contrast VA under simultaneous vision tended to parallel high contrast VA, with a relative average reduction of 32 %.

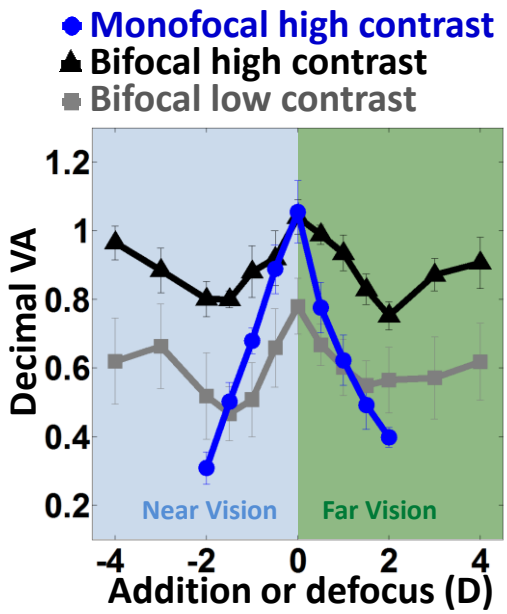

Figure 6.5. Average Decimal VA in the presence of addition (for bifocal vision) or defocus (through focus monofocal visionO through-focus): Bifocal HC VA (black line and symbols) and Bifocal LC VA (gray line and symbols); Monofocal HC VA (blue line and symbols). Bifocal near vision at different distances is shown in shaded blue. Bifocal far vision with different additions is shown in shaded green. Error bars stand for standard deviations across subjects.

6.4. Discussion

We have presented results using a new method implemented in this thesis to provide presbyopic (or simulated presbyopic) subjects with a visual experience of pure bifocal simultaneous vision [51]. The instrument is composed of two Badal systems, which allow providing simultaneously a correction for far vision and a near addition. Visual quality (and also optical quality) can therefore be measured simulating critical parameters of a simultaneous bifocal correction such as the amounts of near addition, as shown in this study.

We have measured the impact of the presence of a near addition (of various amounts) on far VA, and alternatively the presence of a defocused far image on near VA (at various viewing distances). The experimental simulation of pure bifocal simultaneous vision on real subjects, without the limitations imposed by the practical implementation of the bifocal corrections (i.e. diffraction effects or abrupt transitions in refractive elements, chromatic effects in diffractive elements, as 4 question of interest (visual degradation of simultaneous vision at different additions) from other factors. We have found that additions in the 0.5-2.0 D range produce the strongest reduction of VA in patients (and also the largest decrease of contrast in the simultaneous images), while larger additions decreased VA more moderately.

Simultaneous images (and even more in the context of this study) can be understood as the superposition of two channels, one in focus and the other one out of focus, that compete in the subject's visual system. It has often been argued that the perception of simultaneous images is driven by neural processes that are able, first, to separate both superimposed channels and, second, to suppress to some extent the blurred one while preserving the sharp one. Our study however points to a primary role of optical factors in visual performance with simultaneous vision.

The fact that VA in our four subjects show a similar trend to that obtained in computer simulations and optical experiments on a diffraction-limited lens suggests that the decrease in performance at low and intermediate additions is not driven by neural factors as much as by optical factors, and also that it is

relatively unaffected by ocular aberrations. This result is of great interest, not only to increase our understanding of how simultaneous images are perceived, but also from a clinical point of view, as it allows identifying the acceptable addition values in a bifocal correction, which, according to our results, should avoid too low near additions.

Our results are consistent with those of Sanders et al. who showed that VA in multifocal contact lens wearers decreased steadily with the amount of addition imposed (1–2.5D) from about 20/16 to 20/19 [111]. The results are in contrast with those from another clinical evaluation of visual performance with soft bifocal contact lenses that showed that the lower the addition the higher the VA for distance viewing conditions in a wide range of contrast conditions [112]. Unfortunately both groups of subjects in Sanders et al. and in Cox et al. were pre-presbyopic (18-25 years and 23-31, respectively) and the accommodation was not paralyzed, which made the interactions between the multifocal designs used and the subject's accommodative response unpredictable [111,112].

Our study is, to our knowledge, the first attempt to evaluate the loss in contrast and VA produced by bifocal vision, systematically and independently from a particular lens design. Although the system uses a refractive principle, these conclusions can be applied generally into the design of diffractive IOLs. Diffractive IOLs come commercially with different focus shifts between near and far, and their performance is independent on the pupil diameter and does not rely on specific distributions of the refractive profile across the pupil.

In the following chapter we will present how an extension of this instrument allows experimental simulations of the effect of different energy distributions in the near and far foci, and different refractive pupil patterns, therefore expanding the range of bifocal solutions that can be simulated. In general, a systematic simulation of a multifocal correction will allow gaining insights on the visual performance under simultaneous vision, the visual tolerance to simultaneous vision and the mechanisms for adaptation to simultaneous vision [113,114].

Bi/multifocal contact lens prescription in the clinical practice normally rely on a trial and error procedure with different designs until (if found) a design

which appears satisfactory to the patient is prescribed [115,116]. The use of multifocal contact lenses has large margins for increase, as a large majority (63%) of presbyopic contact lens wearers still use monofocal lenses [117]. Undoubtedly, prescription of multifocal lenses would benefit from increased knowledge of the visual response of patients to multifocal corrections, and from screening tools for practitioners that decrease trial and error approaches [117,118]. The method described in this study could be used to screen patients suitable to receive a multifocal correction, and more importantly, to identify the optimal design parameters, to prescribe the best suited available bifocal solution, or to customize parameters to a patient. For the screening method, based on the system described in this chapter, a new set of protocols, different from the extensive psychophysical measurements of the current study, and more suitable to a clinical environment, has to be developed and validated.

6.5. Conclusions

The Simultaneous Vision Simulator allows simulating non-invasively bifocal corrections in subjects (or artificial imaging systems) [51]. With this new methodology we showed that VA and contrast were reduced (7-41% depending on the condition) in simultaneous vision, both for far and near. The VA decrease found in all patients is systematically highest for typical additions used in young presbyopic patients (1.5-2 D). The trends shown in VA and contrast as a function of the induced additions are important in the design of new protocols of adaptation for young presbyopic subjects. Those trends are similar across subjects, indicating that suboptimal near additions are relatively independent on the specific aberrations and neural factors in subjects. The simultaneous vision instrument presented in this chapter has proven to be an excellent tool to simulate bifocal vision and to increase our understanding on multifocal solutions for presbyopia. In the next chapters we present computer simulations and experiments carried out with a more sophisticated version of the simultaneous vision instrument which allows simulation of different pupillary distributions of near and far zones.

Chapter-7 Multiple zone multifocal phase designs

This chapter is based on the paper by de Gracia et al.: “Multiple zone multifocal phase designs”, Opt. Lett. **38**, 3526-3529 (2013).

The coauthors of this study were Carlos Dorronsoro and Susana Marcos.

The author of this thesis designed the study, developed the computer routines, performed the simulations, implemented the new components in the instrument, and performed calibrations, experimental measurements and data analysis.

The optical properties of radially and angularly divided multifocal designs are established in this chapter. The results shown pinpoint an angularly divided of three or four zones as the optimum design among the radially and angularly divided designs (from 1 up to 50 zones) tested. The multifocal properties of the designs can be further extended by adding other aberrations (tilt, astigmatism, coma and spherical aberration).

Theoretical and experimental results shown in this chapter allow concluding that near center or far center designs provide better image quality for the distance which correction is implemented in the center of the design. Also the optical performance of 2-zone designs is higher than those with higher number of zones but more dependent of the natural aberrations of the patients (especially coma).

7.1. Introduction

Simultaneous vision lenses include bifocal or trifocal diffractive and refractive designs, or aspheric designs that generally attempt to modulate the spherical aberration of the eye. Refractive designs show different optical zones of different refractive power, normally concentrically in two zones (for example with the central portion providing near vision and the peripheral one providing far vision), multiple zones, or asymmetric zones (with for example, the upper zone providing distance vision and the lower zone providing near vision) [109,119]. Several studies have proposed expanding DOF by increasing the optical aberrations or by introducing specific combinations of aberrations (i.e. 4^{th} and 6^{th} order spherical aberration Zernike terms) [28,31]. Departing from previous chapters in this section we will be dividing the pupil in different areas to evaluate the optical performance of segmented wavefronts.

Some other DOF expansion strategies inspired in beam shaping or imaging (i.e. axicons) have encountered limitations for applications in the eye [120]. Recently, multifocal intraocular lens designs with aspheric optics have been proposed based on a multiconfiguration approach, where the optical quality of the eye plus lens is optimized for multiple foci [121]. Many studies propose the construction of a phase pattern (generally defined by a set of aberrations) that optimize a certain visual quality metric (for example the Visual Optical Transfer Function) over a certain dioptric range [9]. Besides optical predictions, it is possible to simulate visual performance with these designs with the use of Adaptive Optics simulators. Deformable mirrors are capable of reproducing smooth phase patterns (such as those obtained by combination of aberrations). Spatial light modulators can also reproduce steep phase changes such as those produced in certain refractive multifocal designs [122]. Despite the availability of technology to produce phase patterns that combine both segmented regions of different powers or aberration profiles, to our knowledge the multifocal optical (or visual) performance produced by those patterns has never been explored systematically.

In this chapter we present both a theoretical study dedicated to find the best zone distribution in bifocal design and experimental measurements in subjects that show that the theoretical differences once translated to real designs do affect the visual performance of subjects.

7.2. Computer simulations

In the first part of this chapter, we explore computationally the predicted through-focus optical quality of multifocal phase designs consisting of segmented pupils (N zones up to 50) of progressive power in different radial or angular pattern configurations, where the dioptric power in each zone is defined by:

$$D_i = D_f + \left(\frac{D_n - D_f}{N}\right)(i-1) \qquad (7.1)$$

with i referring to the zone number, N the total number of zones, and D_f the optical correction for far, and D_n the optical correction for near.

In general, the phase pattern (W_T) is defined by the wave aberration in each zone, which can be expressed mathematically by,

$$W_T = \sum_{i=1}^{N} w_i(D_i) * \sigma_{jl} \qquad (7.2)$$

where N=n1∗n2, l labels the radial zones (l = 0 to n_1), j labels the angular zones (j = 0 to n_2), w_i represents the wave aberration in each zone, and σ_{jl} represents a mask that equals to 1 in the corresponding zone and 0 elsewhere. The radial coordinate of the mask for each zone (ρ) varies between,

$$\sigma_{jl}(\rho,\theta) = 1 \;\forall\; \rho \in \left[\frac{\rho_m l}{n_1}, \frac{\rho_m (l+1)}{n_1}\right], 0 \; otherwise \qquad (7.3)$$

and the angular coordinate (θ) of each mask varies according to,

$$\sigma_{jl}(\rho,\theta) = 1 \;\forall\; \theta \in \left[\frac{2\pi j}{n_2}, \frac{2\pi (j+1)}{n_2}\right] + \Phi, 0 \; otherwise \qquad (7.4)$$

where Φ stands for an angular shift, common to all zones.

Figure 7.1 illustrates the distribution of segmented zones in several radial and angular designs. For clarification, the separation between zones in radial designs has been highlighted (but for the 50-zone design). We denoted the patterns by N (n1,n2, Φ), where n_1 indicates the number of radial zones, and n_2 the number of angular zones. Wave aberrations w_{ij} in the phase patterns of

Figure 7.1 are defined by defocus terms only (eq. 1). Other phase patterns considered in the study included w_{ij} defined by combinations of high order aberrations (see figs. 4 and 5).

Fourier optics were used to compute the OTF from the pupil function. The Visual Strehl (obtained as the product of the OTF by a general Neural Transfer Function, to emphasize the spatial frequency range most relevant to visual function) was used as an optical quality metric [9,54]. The threshold for acceptable vision was set to 0.12 Visual Strehl contrast modulation, as reported in prior literature [18,31]. Through-focus Visual Strehl curves were computed to evaluate the through-focus performance of the designed phase patterns. DOF was defined as the dioptric range for which Visual Strehl was above threshold. Also, the area under the Visual Strehl (in a Dioptric range of 6 D) was used as an optical quality metric.

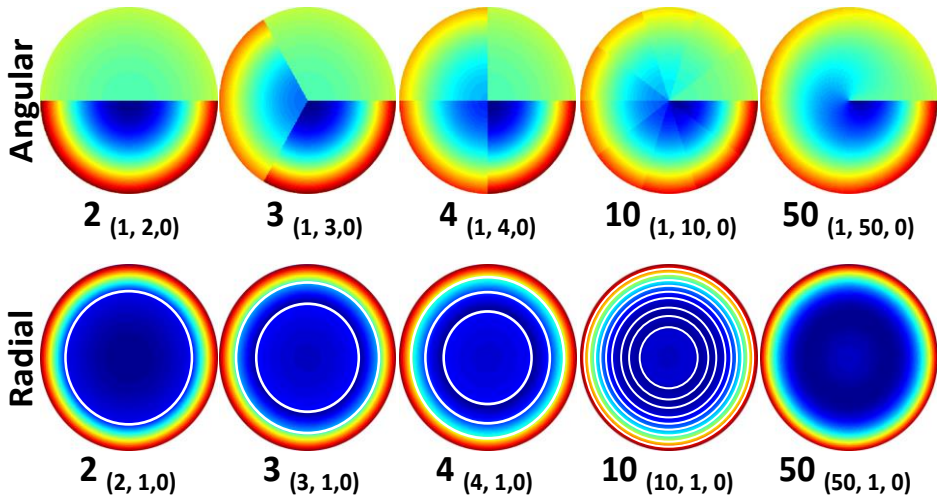

Figure 7.1. W_T for different numbers of angular (top row) and radial (lower row) zones. Maps are represented considering only defocus in angular designs and only a piston term in radial designs in the wave aberration of each zone. Values of [n1,n2,Φ] are shown for each pattern.

Current clinically available multifocal refractive IOL designs use various concentric segmented zones $N_{(N,0,0)}$ according to our notation, i.e. AT Lisa bifocal lens by Carl Zeiss or the ReZoom bifocal lens by Abbot $5_{(5,1,0)}$. To our knowledge only one IOL design uses roughly a two angular zone desing (MPlus lens, by Oculentis, which in a first approximation could be described by $2_{(1,2,0)}$) [123]. Although in some multizonal lens designs aspheric transition zones are included to facilitate smooth variations across zones with different power, multifocality is mostly produced by differences in power in the different zones.

However, to our knowledge, the optimal number of zones in radial and angular zone designs, and potential differences in optical performance of radial versus an angular designs (with equal number of zones and area of the corresponding zones of similar power) have never been tested.

In the second part of this chapter we will show the results of testing the fourteen designs (shown in Fig.7.2). These results are compound by theoretical simulations and experimental measurements in 5 subjects with the system shown in section 2.2.3 of chapter 2 of the methods section. The experimental measurements consisted of a psychophysical paradigm where subjects judged the perceived image quality of the images presented (as described in section 2.4) through pairs of bifocal patterns. All the phase patterns regardless of the number of areas always used half of the total area of the pupil for far vision (represented in black with an addition of 0.5 D) and half of it for near vision (represented in grey with and addition of 3 D). All simulations and measurements in subjects were performed for a pupil size of 4 mm.

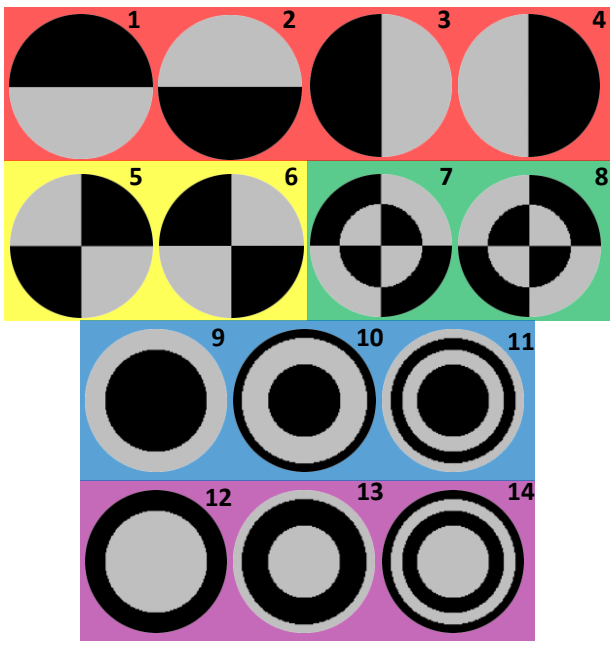

Figure 7.2. Phase patterns tested computationally and in the experiments. First row shows 2-zone designs in 4 different orientations (red background). Second row: four zones designs (yellow background) and 8 zone designs (green background). Third row: Far-center designs with 2, 3 and 4 circular areas. Fourth row: Near-center designs with 2, 3 and 4 circular areas.

To calculate the optical properties through focus of the fourteen designs shown in Fig.7.2, calculations of the Visual Strehl were performed for a through focus range of 6 diopters (from -1 to 5 diopters, 0.0625 D steps)[9,54]. Also it is of great relevance to understand the interaction of these fourteen designs with the aberrations of a normal set of subjects. Therefore these fourteen wavefronts (mimicking bifocal solutions) were combined with aberrations from a personal database of the laboratory that contains data from 100 subjects. The threshold of acceptable vision in terms of Visual Strehl is set to 0.12 as commonly accepted in previous works[18,31] .

The psychophysical measurements involved a 2 alternative forced choice procedure. Measurements were performed in 5 subjects (31.4 ± 5.9 years) with best sphero-cylindrical correction. Subjects were asked to choose the best of the pair of patterns presented by selecting the image with better optical quality. As a result a classification of the quality of the different fourteen phase maps shown in figure 7.2 emerged.

All subjects had undergone an ophthalmological evaluation before performing the experiments and had previous experience in psychophysical tasks. 1% tropicamide was instilled to paralyze accommodation simulating presbyopia and dilating the pupil. Subjects signed a consent form approved by the institutional review boards after they had been informed on the nature of the study and possible consequences. All protocols met the tenets of the Declaration of Helsinki.

Also monochromatic (820 nm) high order aberrations (HOA) were measured using a custom Hartmann-Shack aberrometer described in previous publications [22,28,29] and in chapter 2 of this thesis.

7.3. Results

7.3.1 Computer simulations

We designed multifocal phase patterns with N zones both with radial ($N_{(N,0,0)}$) and angular ($N_{(0,N,0)}$), configurations with N ranging from 1 to 50. Defocus term (C_2^0 in a Zernike expansion notation) was varied linearly and sequentially across zones between -0.2 and -1.7 μm in a 4-mm pupil, equivalent to a power change from +0.35 D for far distance correction to +3 D for near (i.e. near addition). The area of each zone is of equal value in all cases ($\pi*\rho^2$/N mm^2). Figure 7.2 shows the Visual Strehl-based optical performance metrics (DOF vs Area under the Visual Strehl through-focus curve) for radial and angular zone designs of increasing number of zones (up to N=50), always with defocus varying by 2.65 D from the far to near zones. Interestingly, in both cases, increasing the number of zones does not lead to an increase in performance. The best multifocal optical performance (large DOF while preserving a high area under the curve) corresponds to 3-4 zones, in both radial and angular zone designs. Figure 3 shows the Visual Strehl through-focus curves for selected defocus-varying designs with radial zones and angular zones, respectively. In radial zone designs, increasing the number of zones will eventually lead to a spherical aberration phase pattern, as shown by the purple dotted line in Fig. 7.4 for a 1(1,0,0) pupil pattern, where wave aberration WT is defined by a 4th order spherical aberration (C_0^4 = 0.4 μm). Remarkably, this solution (although frequently proposed [31,32]) provides poorer optical performance than a bifocal solution, and is largely exceeded by a trifocal solution (trifocal diffractive IOL designs have been recently released commercially [124,125]). In angular zone designs, increasing the number of zones will eventually lead to a spiral phase plate (or optical vortex), which has been proposed in other areas as a focal beam expander [126], although they appear suboptimal in the current application. Currently clinically available approaches using two angular zones (upper for far and lower for near) could be improved by increasing the number of zones to 3.

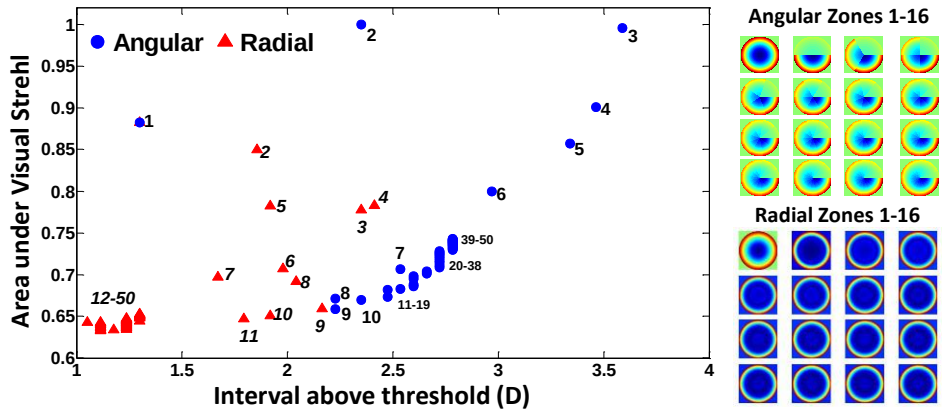

Figure 7.3. Depth-of-focus versus Area under the Visual Strehl through-focus curves, for phase patterns with N angular (blue circles) and radial (red triangles) zones (N ranges from 1 to 50). The labels next to each spot stand for the number of zones of the corresponding design. Insets are examples the phase patterns tested (for N=1 to 16). Area under Visual Strehl normalized by the area of the bifocal angular design.

Interestingly the optical performance of radial and angular zone designs differs for the same number of zones (N) and equivalent values of defocus on each zone. The total area of the pupil is divided in equal subareas in all cases. Our results reveal, for the same number of zones, a higher efficiency in angular designs than in a radial designs (12 % on average across the 50 designs). Besides, the number of zones in the angular design directly translates into increased number of peaks in the through-focus curve (see Fig. 7.4). However a less monotonic behavior occurs with radial designs, which ultimately (for large N) become similar to a spherical aberration phase pattern. An additional advantage of angular designs includes a relative independence of their performance with the natural pupil size.

These results suggest that phase patterns with angularly segmented zones (2-4) are optimal in expanding DOF while preserving acceptable visual performance. This analysis has been performed varying only the defocus term across zones. Previous studies have reported that interactions between high order aberrations occur which may lead to increased optical quality [18,28]. It is likely that combinations of other aberrations than defocus in each zone have also a positive impact on the through-focus optical quality of multifocal phase patterns.

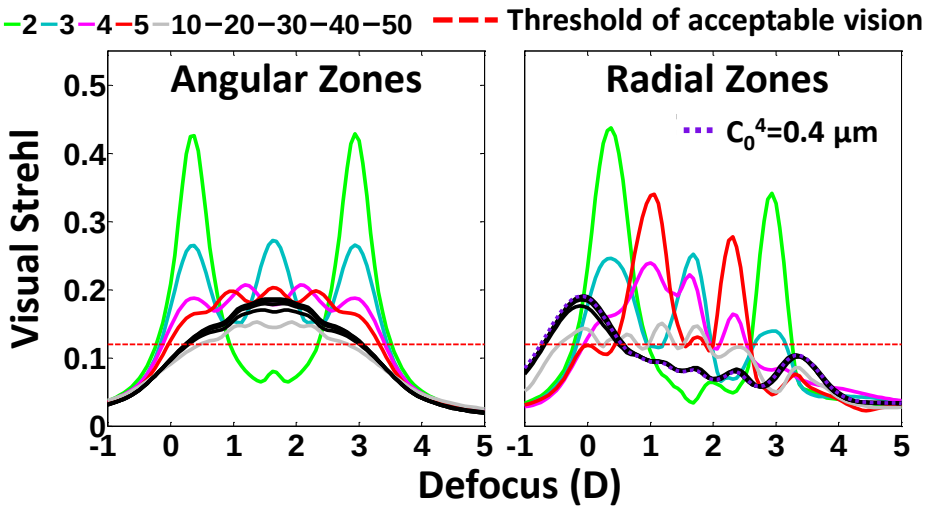

Figure 7.4. Visual Strehl values as a function of defocus for phase patterns generated with 2, 3, 4, 5, 10, 20, 30, 40 and 50 zones. Left panel: Phase patterns with angular zones. Right panel: Phase patterns with radial zones and $C_0^4 = 0.4$ µm.

We have generated 6 angular zone multifocal phase patterns (Fig. 7.5), with $2_{(1,2,0)}$ (a-c) and $4_{(1,4,\pi/4)}$ zone patterns (d-f), and introduced different combinations of aberrations in each zone. Inset in Fig. 7.6 shows the selected Zernike coefficients for each zone of designs a-f. The induction of spherical aberration to expand DOF has been studied before [31,32]. A control condition of 0.22 µm of spherical aberration and 0.8 µm of defocus (this combination of spherical aberration and defocus allowed peak performance for emmetropic patients [31]) has been included for direct comparison with the current state of the art. Pattern a was designed with combinations of positive spherical aberration (0.22 µm) and positive defocus (0.8 µm) in one zone, and same amounts of spherical aberration and defocus, but with a reversed sign of the spherical aberration term in the other zone. This configuration produced a 10% increase DOF with respect to the same amount of only spherical aberration across the entire pupil. Favorable interactions between astigmatism and coma have been found in previous work, for particular amounts of these aberrations and specific relative angles [28,29]. Patterns b, c, d, e and f involve the reported optimal combinations of defocus, astigmatism and coma which increased optical performance in monofocal vision with respect to astigmatism alone [28].

In summary, we have shown important improvements in current multifocal refractive phase patterns over current designs. The theoretical performance of multifocal designs with 3 angular zones of different power expanded DOF 40 % more than current angular bifocal designs; 40 % more than trifocal radial

designs, and 32 % more than a typical spherical aberration phase pattern [31]. For the 3 zone angular design through-focus optical quality also varied with respect to the mentioned conventional designs by -1 %, 14 %, and 23 %, respectively. Our study demonstrates that multizonal angular phase patterns with 3-4 zones are optimal. To our knowledge, there is no multifocal lens available with this configuration, but current IOL designs could be improved combining standard IOL design approaches with the results of this study.

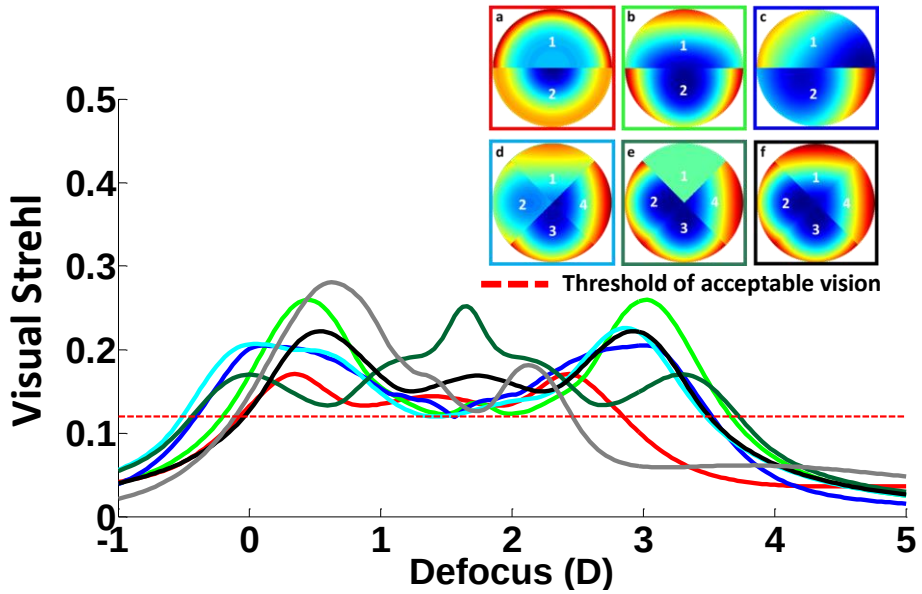

Figure 7.5. Through-focus Visual Strehl for six different multifocal designs (with multiple zones, and different combinations of aberrations in each zone, shown as insets). Each line (colored square box for each pattern) corresponds to a different design. The gray line represents values for a 1-zone multifocal pattern with spherical aberration (0.22 μm). Data are for 4-mm pupil diameters.

In addition (see Fig. 7.6) the dioptric range above threshold can be extended up to 0.5 D by introducing combinations of other aberrations other than defocus with respect to the defocus-varying trifocal angular design (Fig. 7.3).

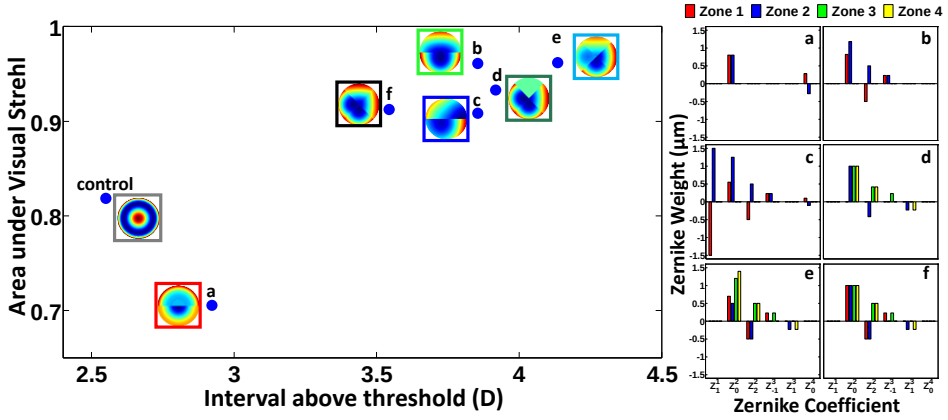

Figure 7.6. DOF versus Area under the Visual Strehl thru-focus curves, for the 6 designs shown in Fig. 4. Area normalized by the one of the bifocal angular design. The inset shows the Zernike coefficients for the different zones of each of the six multifocal designs.

Figure 7.7 shows the optical quality in terms of Visual Strehl for the fourteen bifocal designs as a function of defocus. In absence of the aberrations of subjects all designs that are equal but for a rotation symmetry have identical optical properties: designs (1-4), (5-6) and (7-8). Two-zone designs offer the best optical quality through focus. Although designs 9 and 12 offer the highest peaks of optical quality for far/near vision respectively. It must be pointed out that a 50-50 division of the optical area does not yield equal optical quality for near and far vision when the area is divided radially (concentric circles). The inner area always produces a higher peak of optical quality than the outer one. This effect can be clearly seen in figure 7.7 for designs 9, 11, 12 and 14. On the other hand designs 10 and 13 show a good balance between far and near vision conditions.

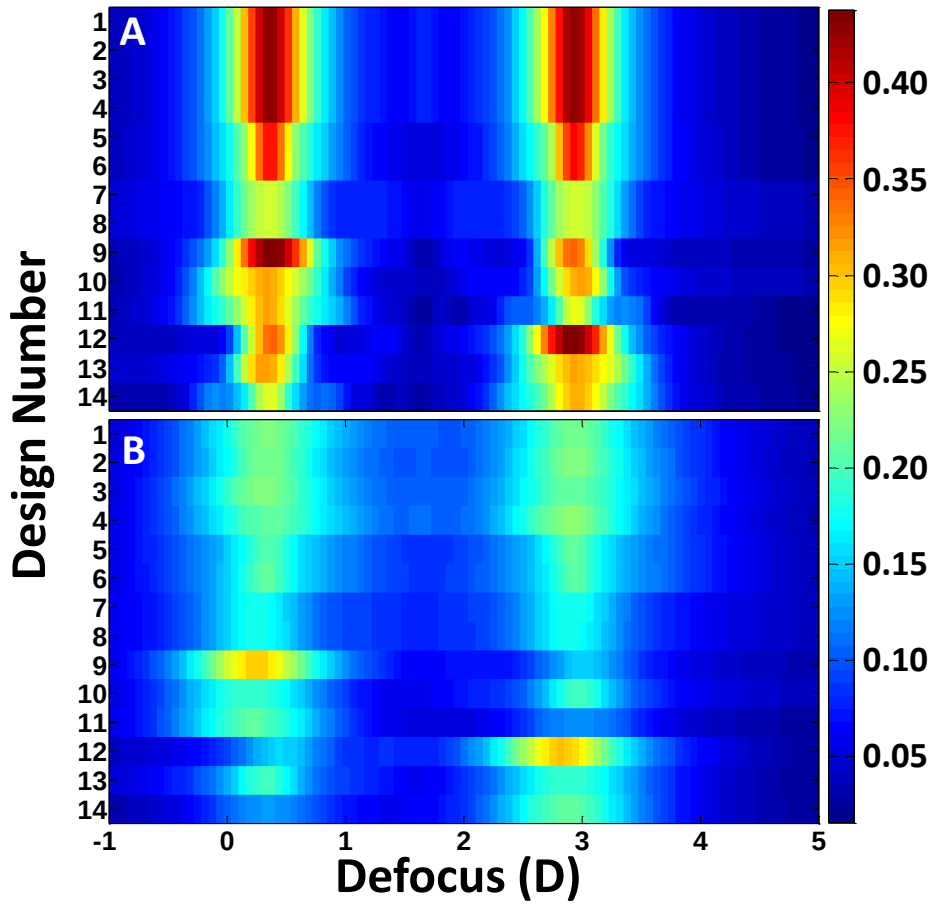

Figure 7.7. Optical performance through focus of eyes provided with 14 bifocal designs in terms of Visual Strehl. A) Assuming no ocular aberrations; B) Average performance in 100 real eyes.

When ocular aberrations of subjects are introduced the interaction between the different designs and the natural aberrations of subjects shifts performance from the predictions in diffraction-limited eyes, particularly producing differences in performance across similar (but just rotated) patterns (see figure 7.7B). Nevertheless their general performance is mainly driven by the design and not by the aberrations of the subjects.

Figure 7.8 shows optical performance of the 100 eyes simulated for intermediate vision conditions (66 cm). Designs 1 to 4 offer an acceptable level of optical quality (Visual Strehl>0.12) for a number of subjects equal to 29, 28, 20 and 24 respectively. From all of the other designs only designs 5, 6, 9 and 12 reach 0.12 for 1, 6, 2 and 2 subjects respectively.

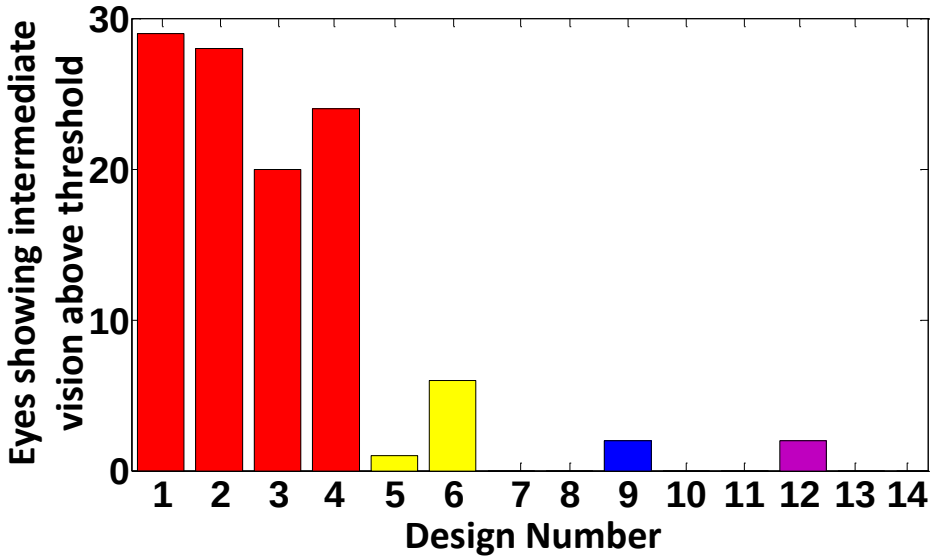

Figure 7.8. Number of eyes showing intermediate vision above threshold (Visual Strehl >= 0.12) , for each of the 14 bifocal eyes of the study. The color of the bars represents the background defined in figure 7.2 where the different designs are represented by their number.

On the other hand the optical quality of designs 1-4 shows more variability across eyes(i.e. most eyes showing best optical quality for design 1 peformed worst for design 2 and vice versa). This occurs also for designs 3 and 4. As the number of optical zones increased optical quality decreased (as for example in designs 7 and 8) the stability of the design to an individual optical aberration pattern, however increased. Figure 7.9 shows the third and fourth order aberrations of those subjects showing the highest optical differences across designs 1 and 2 and designs 3 and 4. These differences are clearly dominated by vertical coma (Z_3^{-1}) in designs 1 and 2 and by horizontal coma (Z_3^1) in designs 3 and 4 for the three distances tested. Potential similar interactions between the eyes spherical aberration and radial designs (9-12) were investigated, but not apparent (perhaps because the bias in the population towards positive spherical aberration, but different signs and orientations of coma.

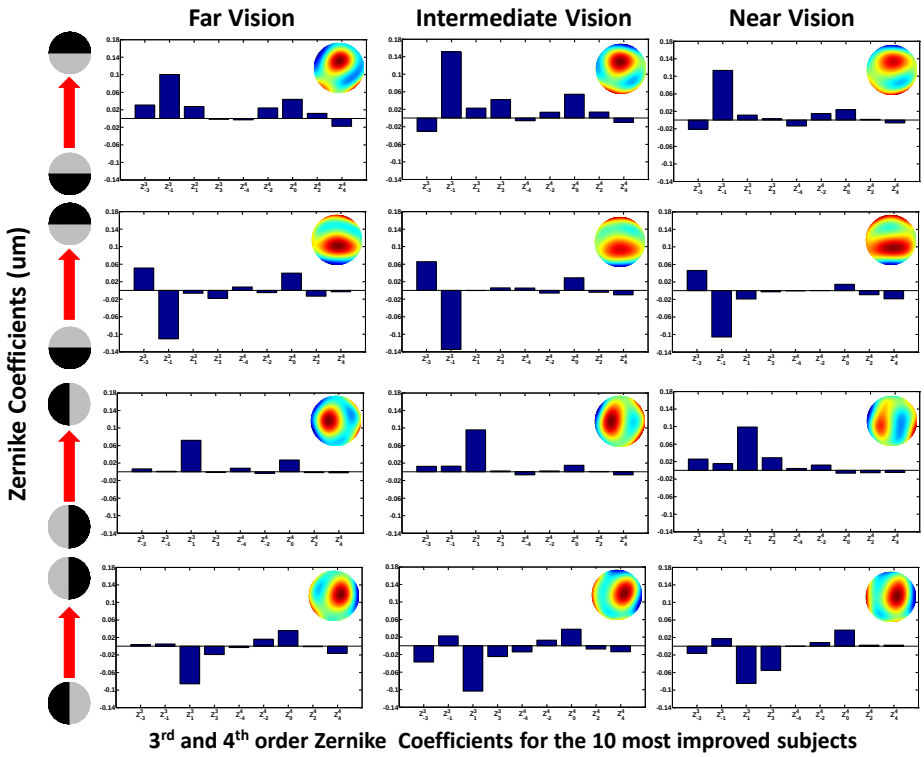

Figure 7.9. Mean of 3rd and 4th order Zernike polynomials from the ocular wave aberrations of the ten eyes that experienced largest differences in optical performance with different designs. Left, middle and right panels depict far, intermediate and near vision conditions. Each horizontal panel (upper to lower) compares two bifocal pairs: 1, 2; 2, 3; 3, 4; 4, 3. Wavefront insets show the averaged wavefront of the ten most improved subjects on each case.

7.3.2 Psychophysical measurements

One way anova revealed statistical differences in the response of the subjects to the bifocal designs for far vision (p= 0.0184); and not for intermediate (p=0.8821) and near (p= 0.0821). When comparing responses for different families of designs (shown by colors in graphs 7.2, 7.8, 7.10 and 7.11), we found that differences between families are statistically significant for all groups in far and near vision conditions ($p<0.01$, $F=5.8$ far, $p<0.01$, $F=4.3$ near), but not in intermediate vision ($p=0.30$, $F=1.2$).

When comparing the rates of selection of the different families between the three distances (far, intermediate and near) no statistical difference was found for angularly or mixed (angularly and radially) divided designs (designs 1-4,

p=0.76, F=0.27; designs 5-6, p=0.91, F=0.1; designs 7-8, p=0.86, F=0.15). On the other hand statistically significant differences across the three distances where found for the other 2 families corresponding to radially segmented designs (designs 9-11, p<0.01, F=0.17; designs 12-14, p<0.01, F=7.42).

Figure 7.10 shows the percentage of times that each pattern is chosen for each working distance by each subject in the 2 alternative forced choice procedure run in subjects. Concentric designs with central far vision were judged as best over near center designs for far vision. Concentric designs with central near vision were chosen as best for near vision. As predicted by the simulations, among all circularly divided designs, designs 10 and 13 provided the least difference in visual performance for far and near vision conditions (see Fig. 7.11).

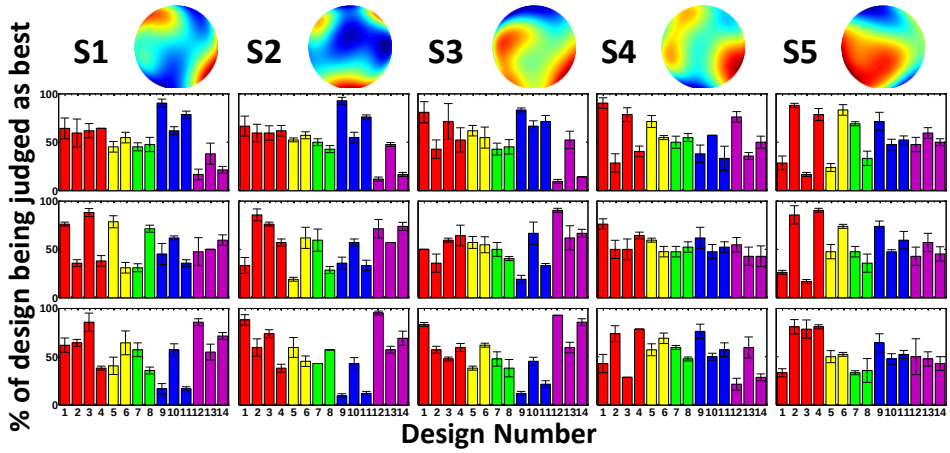

Figure 7.10. Percentage of times that each design is chosen as best by 5 different subjects (wave aberrations shown for each eye, 4-mm pupil). Upper, Middle and Lower panel show results for Far, Intermediate and Near Vision. Error bars stand for standard deviation of the 3 measurements for each condition. The color of the bars represents the background defined in figure 7.2.

Figure 7.11 shows average % of times that each pattern is selected as best, across the five subjects of the study. Color bars refer to the bifocal pattern families shown in Figures 7.2 and 7.10.

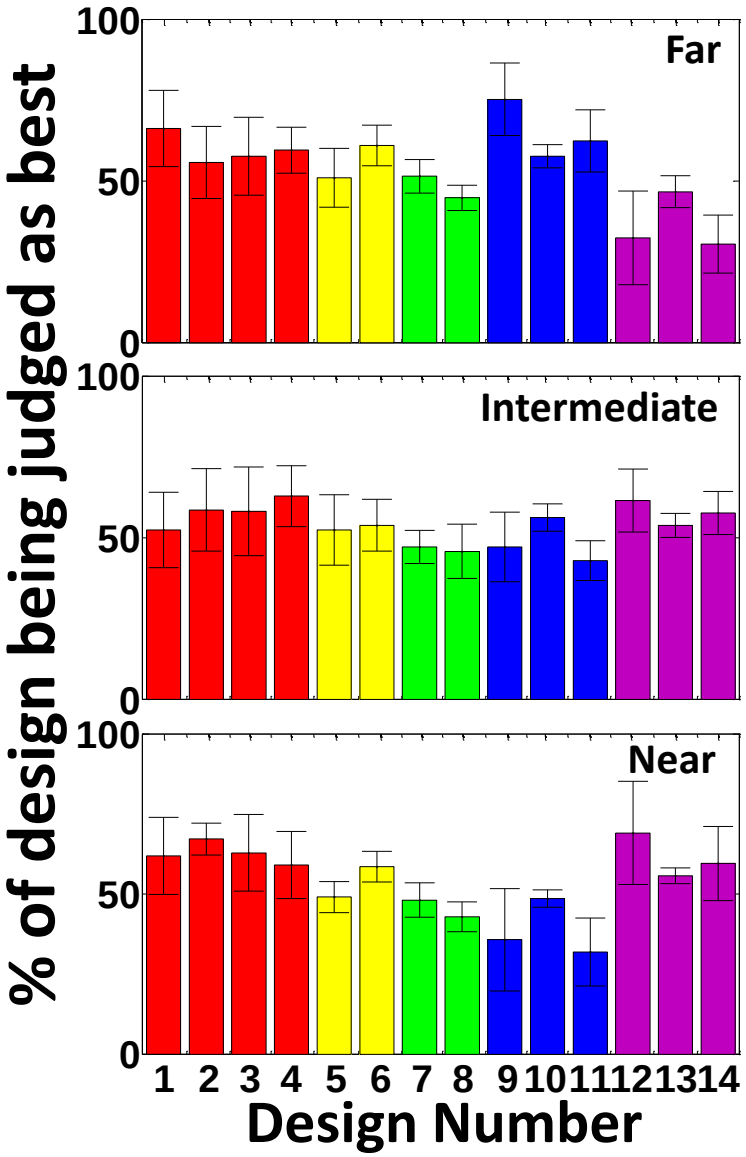

Figure 7.11. Average % of design being judged as best for each of the 14 bifocal designs. Color legend as in Figure 7.2 and 7.10. The color of the bars represents the background defined in figure 7.2 where the different designs are represented by their number. Error bars stand for standard deviation across subjects.

7.4. Discussion

Simulations and measurements in subjects show that the overall optical quality of angularly divided designs is highest than radially divided designs. The optical performance of 2-zone designs is higher than the performance of designs with more zones. Results presented in this chapter also allow concluding that near center or far center designs provide better image quality for the distance that is implemented in the center of the design (far or near). In the other hand the behavior of these designs is the lowest of all of the designs tested for the opposite situation (near or far). The most stable of the radially divided designs are designs 10 and 13 for which almost a 50-50 performance is found both in simulations and in the experiments. This is achieved by placing 3 different areas (near-far-near or far-near-far) where the less effective outer area counteracts the beneficial effects of the inner one.

Experimental measurements shown in this chapter incorporate neural factors, interactions of the multifocal phase patterns with the ocular aberrations of the subject, and potentially the prior visual experience (spatial neural adaptation of the subject) [44]. Considering the natural aberrations of normal eyes has allowed highlighting that 2-zone designs are also more dependent of the natural aberrations of the patients (especially coma). Vision through the presented phase patterns with combinations of HOA of the first part of this chapter can be experimentally simulated in Adaptive Optics (AO) systems provided with spatial light modulators. Also the designed phase patterns can be transferred to surface profiles in contact lenses and intraocular lenses, or implemented in refractive surgery ablation profiles, with the required considerations specific to each correction alternative (including geometrical aspects of the lens, and the corneal versus intraocular position of the correction).

In conclusion: designs based on angular divisions offer better optical quality than if radially divided; segmented designs with 3 or 4 zones produce an optimal optical performance of the design; designs with few divisions offer an optical performance more dependent of the natural aberrations of the eye than designs with a higher number zones; and radially divided profiles offer a higher efficiency in the inner part of the pupil than in the outer one.

Conclusions

Achievements

- Demonstration of the positive optical interactions between coma and astigmatism to produce better optical performance than each one alone.

- Evidence of the neural adaptation of subjects to the previous state of astigmatism present on their eyes.

- Demonstration of the impact of the adaptive optics correction on the improvement of contrast sensitivity, meridionally.

- Development of two new simultaneous vision Instruments: one simulating pure bifocal patterns, the second simulating bifocal patterns with different pupil distributions for near and far vision.

- Experimental demonstration of the impact of the magnitude of the near addition on distance visual acuity

- Simulation of optical performance of new radial and angularly segmented bifocal patterns.

- Experimental measurement of perceived image quality with multizonal bifocal corrections with different pupillary distributions.

Conclusions

This thesis addresses the development of tools to improve current available solutions for presbyopia. During the development of this thesis new combinations of aberrations that improve multifocal performance through focus have been discovered. Also a new optical system that allows the possibility of testing in subjects new multifocal solutions has been developed and tested on subjects.

The development of the new techniques, systems, and software developed in this thesis allows concluding:

1. Certain combinations of non-rotationally symmetric aberrations (coma and astigmatism) can improve retinal image quality over the condition with the same amount of astigmatism alone. A combination of 0.5 D of astigmatism and 0.23 µm of coma produced (for best focus) a peak improvement in Strehl ratio by a factor of 1.7, over having 0.5 D of astigmatism alone (for a 6 mm pupil). The improvement holds over a range of >1.5 D of defocus. The combination of coma with astigmatism improved decimal VA by a 38% in two subjects.

2. Adding coma (0.23 µm for 6-mm pupil) to astigmatism results in a clear increase of VA in subjects with no previous experience under astigmatic conditions, consistently with theoretical optical predictions. While VA decreased when coma was added to astigmatism in subjects with low levels of astigmatism. Subjects with astigmatism but that were habitually corrected did not show a clear improvement or negative effect of adding coma to astigmatism. The fact that the expected performance occurred mainly in eyes with no natural astigmatism suggested relevant neural adaptation effects in eyes normally exposed to astigmatic blur.

3. Correcting the aberrations of the eye produces large increases in retinal image contrast whereas the corresponding improvement factors in the CSF do not match the expected levels of improvement. The trend of improvement it is well reflected both in MTF and CSF behaviours but there

is a difference in the magnitude of the effect. The consistently lower benefit in contrast sensitivity than in the MTF of correcting aberrations suggested a significant role for the neural transfer function in the limit of contrast perception.

4. The largest degradation in contrast and visual acuity under simultaneous vision conditions occurred for additions around ±2 D (25%), while additions of ±4 D produced degradations of less than 14%.

5. Designs providing optimal through-focus performance were found for a maximum of 3-4 zones. Angular zone designs were significantly better (1.95 times on average) than radial zone designs with identical number of zones with the same levels of addition. The optimal design (angular design with 3 zones) surpassed multifocal performance by 33% that of a bifocal angular zone design, and by 32% a standard multifocal phase plate with induced spherical aberration only. By using combinations of low and high order aberrations the through focus range can be extended up to 0.5 D beyond that obtained with the best design of varying optical power.

6. Two-zone bifocal designs offer the best overall optical performance. This advantage of 2-zone designs holds when the optical aberrations of a real population of subjects are taken into account. In the other hand the performance of individual subjects with each of the designs is more variable for designs of 2 zones divided horizontally or vertically than when divided radially or when more zones are present (showing a strong interaction with vertical or horizontal coma) Designs with radial divisions or with a higher number of zones provide overall lower levels of optical performance. Also the simulations and measurements in subjects revealed that the central zone provide much better performance that the outer zone and that in order to equilibrate far and near vision conditions a 50-50 division of the total area should be avoided.

Future Work

A direct follow up of the work presented is to use the simultaneous vision system to reproduce different models of bifocal designs currently in the market to evaluate its performance. Another possible path opened after this thesis is to translate the new multifocal designs to optical elements (intraocular or contact lenses). Also the experimental evaluation in subjects of these new designs will be possible when the next generation of the VioBio adaptive optics system, containing an electromagnetic deformable mirror (with a continuous membrane) and a spatial light modulator (Pluto, HoloEye) will be completed.

Publications associated with this thesis

1. ***Pablo de Gracia***, Carlos Dorronsoro, Enrique Gambra, Gildas Marin, Martha Hernández, Susana Marcos. "Combining coma with astigmatism can improve retinal image over astigmatism alone". Vision Research 50 (2010) 2008-2014.
2. ***Pablo de Gracia***, Carlos Dorronsoro, Enrique Gambra, Gildas Marin, Martha Hernández, Susana Marcos. "Visual acuity under combined astigmatism and coma: Optical and neural adaptation effects", Journal of Vision (2011) February 7, 2011 11(2): 5.
3. ***Pablo de Gracia***, Ankit Mathur, Susana Marcos, David Atchison. 2011 "Contrast sensitivity benefit of adaptive optics correction of ocular aberrations". Journal of Vision (2011), 11(12):5.
4. ***Pablo de Gracia***, Carlos Dorronsoro, Alvaro Sanchez-Gonzalez, Lucie Sawides, Susana Marcos. "Experimental simulation of simultaneous vision". Investigative Ophthalmology and Vision Science (IOVS) (2013), 54(1): 415-422.
5. ***Pablo de Gracia***, Carlos Dorronsoro and Susana Marcos. "Multiple zone multifocal phase designs", Optics Letters 38, 3526-3529 (2013).

Other co-authored publications

1. Lucie Sawides, ***Pablo de Gracia***, Carlos Dorronsoro, Michael Webster, Susana Marcos. "Adapting to blur produced by ocular high order aberrations". Journal of Vision (2011) 11(7):21, 1-11.
2. Lucie Sawides, ***Pablo de Gracia***, Carlos Dorronsoro, Michael Webster, Susana Marcos. "Vision is adapted to the natural level of blur present in the retinal image". PLoS ONE (2011) DOI: 10.1371/journal.pone.0027031.
3. Lucie Sawides, Carlos Dorronsoro, ***Pablo de Gracia***, Maria Vinas, Michael Webster, Susana Marcos. "Dependence of subjective image focus on the magnitude and orientation of High Order Aberrations", Journal of Vision (2012) 12(8):4, 1-12.
4. Maria Vinas, Lucie Sawides, ***Pablo de Gracia***, Susana Marcos. "Perceptual adaptation to the correction of natural astigmatism", PLoS ONE (2012) 7(9): e46361. doi:10.1371/journal.pone.0046361.
5. Maria Vinas, ***Pablo de Gracia***, Carlos Dorronsoro, Lucie Sawides, Gildas Marin, Martha Hernández and Susana Marcos. 2013 "Astigmatism Impact on Visual Performance: Meridional and Adaptational Effects". Optometry and Vision Science, Vol. 90, No. 12, December 2013.

Patents

1. Marin Gildas, Martha Hernandez, ***Pablo de Gracia***, Susana Marcos, Carlos Dorronsoro "A method for providing a spectacle ophthalmic lens by calculating or selecting a design" Patent Owner: Essilor International (COMPAIGNE GENERALE D'OPTIQUE). Pub. No.: WO/2010/072820. International Application No.: PCT/EP2009/067876. Publication Date: 01.07.2010. International Filing Date: 23.12.2009.

Contributions in conferences (personally presented)

1. ***Pablo de Gracia***. "Is the retinal image well represented by a convolution?", Jornadas de Jóvenes Investigadores en Óptica Visual 2010, Red Temática Española en Óptica y Fotónica Visual, Madrid, Spain.
2. ***Pablo de Gracia***, C. Dorronsoro, G. Marin, M. Hernandez, S. Marcos. "Visual Performance with Combined Astigmatism and Coma: Optical and Neural Adaptation Effects", ARVO 2010, The Association for Research in Vision and Ophthalmology, Fort Lauderdale, USA.
3. ***Pablo de Gracia***, Susana Marcos, Ankit Mathur, David Atchison. "Benefit of adaptive optics correction of ocular high order aberrations on contrast sensitivity", 8th International Workshop on Adaptive Optics for Industry and Medicine, June 2011, Murcia, Spain.
4. ***Pablo de Gracia***, C. Dorronsoro, Alvaro Sanchez-Gonzalez, L. Sawides, S. Marcos. "Visual performance under pure simultaneous vision", PARD 2012, Panamerican Research Day. Pan-American Association of Ophthalmology, May 2012, Fort Lauderdale, USA.
5. ***Pablo de Gracia***, C. Dorronsoro, Alvaro Sanchez-Gonzalez, L. Sawides, S. Marcos. "Visual performance under pure simultaneous vision", ARVO 2012, The Association for Research in Vision and Ophthalmology, Fort Lauderdale, USA.
6. ***Pablo de Gracia***, B. I. Gallego, AAO 2012. "A new automatic method for counting microglial cells in healthy and glaucomatous retinas", October 2012, American Academy of Optometry. Phoenix USA.

Invited talks

1. ***Pablo de Gracia,*** "The visual system: from the optical image to the individual perception", February 2012, VIII Seminars in physiology and ocular pathology, Department of Opthalmology, School of Optics and Optometry. Universidad Complutense de Madrid, Spain.
2. ***Pablo de Gracia,*** "Fighting presbyopia: new multifocal solutions and the neural adaptation effects ensued", July 2012, Institute for Theoretical Physics, University of Bremen, Germany.
3. ***Pablo de Gracia,*** "Evaluation of simultaneous vision corrections", Irvin M.Borish Festschrift, October 2012, American Academy of Optometry Meeting. Phoenix, USA.
4. ***Pablo de Gracia,*** "The influence of the amount of power addition in simultaneous vision", Ezell Fellow Gallery, October 2012, American Academy of Optometry Meeting. Phoenix, USA.

Other merits

- ***2011 Irvin M. Borish - William C. Ezell Fellow***, This award is given by the American Academy of Optometry to doctoral students with an outstanding performance in the field of Vision Science, 9500 $.
- ***2012 SPIE Scholarship in Optics and Photonics***, This award is given by the International Society for Optics and Photonics to doctoral students with the potential to outreach during their careers on the field of optics, 2000 $.
- ***2012 Mike Daley - William C. Ezell Fellow***, This award is given by the American Academy of Optometry to doctoral students with an outstanding performance in the field of Vision Science, 9500 $.
- ***2012 Fellow of the American Academy of Optometry, FAAO.***
- ***2013 Bisgrove Scholars Award.*** Conceded by the Arizona Science Foundation this distinction consist in 200.000 $ extended during a 2-year period for the development of a project as post-doc.
- ***Journal reviewer:*** IOVS, JCRS, VR, OVS, COL.

Other contributions in conferences

1. ***Pablo de Gracia***, Carlos Dorronsoro, Lucie Sawides, Enrique Gambra and Susana Marcos. "Experimental test of simulated retinal images using adaptive optics", Frontiers in Optics 2009, San Jose, California, USA, OSA Technical Digest (CD) (Optical Society of America, 2009), paper JWB4.
2. Enrique Gambra, Lucie Sawides, Carlos Dorronsoro, ***Pablo de Gracia***, Jing Yuan, Yinan Wang,Philip B. Kruger, Susana Marcos. "Influence of High Order Aberrations on Accommodation", September 2009, IX Reunión Nacional de Óptica, Orense, Spain.
3. Susana Marcos, Sergio Barbero, Carlos Dorronsoro, Alberto de Castro, ***Pablo de Gracia***, Enrique Gambra, Ignacio Jimenez-Alfaro, Sabine Kling, Lourdes Llorente, Carlos Meneses, Jesus Merayo, Sergio Ortiz, Daniel Pascual, Alfonso Perez-Escudero, Laura Remon, Jose Requejo, Lucie Sawides, DamianSiedlecki. "Lines of Research of the Visual Optics and Biophotonics Laboratory at the Institute of Optics", September 2009, IX Reunión Nacional de Óptica, Orense, Spain.
4. Susana Marcos, Lucie Sawides, ***Pablo de Gracia***, Carlos Dorronsoro, Enrique Gambra, Michael Webster. "Using Adaptive Optics to test the spatial neural adaptation to blur", February 2010, XI Wavefront and Presbyopic Refractive Corrections Meeting, The American Academy of Optometry, San Francisco, USA.
5. L. Sawides, ***Pablo de Gracia***, C. Dorronsoro, E. Gambra, M. Webster, S. Marcos. May 2010 "Adapting to Blur Produced by Ocular High Order Aberration", ARVO 2010, The Association for Research in Vision and Ophthalmology, Fort Lauderdale, USA.
6. C. Dorronsoro, L. Llorente, R.G. Anera, M.J. Gonz·lez, ***Pablo de Gracia***, S. Marcos. "Performance Evaluation of Simultaneous Vision Multifocal Contact Lenses", Treating Presbyopia: Multifocality, Pseudoaccommodation, and Restoring Accommodation - Minisymposium. Fort Lauderdale, Florida. Invited Conference, ARVO 2010, The Association for Research in Vision and Ophthalmology, Fort Lauderdale, USA.

7. Susana Marcos, Lucie Sawides, ***Pablo de Gracia***, Carlos Dorronsoro, M. Webster. "Subjects are naturally adapted to their own optical aberrations", August 2010, EMVPO2010, EOS European Meeting of Vision and Physiological Optics, Stockholm.
8. Gildas Marin, Martha Hernandez, ***Pablo de Gracia***, Carlos Dorronsoro, Enrique Gambra, Susana Marcos. "Etude du bénéfice visuel lié a la combinaison d'aberrations", October 2010, Journées Recherche Industrie de l'Optique Adaptative, Paris France.
9. L. Sawides, ***Pablo de Gracia***, C. Dorronsoro, E. Gambra, M. Webster, S. Marcos. "Exploring the input of optical blur on vision", ARVO 2011, The Association for Research in Vision and Ophthalmology, Fort Lauderdale, USA.
10. Maria Vinas, Lucie Sawides, ***Pablo de Gracia***, Susana Marcos. "Shift of the neutral perceived focus after correction of astigmatism: evidence using adaptive optics", June 2011, Engineering the eye, Benasque, Spain.
11. Maria Vinas, Lucie Sawides, ***Pablo de Gracia***, Susana Marcos. "Adaptive optics as a tool to study changes in the perceived neutral point after correction of astigmatism", June 2011, 8th International Workshop on Adaptive Optics for Industry and Medicine, Murcia, Spain.
12. L. Sawides, ***Pablo de Gracia***, M.Vinas, C. Dorronsoro, M. Webster, S. Marcos. "Adaptive optics to test adaptation to the eye's optics", February 2012, IONS 2012, Optical Society of America, Paris, France.
13. M.Vinas, L. Sawides, ***Pablo de Gracia***, S. Marcos. "Adaptive optics as a tool to study changes in neural adaptation to astigmatism", February 2012, IONS 2012, Optical Society of America, Paris, France.
14. L. Sawides, C. Dorronsoro, ***Pablo de Gracia***, Maria Vinas, M.A. Webster, A. Haun, E. Peli, S. Marcos. "Natural adaptation to the orientation of high order aberrations", ARVO 2012, The Association for Research in Vision and Ophthalmology, Fort Lauderdale, USA.
15. Maria Vinas, L. Sawides, ***Pablo de Gracia***, S. Marcos. ARVO 2012, "Longitudinal changes in perceptual judgment of astigmatic blur", The Association for Research in Vision and Ophthalmology, Fort Lauderdale, USA.

16. L. Sawides, C. Dorronsoro, ***Pablo de Gracia***, Maria Vinas, M.A. Webster, A. Haun, E. Peli, S. Marcos. "Patterns classification strategy to test natural adaptation to the high order aberrations of the eye", September 2012, EMVPO 2012, European Meeting on Visual and Physiological Optics, Dublin, Ireland.
17. M. Vinas, ***Pablo de Gracia***, C. Dorronsoro, L. Sawides, S. Marcos. "Testing the effect of astigmatism on vision with Adaptive Optics", IONS 2013, Optical Society of America, Zurich, Switzerland.
18. Maria Vinas, ***Pablo de Gracia***, C. Dorronsoro, L. Sawides, G. Marin, M. Hernandez, S. Marcos. "Visual acuity in the presence and correction of astigmatism using Adaptive Optics". ARVO 2012. The Association for Research in Vision and Ophthalmology, Seattle, USA.
19. Salazar JJ, Gallego BI, Rojas B, Triviño A, Ramírez JM, ***Pablo de Gracia.*** "A new automatic method for counting microglial cells in wholemount mice retinas". Sircova 2013. The International Society for Research in Retina and Visual Sciences, Valencia, Spain.

Resumen

Capítulo 1

Este capítulo comienza con una breve introducción sobre los conceptos más importantes tratados en esta tesis: como un sensor de frente de onda mide el frente de onda de un sujeto, como los polinomios de Zernike son usaos para modelar el frente de onda, que son las aberraciones de alto y bajo orden y como pueden modificarse con un espejo deformable. Después de esto también se trata como trabaja el mecanismo de la acomodación y como con el envejecimiento la presbicia aparece. También se hace una breve descripción de los distintos métodos para corregir la presbicia y finalmente se enumeran las preguntas aun sin respuesta en el campo sobre las que se ha intentado arrojar luz durante la realización de esta tesis.

Capítulo 2

En el capítulo de métodos se presentan los diferentes sistemas ópticos utilizados y desarrollados en esta tesis. Dos sistemas diferentes de óptica adaptativa han sido utilizados: el primero se encuentra en el laboratorio Viobio en el Instituto de Óptica de Madrid y el segundo en la Queensland University of Technology en Brisbane en el laboratorio de David Atchison. También se presenta un nuevo sistema desarrollado en esta tesis. Se trata de un simulador de visión simultánea que puede, en su segunda versión, reproducir cualquier corrección bifocal refractiva. También se muestra el funcionamiento básico de un modulador espacial de luz. Por último se presentan los algoritmos para la simulación de correcciones multifocales y su evaluación con diferentes métricas.

Capítulo 3

En este capítulo se demuestra que ciertas combinaciones de aberraciones sin simetría de revolución (coma y astigmatismo) pueden mejorar la calidad de la imagen retiniana frente a la que se obtendría añadiendo uno solo de ellos. La calidad de la imagen retiniana es evaluada en términos de la Razón de Strehl y con mediciones de la agudeza visual para distintas cantidades de coma y astigmatismo. La cantidad de coma que produce mejor calidad de imagen en la

retina en las simulaciones es distinta de cero en todos los casos en los que el valor del astigmatismo es distinto de cero. Medidas de agudeza visual en tres casos: sin aberraciones, con astigmatismo y con astigmatismo + coma fueron realizadas en dos sujetos para varios desenfoques. Finalmente se muestra cómo la combinación de coma con astigmatismo mejora la agudeza visual por un factor de 1.28 (28%) y 1.47 (47%) en cada sujeto frente a la obtenida con solo astigmatismo.

Capítulo 4

Después de los resultados teóricos y experimentales que se muestran en el capítulo anterior hemos extendido las medidas de agudeza visual a 20 sujetos. En este capítulo se muestra cómo al añadir coma (0.23 µm para pupilas de 6 mm) a una cantidad de astigmatismo de 0.5 D da lugar a un claro aumento de la agudeza visual en 6 sujetos, de manera coherente con las predicciones teóricas. Mientras que la agudeza visual disminuyó al añadir coma al astigmatismo en 7 pacientes. Además, bajo condiciones de solo astigmatismo la agudeza visual disminuyó más de 10% con respecto a la obtenida con todas las aberraciones corregidas en 13 sujetos. Por último, se describe cómo los efectos beneficiosos de la adición de coma al astigmatismo están relacionados con la presencia de astigmatismo natural y si este está habitualmente corregido o sin corregir. El hecho de que el beneficio esperado se produce principalmente en los ojos sin astigmatismo natural sugiere efectos de adaptación neuronales relevantes en los ojos normalmente expuestos a emborronamiento astigmático.

Capítulo 5

Los capítulos anteriores incluyeron simulaciones teóricas y medidas experimentales de la agudeza visual en sujetos cuyas aberraciones están manipuladas con óptica adaptativa. En este capítulo extendemos el análisis experimental a la medida psicofísica la de sensibilidad al contraste, CSF. En particular, estudiamos la relación de la mejora en la Función de Transferencia de Modulación (MTF) con la mejora en la función de la sensibilidad al contraste (CSF). Esta correspondencia había sido poco explorada en la literatura anterior y ofrecía resultados controvertidos. En este capítulo se presenta la CSF de 4 sujetos con y sin corrección de las aberraciones. Los valores de MTF mejoraron en un promedio de 8 veces mientras que la CSF aumentó una media de 1,35

veces (sólo para las frecuencias espaciales medias y altas). El beneficio consistentemente más bajo en términos de CSF que en valores de la MTF Y las consistentes diferencias meridionales sugieren un papel importante de la función de transferencia neuronal en el límite de percepción del contraste.

Capítulo 6

En este capítulo se presenta y valida un prototipo de un instrumento óptico que permite la simulación experimental de visión bifocal pura. Este sistema se utiliza para evaluar la influencia de diferentes cantidades de adición en el contraste de la imagen y la agudeza visual. El instrumento proporciona al ojo dos imágenes superpuestas, y alineadas con los mismos aumentos, pero con diferentes vergencias. Los sujetos que miran a través del instrumento son capaces de experimentar la visión simultánea pura con corrección de su refracción y para distintos valores de adición. El instrumento se utiliza en este capítulo para investigar el impacto de la cantidad de adición sobre la función visual. El instrumento se validó a través de simulaciones por ordenador del contraste de letras vistas bajo condiciones de visión simultánea y por experimentos ópticos equivalentes con un ojo artificial (cámara). Se presentan las medidas de agudeza visual en cuatro sujetos para letras de bajo y alto contraste y diferentes cantidades de adición. La mayor degradación en el contraste y la agudeza visual (~ 25%) se produjo para adiciones de un valor de alrededor de 2 D, mientras que las adiciones de 4 D produjeron una degradación menor (14%). Valores de adición bajos (1 - 2 D) dan lugar a agudezas visuales inferiores que valores más altos de adición (3-4 D). La visión simultánea induce un patrón de degradación de rendimiento visual, que es bien predicho por la degradación que se encuentra en la calidad de imagen. Debido a esto, los efectos neuronales que se creían cruciales en la tolerancia de la visión simultánea por parte de los pacientes parece no tener un papel decisivo.

Capítulo 7

En este capítulo se presentan nuevos diseños de patrones de fase multifocales encaminados a ampliar la profundidad de foco en el ojo con presbicia. Los diseños se basan en múltiples divisiones (hasta 50) radiales o angulares. Cada zona toma un valor diferente de desenfoque o es creada con un set de polinomios de Zernike diferente. Sus rendimientos a través de foco se evalúan

de acuerdo a dos métricas: el rango de desenfoque para los que la calidad óptica está por encima de un umbral y el área encerrada bajo las generadas de VSOTF través de un intervalo de 6 D. Los mejores diseños fueron encontrados para un máximo de divisiones de 3 o 4. Los diseños con zonas divididas angularmente proporcionaron valores significativamente mejores (1,95 veces en promedio) que los diseños divididos radialmente con los mismos niveles de adición. El diseño óptimo (diseño angular con 3 zonas) superó el rendimiento multifocal de un diseño angular bifocal en un 33% y un 32% el diseño típico basado en inducción de aberración esférica. También se demuestra en este capítulo que utilizando combinaciones de aberraciones de bajo y alto orden se puede extender hasta 0.5 D el rango de desenfoque por encima del umbral sobre el mejor diseño creado con sólo desenfoque. Estos diseños podrán ser testeados en un futuro próximo en sistemas de óptica adaptativa en sujetos. Y en una última fase ser transferidos a diseños de lentes de contacto multifocales, superficies de las lentes intraoculares o perfiles de ablación corneal para técnicas de láser aplicadas a la presbicia.

Por último se evalúan catorce patrones bifocales diferentes en tres distancias de trabajo: lejos, intermedia (66 cm) y cerca (25 cm). Los resultados se presentan en simulaciones computacionales y en medidas en 5 sujetos. Con el fin de probar experimentalmente los catorce diseños bifocales un nuevo sistema bifocal que permite un control completo de la pupila mediante el uso de un modulador espacial de luz ha sido desarrollado. De los 14 diseños a prueba el mejor rendimiento (en ausencia de otras aberraciones) es el de diseños que sólo tienen 2 zonas, independientemente de que la división sea horizontal o vertical (diseños 1-4). Todos los otros diseños (10) muestran niveles más bajos de rendimiento óptico. Esta ventaja de los diseños de dos zonas (parecidos a la lente intraocular Oculentis Mplus) se mantiene cuando se toman en cuenta las aberraciones ópticas de una población real de pacientes (100 sujetos). Por otro lado el rendimiento de los sujetos individuales con cada uno de los diseños es más variable para los diseños de 2 zonas divididas horizontalmente o verticalmente que cuando se divide radialmente o cuando se aplican más zonas. Los frentes de onda de los mejores y peores sujetos cuando se evalúan con diseños de 2 zonas están claramente dominados por coma en todos los casos (para las tres distancias de

trabajo). Los resultados experimentales en 5 sujetos muestran que los diseños radialmente segmentados de dos zonas ofrecen propiedades ópticas mejores que los diseños circularmente segmentados o con mayor número de zonas. También se ve claramente tanto en las simulaciones como en las medidas experimentales que en los diseños radialmente divididos (áreas repartidas al 50%) siempre se obtiene mejor visión para la distancia que se coloca en la parte central del diseño.

Bibliography

1 Ilardi, V. Eyeglasses and concave lenses in fifteenth-century Florence and Milan: new documents. *Renaissance quarterly* **29**, 341-360 (1976).

2 Atchison, D. A. & Charman, W. N. Thomas Young's contribution to visual optics: The Bakerian lecture “On the mechanism of the eye”. *Journal of Vision* **10**, doi:10.1167/10.12.16 (2010).

3 Smirnov, M. S. Measurement of the wave aberration of the human eye. *Biofizika* **6**, 687-703 (1961).

4 Platt, B. C. & Shack, R. History and principles of Shack-Hartmann wavefront sensing. *J Refract Surg* **17**, S573-577 (2001).

5 Liang, J., Grimm, B., Goelz, S. & Bille, J. F. Objective measurement of wave aberrations of the human eye with the use of a Hartmann-Shack wave-front sensor. *Journal of the Optical Society of America A* **11**, 1949-1957 (1994).

6 Cubalchini, R. Modal wave-front estimation from phase derivate measurements. *Journal of the Optical Society of America A* **69**, 972-977 (1979).

7 Thibos, L. N., Applegate, R. A., Schwiegerling, J. T., Webb, R. H. & Members, V. S. T. Standards for reporting the optical aberrations of eyes. *Vision Science and its Applications, OSA Trends in Optics & Photonics* **35**, 110-130 (2000).

8 Guirao, A. & Williams, D. A method to predict refractive errors from wave aberration data. *Optom Vis Sci.* **80**, 36-42 (2003).

9 Marsack, J. D., Thibos, L. N. & Applegate, R. A. Metrics of optical quality derived from wave aberrations predict visual performance. *Journal of Vision* **4**, 322-328 (2004).

10 Williams, D. R. Visibility of interference fringes near the resolution limit. *Journal of the Optical Society of America A* **7**, 1087-1093 (1985).

11 Yoon, G., Cox, I. & Williams, D. R. The visual benefit of the static correction of the monochromatic wave aberration. *Investigative of Ophthalmology Visual Science (Suppl.)* **40**, 40 (1999).

12 Tyson, R. K. *Principles of Adaptive Optics*. (Academic Press, 1991).

13 Lukin, V. P. *Atmospheric Adaptive Optics*. (SPIE Optical Engineering Press, 1995).

14 Liang, J., Williams, D. R. & Miller, D. T. Supernormal vision and high resolution retinal imaging through adaptive optics. *Journal of the Optical Society of America A* **14**, 2884-2892 (1997).

15 Dreher, A. W., Bille, J. F. & Weinreb, R. N. Active optical depth resolution improvement of the laser tomographic scanner. *Appl. Opt.* **28**, 804-808 (1989).

16 Liang, J. & Williams, D. R. Aberrations and retinal image quality of the normal human eye. *Journal of the Optical Society of America A* **14**, 2873-2883 (1997).

17 Applegate, R. A., Marsack, J. D., Ramos, R. & Sarver, E. J. Interaction between aberrations to improve or reduce visual performance. *Journal of Cataract and Refractive Surgery* **29**, 1487-1495 (2003).

18 Cheng, X., Bradley, A. & Thibos, L. N. Predicting subjective judgment of best focus with objective image quality metrics. *Journal of Vision* **4**, 310-321 (2004).

19 Yoon, G. & Williams, D. Visual performance after correcting the monochromatic and chromatic aberrations of the eye. *Journal of the Optical Society of America A.* **19**, 266-275 (2002).

20 Artal, P., Manzanera, S., Piers, P. & Weeber, H. Visual effect of the combined correction of spherical and longitudinal chromatic aberrations. *Opt. Express* **18**, 1637-1648 (2010).

21 Li, S. *et al.* Effects of monochromatic aberration on visual acuity using adaptive optics. *Optom Vis Sci* **86**, 868-874, doi:10.1097/OPX.0b013e3181adfdff (2009).

22 Marcos, S., Sawides, L., Gambra, E. & Dorronsoro, C. Influence of adaptive-optics ocular aberration correction on visual acuity at different luminances and contrast polarities. *Journal of Vision* **8**, 12, doi:110.1167/8.13.1 (2008).

23 Sawides, L., Gambra, E., Pascual, D., Dorronsoro, C. & Marcos, S. Visual performance with real-life tasks under Adaptive-Optics ocular aberration correction. *Journal of Vision* **10**, doi:10.1167/10.5.19 (2010).

24 Marcos, S. Refractive Surgery and Optical Aberrations. *Optics and Photonics News* **12**, 22-25 (2001).

25 Guo, H., Atchison, D. A. & Birt, B. J. Changes in through-focus spatial visual performance with adaptive optics correction of monochromatic aberrations. *Vision Research* **48**, 1804-1811, doi:10.1016/j.visres.2008.04.033 (2008).

26 Legras, R., Benard, Y. & Rouger, H. Through-focus visual performance measurements and predictions with multifocal contact lenses. *Vision Research* **50**, 1185-1193, doi:10.1016/j.visres.2010.04.001 (2010).

27 Piers, P. A., Fernandez, E. J., Manzanera, S., Norrby, S. & Artal, P. Adaptive optics simulation of intraocular lenses with modified spherical aberration. *Invest Ophthalmol Vis Sci* **45**, 4601-4610, doi:10.1167/iovs.04-0234 (2004).

28 de Gracia, P. *et al.* Combining coma with astigmatism can improve retinal image over astigmatism alone. *Vision Research* **50**, 2008-2014, doi:DOI: 10.1016/j.visres.2010.07.014 (2010).

29 de Gracia, P., Dorronsoro, C., Marin, G., Hernández, M. & Marcos, S. Visual acuity under combined astigmatism and coma: Optical and neural adaptation effects. *Journal of Vision* **11**, doi:10.1167/11.2.5 (2011).

30 de Gracia, P., Marcos, S., Mathur, A. & Atchison, D. A. Contrast sensitivity benefit of adaptive optics correction of ocular aberrations. *Journal of Vision* **11**, doi:10.1167/11.12.5 (2011).

31 Yi, F., Robert Iskander, D. & Collins, M. Depth of focus and visual acuity with primary and secondary spherical aberration. *Vision Research* **51**, 1648-1658, doi:10.1016/j.visres.2011.05.006 (2011).

32 Benard, Y., Lopez-Gil, N. & Legras, R. Optimizing the subjective depth-of-focus with combinations of fourth- and sixth-order spherical aberration. *Vision Research* **51**, 2471-2477, doi:10.1016/j.visres.2011.10.003 (2011).

33 Nishi, Y., Mireskandari, K., Khaw, P. & Findl, O. Lens refilling to restore accommodation. *Journal of Cataract and Refractive Surgery* **35**, 374-382, doi:10.1016/j.jcrs.2008.10.054 (2009).

34 Han, S. C., Graham, A. D. & Lin, M. C. Clinical assessment of a customized free-form progressive add lens spectacle. *Optometry & Vision Science* **88**, 234-243 (2011).

35 Bennett, E. S. Contact lens correction of presbyopia. *Clinical and Experimental Optometry* **91**, 265-278, doi:10.1111/j.1444-0938.2007.00242.x (2008).

36 Evans, B. J. W. Monovision: a review. *Ophthalmic and Physiological Optics* **27**, 417-439, doi:10.1111/j.1475-1313.2007.00488.x (2007).

37 Buznego, C. & Trattler, W. B. Presbyopia-correcting intraocular lenses. *Current Opinion in Ophthalmology* **20**, 13-18 (2009).

38 Bradley, A., Abdul Rahman, H., Soni, P. S. & Zhang, X. Effects of target distance and pupil size on letter contrast sensitivity with simultaneous vision bifocal contact lenses. *Optometry & Vision Science* **70**, 476-481 (1993).

39 Institute, G. P. L. *http://www.gpli.info/asp/search.aspx GPLI's searchable database of GP lenses* 2012).

40 Roorda, A. Adaptive optics for studying visual function: A comprehensive review. *Journal of Vision* **11**, doi:10.1167/11.5.6 (2011).

41 Sawides, L., Gambra, E., Pascual, D., Dorronsoro, C. & Marcos, S. Visual performance with real-life tasks under Adaptive-Optics ocular aberration correction. *Journal of Vision* **10**, doi:10.1167/10.5.19 (2010).

42 Gambra, E., Sawides, L., Dorronsoro, C. & Marcos, S. Accommodative lag and fluctuations when optical aberrations are manipulated. *Journal of Vision* **9**, 1-15 (2009).

43 Sawides, L., de Gracia, P., Dorronsoro, C., Webster, M. & Marcos, S. Adapting to blur produced by ocular high-order aberrations. *Journal of Vision* **11**, doi:10.1167/11.7.21 (2011).

44 Sawides, L., de Gracia, P., Dorronsoro, C., Webster, M. A. & Marcos, S. Vision Is Adapted to the Natural Level of Blur Present in the Retinal Image. *PLoS ONE* **6**, e27031, doi:10.1371/journal.pone.0027031 (2011).

45 Sawides, L. *et al.* in *ARVO* (Fort Lauderdale, Miami, EEUU, 2010).

46 Vinas, M., Sawides, L., de Gracia, P. & Marcos, S. Perceptual Adaptation to the Correction of Natural Astigmatism. *PLoS ONE* **7**, e46361, doi:10.1371/journal.pone.0046361 (2012).

47 Atchison, D. A., Guo, H., Charman, W. N. & Fisher, S. W. Blur limits for defocus, astigmatism and trefoil. *Vision Research* **49**, 2393-2403, doi:DOI: 10.1016/j.visres.2009.07.009 (2009).

48 Atchison, D. A., Guo, H. & Fisher, S. W. Limits of spherical blur determined with an adaptive optics mirror. *Ophthalmic and Physiological Optics* **29**, 300-311, doi:10.1111/j.1475-1313.2009.00637.x (2009).

49 Guo, H. & Atchison, D. A. Subjective blur limits for cylinder. *Optom Vis Sci* **87**, E549-559, doi:10.1097/OPX.0b013e3181e61b8f (2010).

50 Atchison, D. A. & Guo, H. Subjective blur limits for higher order aberrations. *Optom Vis Sci* **87**, E890-898, doi:10.1097/OPX.0b013e3181f6fb99 (2010).

51 Dorronsoro, C. & Marcos, S. Instrument for simulating multifocal ophthalmic corrections USA patent WO/2010/116019 (2009).

52 de Gracia, P., Dorronsoro, C., Sánchez-González, Á., Sawides, L. & Marcos, S. Experimental Simulation of Simultaneous Vision. *Investigative Ophthalmology & Visual Science* **54**, 415-422, doi:10.1167/iovs.12-11219 (2013).

53 Goodman, J. W. *Introduction to Fourier Optics*. 2nd edn, (McGraw-Hill International Editions, 1996).

54 Iskander, D. R. Computational Aspects of the Visual Strehl Ratio. *Optometry & Vision Science* **83**, 57-59 (2006).

55 Brainard, D. H. The psychophysics toolbox. *Spatial Vision* **10**, 433-436 (1997).

56 Applegate, R. A., Ballentine, C., Gross, H., Sarver, E. J. & Sarver, C. A. Visual acuity as a function of Zernike mode and level of root mean square error. *Optometry and Vision Science* **80**, 97-105 (2003).

57 Thibos, L. N., Hong, X., Bradley, A. & Applegate, R. A. Accuracy and precision of objective refraction from wavefront aberrations. *Journal of Vision* **4**, 329-351 (2004).

58 McLellan, J. S., Prieto, P., Marcos, S. & Burns, S. Are the eye's wave aberrations random? *Vision Res.* **46**, 2546-2553 (2006).

59 McLellan, J. S., Marcos, S., Prieto, P. M. & Burns, S. A. Imperfect optics may be the eye's defence against chromatic blur. *Nature* **417**, 174-176 (2002).

60 Thibos, L. N. Calculation of the influence of lateral chromatic aberration on image quality across the visual field. *Journal of the Optical Society of America A* **4**, 1673-1680. (1987).

61 Vitale, S., Ellwein, L., Cotch, M. F., Ferris, F. L., III & Sperduto, R. Prevalence of Refractive Error in the United States, 1999-2004. *Arch Ophthalmol* **126**, 1111-1119, doi:10.1001/archopht.126.8.1111 (2008).

62 Castejon-Mochon, F. J., Lopez-Gil, N., Benito, A. & Artal, P. Ocular wave-front aberration statistics in a normal young population. *Vision Research* **42**, 1611-1617 (2002).

63 Thibos, L., Hong, X., Bradley, A. & Cheng, X. Statistical variation of aberration structure and image quality in a normal population of healthy eyes. *J Opt Soc Am A* **19**, 2329-2348 (2002).

64 Howland, H. C. & Howland, B. A subjective method for the measurement of the monochromatic aberrations of the eye. *Journal of the Optical Society of America A* **67**, 1508-1518 (1977).

65 Charman, W. N. The eye in focus: accommodation and presbyopia. *Clinical and Experimental Optometry* **91**, 207-225, doi:10.1111/j.1444-0938.2008.00256.x (2008).

66 Navarro, R., Moreno, E. & Dorronsoro, C. Monochromatic aberrations and point-spread functions of the human eye across the visual field. *Journal of the Optical Society of America A* **15**, 2522-2529 (1998).

67 Gustafsson, J., Terenius, E., Buchheister, J. & Unsbo, P. Peripheral astigmatism in emmetropic eyes. *Ophthalmic and Physiological Optics* **21**, 393-400, doi:10.1046/j.1475-1313.2001.00606.x (2001).

68 Barbero, S., Marcos, S., Merayo-Lloves, J. & Moreno-Barriuso, E. Validation of the estimation of corneal aberrations from videokeratography in keratoconus. *Journal of Refractive Surgery* **18**, 263-270 (2002).

69 Villegas, E. A. & Artal, P. Spatially Resolved Wavefront Aberrations of Ophthalmic Progressive-Power Lenses in Normal Viewing Conditions. *Optometry & Vision Science* **80**, 106-114 (2003).

70 Marcos, S., Rosales, P., Llorente, L. & Jimenez-Alfaro, I. Change in corneal aberrations after cataract surgery with 2 types of aspherical intraocular lenses. *Journal of Cataract and Refractive Surgery* **33**, 217-226 (2007).

71 Legras, R., Chateau, N. & Charman, W. N. Assessment of just-noticeable differences for refractive errors and spherical aberration using visual simulation. *Optometry and Vision Science* **81**, 718-728 (2004).

72 Sawides, L. *et al.* Adaptation to astigmatic blur. *Journal of Vision* **10**, doi:10.1167/10.12.22 (2010).

73 Collins, F. L., Ricci, J. A. & Burkett, P. A. Behavioral training for myopia: long term maintenance of improved acuity. *Behaviour Research and Therapy* **19**, 265-268 (1981).

74 Pesudos, K. & Brennan, N. A. Decreased Uncorrected Vision After a Period of Distance Fixation with Spectacle Wear. *Optometry & Vision Science* **70**, 528-531 (1993).

75 George, S. & Rosenfield, M. Blur Adaptation and Myopia. *Optometry & Vision Science* **81**, 543-547 (2004).

76 Webster, M. A., Georgeson, M. A. & Webster, S. M. Neural adjustments to image blur. *Nature Neuroscience* **5**, 839-840 (2002).

77 Georgeson, M. A. & Sullivan, G. D. Contrast constancy: deblurring in human vision by spatial frequency channels. *The Journal of Physiology* **252**, 627-656 (1975).

78 Cufflin, M. P., Mankowska, A. & Mallen, E. A. H. Effect of blur adaptation on blur sensitivity and discrimination in emmetropes and myopes. *Investigative Ophthalmology & Visual Science* **48**, 2932-2939 (2007).

79 Freeman, R. D. Asymmetries in human accommodation and visual experience. *Vision Research* **15**, 483-492 (1975).

80 Dobson, V., Miller, J. M., Harvey, E. M. & Mohan, K. M. Amblyopia in astigmatic preschool children. *Vision Research* **43**, 1081-1090 (2003).

81 Gwiazda, J., Mohindra, I., Brill, S. & Held, R. Infant astigmatism and meridional amblyopia. *Vision Research* **25**, 1269-1276 (1985).

82 Tan, J. *et al.* Performance Standards for Toric Soft Contact Lenses. *Optometry & Vision Science* **84**, 422-428 410.1097/OPX.1090b1013e318059063b (2007).

83 Amos, J. F. *Diagnosis and management in vision care*. (Butterworth-Heinemann, 1987).

84 Guyton, D. L. Prescribing cylinders: The problem of distortion. *Survey of Ophthalmology* **22**, 177-188 (1977).

85 Campbell, F. W. & Green, D. G. Optical and retinal factors affecting visual resolution. *Journal of Physiology (London)* **181**, 576-593 (1965).

86 Dalimier, E., Dainty, C. & Barbur, J. L. Effects of higher-order aberrations on contrast acuity as a function of light level. *Journal of Modern Optics* **55**, 791-803 (2008).

87 Elliott, S. L. *et al.* Role of high-order aberrations in senescent changes in spatial vision. *Journal of Vision* **9**, doi:10.1167/9.2.24 (2009).

88 Murray, I. J. *et al.* The oblique effect has an optical component: Orientation-specific contrast thresholds after correction of high-order aberrations. *Journal of Vision* **10**, doi:10.1167/10.11.10 (2010).

89 Campbell, F. W. & Kulikowski, J. J. Orientational selectivity of the human visual system. *The Journal of Physiology* **187**, 437-445 (1966).

90 Furchner, C. & Young, S. Recovery from adaptation as a function of stimulus orientation. *Attention, Perception, & Psychophysics* **17**, 117-124, doi:10.3758/bf03203875 (1975).

91 Li, B., Peterson, M. R. & Freeman, R. D. Oblique Effect: A Neural Basis in the Visual Cortex. *Journal of Neurophysiology* **90**, 204-217, doi:10.1152/jn.00954.2002 (2003).

92 Huang, C.-B., Zhou, Y. & Lu, Z.-L. Broad bandwidth of perceptual learning in the visual system of adults with anisometropic amblyopia.

Proceedings of the National Academy of Sciences **105**, 4068-4073, doi:10.1073/pnas.0800824105 (2008).

93 Hua, T. *et al.* Perceptual Learning Improves Contrast Sensitivity of V1 Neurons in Cats. *Current biology : CB* **20**, 887-894 (2010).

94 Woods, R. L., Bradley, A. & Atchison, D. A. Consequences of monocular diplopia for the contrast sensitivity function. *Vision Research* **36**, 3587-3596 (1996).

95 Atchison, D. A., Woods, R. L. & Bradley, A. Predicting the effects of optical defocus on human contrast sensitivity. *Journal of the Optical Society of America A* **15**, 2536-2544 (1998).

96 Atchison, D. A. & Scott, D. H. Contrast sensitivity and the Stiles-Crawford effect. *Vision Research* **42**, 1559-1569, doi:Doi: 10.1016/s0042-6989(02)00084-6 (2002).

97 Marcos, S. Aberrations and visual performance following standard laser vision correction. *J. Refract. Surgery* **17**, 596-601 (2001).

98 Timney, B. & Muir, D. Orientation anisotropy: incidence and magnitude in Caucasian and Chinese subjects. *Science* **193**, 699-701, doi:10.1126/science.948748 (1976).

99 Tahir, H. J., Parry, N. R. A., Brahma, A., Ikram, K. & Murray, I. J. The importance of grating orientation in contrast sensitivity following refractive surgery. *Ophthalmic and Physiological Optics* **29**, 518-525, doi:10.1111/j.1475-1313.2009.00676.x (2009).

100 Fernandez, E. J. *et al.* Adaptive optics with a magnetic deformable mirror: applications in the human eye *Optics Express* **14**, 8900-8917 (2006).

101 Love, G. D. Wave-front correction and production of Zernike modes with a liquid-crystal spatial light modulator. *Applied Optics* **36**, 1517-1524 (1997).

102 Prieto, P., Fernández, E., Manzanera, S. & Artal, P. Adaptive optics with a programmable phase modulator: applications in the human eye. *Optics Express* **12**, 4059-4071 (2004).

103 Márquez, A., Iemmi, C., Campos, J., Escalera, J. & Yzuel, M. Programmable apodizer to compensate chromatic aberration effects using a liquid crystal spatial light modulator. *Optics Express* **13**, 716-730 (2005).

104 Weiner, A. M. Femtosecond pulse shaping using spatial light modulators. *Review of Scientific Instruments* **71**, 1929-1960 (2000).

105 Williamson, W., Poirier, L., Coulon, P. & Verin, P. Compared optical performances of multifocal and monofocal intraocular lenses (contrast

sensitivity and dynamic visual acuity). *British Journal of Ophthalmology* **78**, 249-251 (1994).

106 Alfonso, J. F., Fernández-Vega, L., Puchades, C. & Montés-Micó, R. Intermediate visual function with different multifocal intraocular lens models. *Journal of Cataract & Refractive Surgery* **36**, 733-739, doi:10.1016/j.jcrs.2009.11.018 (2010).

107 Gupta, N., Naroo, S. A. & Wolffsohn, J. S. Visual comparison of multifocal contact lens to monovision. *Optometry & Vision Science* **86**, 98-105 (2009).

108 Chateau, N. & Baude, D. Simulated in situ optical performance of bifocal contact lenses. *Optometry & Vision Science* **74**, 532-539 (1997).

109 Martin, J. A. & Roorda, A. Predicting and assessing visual performance with multizone bifocal contact lenses. *Optometry & Vision Science* **80**, 812-819 (2003).

110 Maxwell, W. A., Lane, S. S. & Zhou, F. Performance of presbyopia-correcting intraocular lenses in distance optical bench tests. *Journal of Cataract & Refractive Surgery* **35**, 166-171, doi:10.1016/j.jcrs.2008.10.026 (2009).

111 Sanders, E., Wagner, H. & Reich, L. N. Visual acuity and "balanced progressive" simultaneous vision multifocal contact lenses. *Eye Contact Lens* **34**, 293-296, doi:10.1097/ICL.0b013e318185d271 (2008).

112 Cox, I., Apollonio, A. & Erickson, P. The effect of add power on simultaneous vision, monocentric, bifocal, soft lens visual performance. *International Contact Lens Clinic* **20**, 18-22, doi:10.1016/0892-8967(93)90050-2 (1993).

113 Pepin, S. M. Neuroadaptation of presbyopia-correcting intraocular lenses. *Current Opinion in Ophthalmology* **19**, 10-12 10.1097/ICU.1090b1013e3282f31758 (2008).

114 Sheedy, J. E., Harris, M. G. & Gan, C. M. Does the presbyopic visual system adapt to contact lenses? *Optometry & Vision Science* **70**, 482-486 (1993).

115 Efron, N. (ed Elsevier Health Sciences) 502 (Elsevier, 2002).

116 Bennett, E. S. & Henry, V. A. (ed Lippincott Williams & Wilkins) (Wolters Kluwer, 2008).

117 Morgan, P. B., Efron, N. & Woods, C. A. An international survey of contact lens prescribing for presbyopia. *Clinical and Experimental Optometry* **94**, 87-92, doi:10.1111/j.1444-0938.2010.00524.x (2011).

118 Jones, L., Jones, D., Langley, C. & Houlford, M. Reactive or proactive contact lens fitting — Does it make a difference? *Journal of The British Contact Lens Association* **19**, 41-43, doi:10.1016/s0141-7037(96)80031-0 (1996).

119 Lichtinger, A. & Rootman, D. S. Intraocular lenses for presbyopia correction: past, present, and future. *Current Opinion in Ophthalmology* **23**, 40-46 (2012).

120 Zlotnik, A. *et al.* Extended depth of focus intra-ocular lens: a solution for presbyopia and astigmatism. 75500A-75500A, doi:10.1117/12.846682 (2010).

121 Fernández, D., Barbero, S., Dorronsoro, C. & Marcos, S. Multifocal intraocular lens providing improved visual quality. (P201232043, Spanish patent application, 2012).

122 Manzanera, S., Prieto, P. M., Ayala, D. B., Lindacher, J. M. & Artal, P. Liquid crystal Adaptive Optics Visual Simulator: Application to testing and design of ophthalmic optical elements. *Optics Express* **15**, 16177-16188 (2007).

123 Angerlo, B. & Arnhem, B. Ophthalmic lens with optical sectors. US patent (US20120029631, US patent number, 2012).

124 Fiala, W. & Gerlach, M. Multifocal lens. US Patent Application 20130050640 (20130050640, US patent application, 2012).

125 Gatinel, D., Pagnoulle, C., Houbrechts, Y. & Gobin, L. Design and qualification of a diffractive trifocal optical profile for intraocular lenses. *Journal of Cataract & Refractive Surgery* **37**, 2060-2067 (2011).

126 Lee, W. M., Yuan, X. C. & Cheong, W. C. Optical vortex beam shaping by use of highly efficientirregular spiral phase plates for optical micromanipulation. *Opt. Lett.* **29**, 1796-1798 (2004).